To the Graduate Council:

I am submitting herewith a thesis written by Katherine Samuels Crabb entitled "Mass Transfer in Vacuum Sorption Pumping of Pure Gases on Molecular Sieves." I have examined the final copy of this thesis for form and content and recommend that it be accepted in partial fulfillment of the requirements for the degree of Master of Science, with a major in Chemical Engineering.

Joseph J. Perona, Major Professor

We have read this thesis
and recommend its acceptance:

Charles H. Byers

John W. Holmes

Jack D. Watson

Accepted for the Council:

The Graduate School

MASS TRANSFER IN VACUUM SORPTION PUMPING OF PURE GASES ON MOLECULAR SIEVES

A Thesis

Presented for the

Master of Science

Degree

The University of Tennessee, Knoxville

Katherine Samuels Crabb

August 1984

ACKNOWLEDGMENTS

For their time and consideration, the author extends a sincere thank you to the members of the thesis committee: Dr. J. J. Perona, Dr. J. S. Watson, Dr. C. H. Byers, and Dr. J. M. Holmes. Special thanks go to Dr. Perona, the research director, for his guidance and friendship and to Dr. Byers, who shared many of the day-to-day trials.

The assistance and patience of Mr. M. R. Gibson were invaluable in obtaining the experimental data and are greatly appreciated. The author also gratefully acknowledges the help of Mr. R. M. Wham in implementing a computer system for data acquisition. The work of Ms. B. K. Breeden in preparing the manuscript was truly excellent.

Not to be overlooked or unappreciated is the author's husband, Dr. C. C. Crabb. Thanks Chuck, not only for understanding and support but also for many good ideas.

The work was sponsored by the U.S. Department of Energy, Office of Basic Energy Sciences.

ABSTRACT

The major objective of this work was to develop a mathematical model to quantitatively describe the hydrodynamic and diffusive mass transfer processes involved in the vacuum sorption pumping of single-component gases on cylindrical sorbent beds. A set of equations describing these processes in terms of the pressure above and through the bed and the solid loading was derived from theory, and a finite difference solution of the set of partial differential equations was developed. The model shows hydrodynamic mass transfer through the bed interstices to be characterized by an interstitial mass transfer coefficient, κ, that is a function of only the channel geometry and the temperature and molecular weight of the flowing gas.

Sorption pumping experiments were conducted using nitrogen and carbon dioxide on Davison 4A zeolite molecular sieves. For N_2, the theoretical model predicted well both the pressure above and total pressure drop across the bed for times up to saturation of the sieves. The model also described accurately the pressure profiles obtained with CO_2 but failed to fit the pressure drop data.

Estimates of κ obtained from N_2 runs using two different sorbent particle sizes indicated that κ is proportional to the particle radius; this supports the assertion that κ is a function of channel geometry. From κ for one gas, it should be possible to estimate κ for another gas moving through the same bed. The κ's predicted theoretically for CO_2 from those for N_2 did not successfully model the experimental data.

TABLE OF CONTENTS

LIST OF TABLES

LIST OF FIGURES

FIGURE PAGE

FIGURE PAGE

LIST OF SYMBOLS

A	channel or bed cross-sectional area, cm^2
c	fluid-phase concentration, mol/cm^3
d	molecular diameter, cm
D	effective solid-phase diffusivity, cm^2/s
D^*	preexponential factor for diffusion, cm^2/s
D_c	interstitial channel diameter, cm
D_H	hydraulic diameter of channel, cm
E	energy of activation for diffusion, kcal/mol
F	mass flux into bed, mol/cm^2-s
H	channel perimeter, cm
I	constant mass flow rate into void above bed, mol/s
k	Langmuir isotherm constant, $torr^{-1}$
k_B	Boltzmann constant, J/K
L	channel or bed length, cm
p	fluid-phase pressure, torr
p_R	reference pressure, torr
q	solid-phase concentration at r
$\overline{q}$	average solid-phase concentration, mol/g
q_m	Langmuir isotherm constant, mol/g
q_S	solid-phase concentration at sorbent particle surface, mol/g
Q	gas throughput, $torr\text{-}cm^3/s$
r	radial position, cm
R	universal gas constant, $torr\text{-}cm^3/mol\text{-}K$
S	sorbent particle radius, cm

t	time, s
T	absolute temperature, K
T_a	absolute ambient temperature, K
T_b	absolute temperature of sorbent bed, K
v	fluid velocity, cm/s
v_m	average molecular velocity, cm/s
V	volume, cm^3
V_f	volumetric flow rate, cm^3/s
x	dimensionless variable for pressure
$\overline{y}$	dimensionless variable for average solid-phase concentration
z	axial position in bed, cm
Z	dimensionless variable for axial position in bed

Greek Letters

ϵ	void fraction of bed, cm^3 void/cm^3 bed
Θ	dimensionless variable for time
κ	interstitial mass transfer coefficient, cm^2/s
λ	mean free path of gas molecule, cm
ρ_B	bulk density of sorbent, g/cm^3

I. INTRODUCTION

Cryosorption pumping of gases on deep beds of sorbents is becoming an important process in several areas of energy production. Sorption pumping differs from most sorption processes in that the usual goal is not separation. No carrier gas is used, and there is no forced convection through the sorbent bed. As sorption proceeds, the bed acts as a pump to transfer gas from a closed system. Dewar first used sorption pumping to evacuate an enclosed space 80 years ago (O'Hanlon, 1980). Today, small cryosorption pumps are commonly used in laboratory applications to evacuate volumes on the order of 10 L; typically, these employ several pounds of synthetic zeolite molecular sieves at liquid nitrogen temperature (Roth, 1976). Commercially available units are used to pump small volumes from atmospheric pressure to about 10^{-2} torr (mm Hg).

Many of the advantages of sorption pumps are immediately apparent. With no moving mechanical parts, they are compact, reliable, and easily maintained. They are also economical. The molecular sieves can be regenerated after each pumpdown, making the liquid nitrogen the major operating cost. Most important, however, they introduce no foreign materials (e.g., oil) to the system and provide no path for escape of pumped gases.

A need for clean roughing pumps exists in both the current development and future use of fusion energy (Conn, 1977 and 1983). In experiments at the Oak Ridge National Laboratory, large cryosorption pumps are now being used to evacuate volumes of 10^3 L. In future applications, such pumps will be used to rough fusion power reactors (volumes of about

10^5 L) as well as the vacuum buildings that house the reactors (volumes on the order of 10^7 L).

Although small-scale pumps are currently in use and their advantages are easily delineated, the mass and heat transfer phenomena occurring within the sorbent bed are not well understood. The pumping characteristics of sorption pumps change as the sorbent bed becomes saturated. Successful scale-up of the laboratory pump for fusion energy applications can be achieved most effectively through developing mathematical models that quantitatively describe these transport phenomena. This development requires not only physical property data available in the literature, such as equilibrium adsorption isotherms and sorbent characteristics, but also parameters that must be determined experimentally.

The goal of the research reported here was to determine the mass transfer parameters necessary to characterize cryosorption pump performance. A theoretical model was developed to describe the behavior of a pump in sorbing pure gases at isothermal conditions. The model predicts the pressure above and through the sorbent bed and the quantity of gas sorbed as functions of time. Application of the model, however, required values of parameters that could not be readily calculated or measured.

To determine these parameters, experiments were conducted in which nitrogen and carbon dioxide were sorbed isothermally in deep cylindrical beds of artificial zeolite sieves. The pressure profile above and through the bed was recorded as gas was pumped into the bed over long time intervals. Comparisons of the pressure profiles generated by the

theoretical model with experimental results allowed determination of the necessary parameters. The general applicability of the model to various conditions was then tested by further comparisons with experimental data.

The following pages report the research beginning with a survey of related literature. Following is a discussion of the theoretical model and the numerical methods used in solving the set of equations that comprise the model. The experimental program is then summarized, the results are presented, and comparisons are made between the theoretical model and experimental data. The report ends with a summary of the results and the conclusions drawn from them along with recommendations for future work.

II. LITERATURE SURVEY

Although Dewar first used cryosorption pumping to evacuate an enclosure about 80 years ago, active interest in this pumping technique did not begin until the late fifties and early sixties. This growth seems to have stemmed from the commercial development of synthetic zeolite sieves that began in 1948 (Breck, 1974). Designs for cryosorption pumps using synthetic zeolite sorbents began to appear in the late fifties along with studies of the sorbent properties of the sieves. For discussion here, the extensive body of literature concerned with vacuum technologies and zeolite sieves will be grouped into three categories: (1) cryosorption pumping, (2) molecular sieves as sorbents, and (3) modeling of molecular sieve columns.

Cryosorption Pumping

Numerous texts describe the properties of gases in vacuum and the technologies for achieving low pressures. The reference most often cited by early researchers is a book by Dushman (1949) in which he reviews the important developments in vacuum technology throughout the 1900's. He makes only brief mention of adsorption on naturally occurring zeolites while discussing sorption pumping using activated charcoal. More recently, Roth (1976) and O'Hanlon (1980) discuss the properties of gases in and the production and measurement of vacuum. Roth presents extensive references related to molecular sieve cryosorption pump designs. These studies are of interest primarily in that they provide an understanding of the performance characteristics of

cryosorption pumps and of the techniques for measuring temperatures and pressures at vacuum conditions.

Molecular Sieves as Sorbents

Since the fifties, countless papers have dealt with the kinetics and equilibria of adsorption on synthetic zeolites. Because the work proposed here will study vacuum sorption of nitrogen and carbon dioxide on zeolite 4A, the literature search focused primarily on these systems.

The pioneer in this field was R. M. Barrer, whose first publications appeared in the late thirties. In a 1978 text he summarizes much of his as well as others studies of molecular sieves as sorbents, presenting numerous literature citations (Barrer, 1978). Much of his work deals with monatomic and diatomic molecules on naturally occurring zeolites. Another valuable reference text is by Breck (1974), one of the workers who followed Barrer's lead into the fifties and sixties. He presents an extensive review of the structure, chemistry, and use of molecular sieves. Included are equilibrium sorption isotherms for CO_2 on 4A at temperatures from 198 K and for N_2 from 77 K as well as diffusion constants for N_2 over a range from 150 to 200 K. In addition, Habgood (1958) presents equilibrium isotherms and diffusion coefficients for N_2 on 4A at temperatures down to 193.7 K. Harper, Stifel, and Anderson (1969) studied both the N_2-4A and CO_2-4A systems at 197 K.

Most recently, Ruthven and coworkers at the University of New Brunswick have published numerous articles on the diffusion of gases in zeolites. They present measured diffusivities and sorption isotherms for many systems as well as models and theories describing these

processes. Specific problems addressed include (1) the effect of crystal size and shape distribution on measured diffusivities (Loughlin, Derrah, and Ruthven, 1971; Ruthven and Loughlin, 1971, 1972a, and 1972b), (2) the concentration dependence of diffusivity (Loughlin, Derrah, and Ruthven, 1971; Garg and Ruthven, 1972; Yucel and Ruthven, 1980), (3) the relative effects of micropore (intracrystalline) and macropore (intercrystalline) diffusion in manufactured sieve particles (Ruthven and Loughlin, 1972b), and (4) the kinetics of nonisothermal sorption (Lee and Ruthven, 1979; Ruthven, Lee, and Yucel, 1980). In general, they have studied single and multicomponent systems of monatomic and diatomic gases and light hydrocarbons on zeolite types A and X at temperatures above 200 K. Of particular interest here are studies of N_2 and CO_2 on 4A crystals (Ruthven and Derrah, 1975; Yucel and Ruthven, 1980).

Modeling of Molecular Sieve Columns

Numerous studies exist of the performance of fixed bed adsorbers in which the controlling mechanism is diffusion into solid particles. Most have considered isothermal sorption from dilute feed streams at standard conditions. The models predict the "breakthrough curve," which is the effluent concentration as a function of time in response to a step increase in sorbate concentration.

For example, Rosen (1952) develops a model for a fixed bed that assumes a linear equilibrium isotherm. Hall et al. (1966) consider constant pattern behavior (sorption front moves at constant velocity through the bed) for solid diffusion and pore diffusion assuming a

Langmuir isotherm. They define solid diffusion as movement of molecules from the exterior of the sorbent molecules in condensed form and pore diffusion as movement in fluid phase into the pores followed by stationary adsorption on the surface. Fleck, Kirwan, and Hall (1973) extend this work by considering combined resistances.

Garg and Ruthven have published several studies concerned specifically with molecular sieve columns. In one series, they develop a model that successfully predicts experimental saturation and regeneration curves for systems exhibiting a Langmuir isotherm and controlled by micropore diffusion (Garg and Ruthven, 1973a, 1973b, and 1974).

The model considers the response to a step increase in concentration of a dilute sorbate in an inert carrier at standard conditions. The numerous simplifying assumptions on which it is based include several not applicable to the sorbent bed of a cryosorption pump. Most important is that they assume constant fluid velocity through the bed — an assumption that does not hold for the pump. Thus the differential fluid-phase mass transfer equation they solve differs significantly from that required here. However, the equations they develop modeling solid-phase diffusion and relating solid-phase and fluid-phase concentrations are applicable.

In subsequent work, Garg and Ruthven modify their original model to account for macropore diffusion (1973c), for a linear driving force for solid-phase mass transfer (1975a), and for longitudinal diffusion (1975b). Ruthven has also considered the performance of nonisothermal columns (Ruthven, Garg, and Crawford, 1975; Ruthven and Lee, 1981). Most recently, Raghavan and Ruthven (1983) have compared different

numerical methods for solving the set of partial differential equations that make up the theoretical model; specifically, they consider orthogonal collocation as opposed to standard finite difference methods.

III. THEORETICAL MODEL

Figure 1 sketches the physical system being modeled. A single-component gas flows at constant flux into a void space above a sorbent bed. The void space is at ambient temperature while the bed is cooled using a liquid refrigerant; the bed temperature is determined by the sorbent and sorbate gas. The system is initially under vacuum. In the work conducted here, the starting pressure was about 10^{-3} torr.

As the gas molecules flow into the cooled bed, they are adsorbed on the porous sorbent particles. A pressure gradient is maintained across the bed, and gas continues to flow into the bed until the sorbent approaches saturation. Two transport processes occur as gas moves into the bed. Hydrodynamic transport takes place as gas flows through the bed interstices, and diffusive transfer occurs as adsorbed molecules move from the surface to the interior of the sorbent particles.

The two transport processes can be related by a mass balance around a differential length of bed:

$$\varepsilon \frac{\partial c}{\partial t} + \rho_B \frac{\partial \bar{q}}{\partial t} + \varepsilon \frac{\partial (vc)}{\partial z} = 0 \ , \qquad (1)$$

where

ε = void fraction of bed,

c = fluid-phase concentration,

ρ_B = bulk density of sorbent,

$\bar{q}$ = average solid-phase concentration,

v = fluid velocity, and

z = axial position in bed.

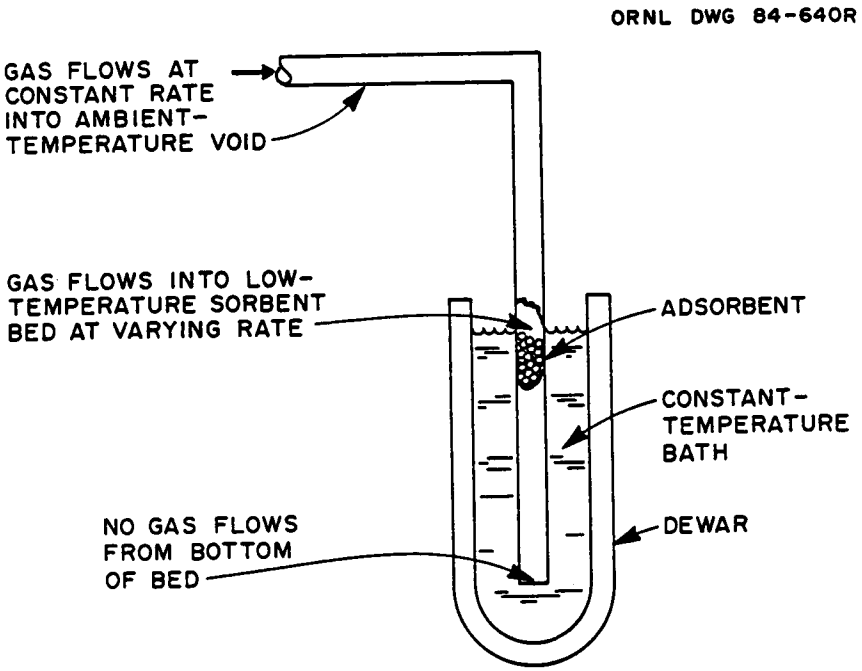

Figure 1. Gas flow in experimental sorption pumping system.

In words, the change in flux across a section of the bed equals the accumulation in the fluid phase plus the accumulation in the solid phase. By relating the three dependent variables c, v, and $\bar{q}$ to the more easily measured quantity of pressure, p, Equation (1) can be used to develop a model that predicts the pressure and solid loading in the bed as a function of time and position.

First consider that the gas concentration, c, for a single-component system is simply the molar gas density. At the low pressures considered here (up to 1 torr), ideal gas behavior can be assumed, and

$$c = \frac{n}{V} = \frac{p}{RT} . \tag{2}$$

The flow rate of gas into the system for the cases studied is on the order of 10^{-8} mol/s. For the resulting low adsorption fluxes, the heat of adsorption will be low, and T in Equation (2) can be assumed constant.

Consider next the velocity of the gas through the bed interstices. Most models of fixed-bed adsorption columns consider adsorption of a dilute component from a fluid mixture flowing through the bed by forced convection. When sorbing a dilute component, the velocity is essentially constant. In the work conducted here, a single-component gas is drawn into the bed because of a pressure gradient, and there is no flux out of the bed. Consequently, a large variation in interstitial velocity will occur along the bed.

In addition, because of the low temperatures and pressures and the small channel size, flow through the bed interstices is in the molecular

flow regime rather than the more familiar laminar and turbulent regimes. By definition, molecular flow occurs when the mean free path of the gas molecules is large compared to the cross section of the channel through which the gas is passing. Recall that the mean free path is directly proportional to temperature and inversely proportional to pressure.

A quantity often used to describe the molecular flow of gases is the throughput, Q, which is the volume of gas at a known pressure and temperature passing a plane per unit time. It is defined by

$$Q = pV_f \tag{3}$$

where V_f is the volumetric flow rate. Rewriting V_f in terms of velocity through a channel,

$$Q = pvA \ , \tag{4}$$

where A is the channel cross section.

For molecular flow through long tubes and channels, Knudsen derived the following expression for Q (Dushman, 1949):

$$Q = -\frac{4}{3} \frac{v_m}{\int_0^L \frac{H}{A^2} dL} (p_2 - p_1) \ , \tag{5}$$

where

v_m = average molecular velocity,

H = channel perimeter,

L = channel length, and

$(p_2 - p_1)$ = pressure drop along channel.

The average molecular velocity, v_m, depends only on the temperature and molecular weight of the gas. The integral depends on the channel geometry. In using this equation to model flow through the interstices of a packed bed, where the channel is the void volume between particles, the integral is intractable. However, by estimating the ratio H/A^2 by an average value over the length of the channel, the integral simplifies to

$$\int_0^L \frac{H}{A^2}\, dL = \left(\frac{H}{A^2}\right)_{avg} L \,. \tag{6}$$

Equations (4), (5), and (6) can now be combined to yield the velocity at p_1,

$$v = -\left[\frac{4}{3}\,\frac{v_m}{\left(\frac{H}{A}\right)_{avg}}\right]\frac{1}{p_1}\,\frac{p_2 - p_1}{L} \,. \tag{7}$$

Because of the complex channel geometry, the group of constants, represented by the symbok κ, must be determined experimentally. For a differential length of channel, Equation (7) becomes

$$v = -\frac{\kappa}{p}\frac{\partial p}{\partial z} \,. \tag{8}$$

To relate $\bar{q}$ to p, consider the solid-phase mass transfer phenomena. Movement of gas into the solid involves two steps: surface adsorption of individual molecules followed by inward diffusion. Mass transport

within the molecular sieve particles is modeled as a radial diffusion process characterized by an effective mass diffusivity (e.g., Garg and Ruthven, 1973a). If the particles are represented as spheres, the governing equation is

$$\frac{\partial q}{\partial t} = \frac{D}{r^2} \frac{\partial}{\partial r} \left(r^2 \frac{\partial q}{\partial r} \right), \tag{9}$$

where

q = solid-phase concentration at r,

D = effective diffusivity, and

r = radial position.

The use of Equation (9) depends on several assumptions. Commercial molecular sieve adsorbents consist of synthetic zeolite crystals in an inert binder. Thus two mass transfer resistances occur: the macropore (intercrystalline) diffusional resistance of the pellet and the micropore (intracrystalline) resistance of the zeolite crystals. The sorption behavior can be described by Equation (9) only if one of the resistances is dominant and if the resistance can be assumed independent of concentration (Garg and Ruthven, 1973c). These assumptions appear valid in developing a first model of the movement of monatomic and diatomic gases in 4A sieves (Perona et al., 1983).

The solid-phase concentration, q, varies with radial position within the particles. The quantity required in the material balance is the average loading per unit weight of sorbent, $\bar{q}$, at a given bed position; $\bar{q}$ is defined by

$$\bar{q} = \frac{\int_0^S q 4\pi r^2 dr}{\frac{4}{3}\pi S^3} , \tag{10}$$

or

$$\bar{q} = \frac{3}{S^3} \int_0^S q r^2 \, dr , \tag{11}$$

where S is the particle radius. To obtain the change in $\bar{q}$ with time, begin by differentiating Equation (11) with respect to time:

$$\frac{\partial \bar{q}}{\partial t} = \frac{3}{S^3} \int_0^S \frac{\partial q}{\partial t} r^2 \, dr . \tag{12}$$

Substituting Equation (9) for $\partial q/\partial t$,

$$\frac{\partial \bar{q}}{\partial t} = \frac{3}{S^3} \int_0^S D \frac{\partial}{\partial r}\left(r^2 \frac{\partial q}{\partial r}\right) dr . \tag{13}$$

On integrating, this yields

$$\frac{\partial \bar{q}}{\partial t} = \frac{3D}{S}\left[\frac{\partial q}{\partial r}\right]_{r = S} . \tag{14}$$

At this point, it is convenient to assume a parabolic form for the solid-phase concentration profile. This approximation has been used in adsorption and ion exchange work for at least thirty years and has generally given good results (Liaw et al., 1979). Thus,

$$q = a_0 + a_2 r^2 \ , \tag{15}$$

where a_0 and a_2 vary with time.

Using the parabolic concentration profile in the integral expression for $\bar{q}$, Equation (11), one obtains

$$\bar{q} = \frac{3}{S^3} \int_0^S (a_0 + a_2 r^2) r^2 dr \ , \tag{16}$$

or, after integrating,

$$\bar{q} = a_0 + \frac{3}{5} a_2 S^2 \ . \tag{17}$$

Equation (15) is next evaluated at S to obtain the solid-phase concentration at the particle surface, q_S, and Equation (17) is subtracted from q_S to yield

$$q_S - \bar{q} = \frac{2}{5} a_2 S^2 \ . \tag{18}$$

Solving for a_2,

$$a_2 = \frac{5}{2S^2} (q_S - \bar{q}) \ . \tag{19}$$

Equation (15) is now differentiated with respect to r to yield the concentration gradient at the particle surface:

$$\left.\frac{\partial q}{\partial r}\right|_{r=S} = 2a_2 S \ . \tag{20}$$

Eliminating a_2 by means of Equation (19),

$$\left.\frac{\partial q}{\partial r}\right|_{r=S} = \frac{5}{S}(q_S - \bar{q}) \ . \tag{21}$$

Equation (21) is then substituted into Equation (14) to yield

$$\frac{\partial \bar{q}}{\partial t} = \frac{15D}{S^2}(q_S - \bar{q}) \ . \tag{22}$$

For a single-component system, no gas-phase resistance to mass transfer occurs at the particle surface, and q_S is the surface loading in equilibrium with the gas pressure. Garg and Ruthven (e.g., 1973a) have shown that a Langmuir form of adsorption isotherm can successfully model surface adsorption in commercial synthetic zeolites. Thus,

$$\frac{q_S}{q_m} = \frac{kp}{1 + kp} \ , \tag{23}$$

where q_m is usually considered the amount of gas required to form a monolayer and k is a constant. In using Equation (23) to model surface adsorption on molecular sieves, Garg and Ruthven (1973a) note that q_m and k should both be regarded as empirical constants.

The three dependent variables have now all been related to the one variable of the gas pressure in the bed. The equations for c and v, Equation (2), p. 11, and Equation (8), p. 13, can now be substituted into the material balance, Equation (1), p. 9:

$$\frac{\varepsilon}{RT_b}\frac{\partial p}{\partial t} + \rho_B \frac{\partial \bar{q}}{\partial t} - \frac{\varepsilon\kappa}{RT_b}\frac{\partial^2 p}{\partial z^2} = 0 \ , \tag{24}$$

where T_b is, specifically, the temperature of the sorbent bed. This equation along with Equations (22) and (23),

$$\frac{\partial \bar{q}}{\partial t} = \frac{15D}{s^2}(q_s - \bar{q}) \tag{25}$$

and

$$q_s = \frac{q_m k p}{1 + kp} \ , \tag{26}$$

form the set that must be solved to model mass transfer in the bed in terms of pressure and solid loading.

Solution of this set requires appropriate initial and boundary conditions. The initial conditions are simply that

$$\text{At } t = 0, \text{ for all } z, \ p = 0 \text{ and } \bar{q} = 0 \ . \tag{27}$$

The fluid-phase boundary condition at the bottom of the bed is equally straightforward:

$$\text{At } z = L, \ t > 0, \ \frac{\partial p}{\partial z} = 0 \ . \tag{28}$$

The condition at the top of the bed is more complicated. As seen from Figure 1, p. 10, gas flows into the void above the bed at a constant rate; however, the flux into the bed itself changes with time.

To account for the changing boundary condition, begin with a material balance around the void space above the sorbent bed:

$$I - FA = \frac{V}{RT_a} \frac{\partial p}{\partial t} , \tag{29}$$

where

I = constant mass flow into void,

F = mass flux into bed,

A = cross-sectional area of bed,

V = volume of void space, and

T_a = temperature of the void volume.

The first term accounts for the constant flow of gas into the void above the bed, the second for the flow of gas from the void into the bed, and the third for the accumulation of gas in the void in terms of the resultant pressure increase.

The axial flux within the bed, based on the total cross-sectional area, is given by

$$F = \varepsilon v c . \tag{30}$$

As derived previously for molecular flow,

$$v = - \frac{\kappa}{p} \frac{\partial p}{\partial z} . \tag{31}$$

Eliminating v by Equation (31) and c by Equation (2), p. 11, Equation (30) yields

$$F = -\frac{\varepsilon\kappa}{RT_b}\frac{\partial p}{\partial z} . \tag{32}$$

Using Equation (32) in Equation (29), the boundary condition at the top of the bed is

$$I + \frac{\varepsilon\kappa A}{RT_b}\frac{\partial p}{\partial z}\bigg|_{z=0} = \frac{V}{RT_a}\frac{\partial p}{\partial t}\bigg|_{z=0} . \tag{33}$$

Equations (24) through (28) and Equation (33) form the complete set of equations to be solved. They will be solved by numerical methods.

IV. NUMERICAL SOLUTION OF THEORETICAL MODEL

Modeling the mass transfer phenomena in the vacuum sorption pump requires obtaining a numerical solution to the two partial differential equations

$$\frac{\varepsilon}{RT_b}\frac{\partial p}{\partial t} + \rho_B \frac{\partial \bar{q}}{\partial t} - \frac{\varepsilon\kappa}{RT_b}\frac{\partial^2 p}{\partial z^2} = 0 \tag{34}$$

and

$$\frac{\partial \bar{q}}{\partial t} = \frac{15D}{S^2}(q_S - \bar{q}) \ , \tag{35}$$

which are coupled by the relationship

$$q_S = q_m \frac{kp}{1 + kp} \tag{36}$$

and bounded by

$$\bar{q} = 0 \text{ and } p = 0 \text{ for } t = 0 \text{ and all } z, \tag{37}$$

$$\frac{\partial p}{\partial z} = 0 \text{ for } t > 0 \text{ and } z = L, \text{ and} \tag{38}$$

$$I + \frac{\varepsilon\kappa A}{RT_b}\frac{\partial p}{\partial z} = \frac{V}{RT_a}\frac{\partial p}{\partial t} \text{ for } t > 0 \text{ and } z = 0 \ . \tag{39}$$

The steps involved in obtaining a solution include

1. Expressing the equations in dimensionless form,
2. Selecting a solution method,
3. Obtaining solutions for various sets of parameters, and
4. Assessing the validity of the solution.

The first two steps are detailed below; the latter two are discussed in subsequent chapters.

The first step in obtaining a general solution is recasting the equations in terms of dimensionless variables. The dimensionless variables for time, bed position, pressure, and solid loading are defined by

$$\Theta = \frac{\kappa t}{L^2} , \tag{40}$$

$$Z = \frac{z}{L} , \tag{41}$$

$$x = \frac{p}{p_R} , \text{ and} \tag{42}$$

$$\bar{y} = \frac{\rho_B R T_b \bar{q}}{p_R \epsilon} , \tag{43}$$

respectively, where p_R is a reference pressure. In dimensionless terms, Equations (34) through (39) become

$$\frac{\partial x}{\partial \Theta} + \frac{\partial \bar{y}}{\partial \theta} - \frac{\partial^2 x}{\partial Z^2} = 0 , \tag{44}$$

$$\frac{\partial \overline{y}}{\partial \Theta} = \frac{15D}{S^2} (y_S - \overline{y}) , \tag{45}$$

$$y_S = \frac{\rho_B R T_b}{p_R \varepsilon} \left(\frac{q_m k p_R x}{1 + k p_R x} \right) , \tag{46}$$

$$\overline{y} = 0 \text{ and } x = 0 \text{ for } \Theta = 0 \text{ and } 0 \leq Z \leq 1 , \tag{47}$$

$$\frac{\partial x}{\partial Z} = 0 \text{ for } \Theta > 0 \text{ and } Z = 1, \text{ and} \tag{48}$$

$$I + \frac{\varepsilon \kappa A p_R}{R T_b L} \frac{\partial x}{\partial Z} = \frac{V p_R^{\kappa}}{R T_a L^2} \frac{\partial x}{\partial \Theta} \text{ for } \Theta > 0 \text{ and } Z = 0 . \tag{49}$$

The finite difference method was chosen for solving the equation set because the method is easily implemented and has proven successful in solving similar problems (Garg and Ruthven, 1973b). The basic idea is to approximate the partial derivatives by the finite changes in the dependent variables resulting from differential changes in the independent variables. The solution yields values of the dependent variables at a set of discrete points.

Consider dividing the bed into N increments, or N+1 discrete points, positioned evenly from Z = 0 to Z = 1. The increment length, ΔZ, is simply 1/N, and the N+1 points can be located by $Z_i = i(\Delta Z)$, where i ranges from 0 to N. Similarly, by specifying a time increment $\Delta\Theta$, any time Θ can be expressed as $\Theta_j = j(\Delta\Theta)$, were j ranges from 0. The first derivatives are approximated by forward-difference formulas; that is,

$$\frac{\partial x}{\partial \Theta} = \frac{x_i^{j+1} - x_i^{j}}{\Delta \Theta} , \tag{50}$$

$$\frac{\partial \bar{y}}{\partial \Theta} = \frac{\bar{y}_i^{j+1} - \bar{y}_i^{j}}{\Delta \Theta} , \tag{51}$$

and

$$\frac{\partial x}{\partial Z} = \frac{x_{i+1}^{j+1} - x_i^{j+1}}{\Delta Z} . \tag{52}$$

For the second derivative term, a Crank-Nicholson implicit approximation is used:

$$\frac{\partial^2 x}{\partial Z^2} = \frac{(x_{i-1}^{j+1} - 2x_i^{j+1} + x_{i+1}^{j+1}) + (x_{i-1}^{j} - 2x_i^{j} + x_{i+1}^{j})}{2(\Delta Z)^2} . \tag{53}$$

Again, the i subscript refers to the position variable and the j superscript to the time variable. The expression x_i^{j+1}, for example, is shorthand for $x(\Theta_{j+1}, Z_i)$. In each term, the values of x and $\bar{y}$ at Θ_j are known. From these known conditions, x and $\bar{y}$ at Θ_{j+1} will be determined.

Using the finite difference approximations for the partial derivatives in Equations (44) through (46), one obtains

$$\frac{x_i^{j+1} - x_i^{j}}{\Delta \Theta} + \frac{\bar{y}_i^{j+1} - \bar{y}_i^{j}}{\Delta \Theta}$$

$$- \frac{(x_{i-1}^{j+1} - 2x_i^{j+1} + x_{i+1}^{j+1}) + (x_{i-1}^{j} - 2x_i^{j} + x_{i+1}^{j})}{2(\Delta Z)^2} = 0 \tag{54}$$

and

$$\frac{\bar{y}_i^{j+1} - \bar{y}_i^{j}}{\Delta\Theta} = \frac{15D}{S^2}\left[\frac{\rho_B R T_b}{p_R \varepsilon}\left(\frac{q_m k p_R x_i^{j+1}}{1 + k p_R x_i^{j+1}}\right) - \bar{y}_i^{j+1}\right] , \qquad (55)$$

where Equation (46) has been used to eliminate y_S from Equation (45). Equation (54) is now solved for the unknown values of x and Equation (55) for the unknown value of $\bar{y}$:

$$x_{i-1}^{j+1} - \left(2 + \frac{2(\Delta Z)^2}{\Delta\Theta}\right) x_i^{j+1} + x_{i+1}^{j+1} = \frac{2(\Delta Z)^2}{\Delta\Theta}\left(\bar{y}_i^{j+1} - \bar{y}_i^{j} - x_i^{j}\right)$$

$$- \left(x_{i-1}^{j} - 2x_i^{j} + x_{i+1}^{j}\right) , \qquad (56)$$

and

$$\bar{y}_i^{j+1} = \frac{\bar{y}_i^{j} + \left(\frac{15D\Delta\Theta}{S^2}\right)\left(\frac{\rho_B R T_b}{p_R \varepsilon}\right)\left(\frac{q_m k p_R x_i^{j+1}}{1 + k p_R x_i^{j+1}}\right)}{\left(1 + \frac{15D\Delta\Theta}{S^2}\right)} . \qquad (57)$$

As will be explained, at Θ_{j+1} the terms on the right side of Equations (56) and (57) are considered known and are used to calculate the unknowns on the left.

For any Θ_j and Θ_{j+1}, the material balance equation, Equation (56), can be used to obtain N-1 equations in the N+1 unknowns $x_0, x_1, \ldots, x_N$. Solving for the unknowns requires two additional equations; these

are provided by the boundary conditions. In finite difference notation, the boundary conditions, Equations (48) and (49), are

$$\frac{x_N^{j+1} - x_{N-1}^{j+1}}{\Delta Z} = 0 \tag{58}$$

and

$$I + \frac{\varepsilon \kappa A p_R}{RT_b L} \frac{(x_1^{j+1} - x_0^{j+1})}{\Delta Z} = \frac{V p_R \kappa}{RT_a L^2} \frac{(x_0^{j+1} - x_0^{j})}{\Delta \Theta} . \tag{59}$$

Equation (59) is solved for x_0^{j+1} and used to eliminate x_0^{j+1} from the material balance written for x_0, x_1, and x_2. Similarly, Equation (58) is used to eliminate x_N from Equation (56) written for x_{N-2}, x_{N-1}, and x_N. The result is a set of N-1 equations in N-1 unknowns that can be written in matrix notation as shown in Figure 2.

A problem arises at this point because the $\bar{y}_i^{j+1}$ terms on the right side of Equation (56) are actually not known. This is resolved by using a backward-difference formula for $\partial \bar{y}/\partial t$; that is,

$$\frac{\partial \bar{y}}{\partial t} = \frac{\bar{y}_i^{j} - \bar{y}_i^{j-1}}{\Delta \Theta} . \tag{60}$$

Figure 2 uses this formula in its notation for the right-side terms.

The algorithm used to obtain the dimensionless pressure and solid loading profiles at discrete times can now be summarized.

$$\begin{bmatrix} \alpha & 1 & & & & & \\ 1 & \beta & 1 & & & & \\ & 1 & \beta & 1 & & & \\ & & \cdot & & & & \\ & & & \cdot & & & \\ & & & & \cdot & & \\ & & & & 1 & \beta & 1 \\ & & & & & 1 & \gamma \end{bmatrix} \begin{bmatrix} x_1^{j+1} \\ x_2^{j+1} \\ x_3^{j+1} \\ \cdot \\ \cdot \\ \cdot \\ x_{N-2}^{j+1} \\ x_{N-1}^{j+1} \end{bmatrix} = \begin{bmatrix} R_1 \\ R_2 \\ R_3 \\ \cdot \\ \cdot \\ \cdot \\ R_{N-2} \\ R_{N-1} \end{bmatrix},$$

where

$$\alpha = \frac{\left(\frac{\epsilon A L T_a}{V T_b}\right)\left(\frac{\Delta\theta}{\Delta Z}\right)}{1 + \left(\frac{\epsilon A L T_a}{V T_b}\right)\left(\frac{\Delta\theta}{\Delta Z}\right)} - 2 - \frac{2(\Delta Z)^2}{\Delta\theta},$$

$$\beta = -2 - \frac{2(\Delta Z)^2}{\Delta\theta},$$

$$\gamma = -1 - \frac{2(\Delta Z)^2}{\Delta\theta},$$

$$R_1 = \frac{2(\Delta Z^2)}{\Delta\theta}\left(y_1^j - y_1^{j-1} - x_1^j\right) - \left[\frac{x_0^j + \frac{I R T_a L^2}{V p_R \kappa}}{1 + \left(\frac{\epsilon A L T_a}{V T_b}\right)\left(\frac{\Delta\theta}{\Delta Z}\right)}\right] - \left(x_0^j - 2x_1^j + x_2^j\right), \text{ and}$$

$$R_2, R_3, \ldots, R_i, \ldots, R_{N-1} = \frac{2(\Delta Z)^2}{\Delta\theta}\left(\underline{y}_i^j - \underline{y}_i^{j-1} - x_i^j\right) - \left(x_{i-1}^j - 2x_i^j + x_{i+1}^j\right).$$

Figure 2. Simultaneous set of material balance equations written for N-1 points in dimensionless sorption pump.

1. Let x_i^j and $\overline{y}_i^j$ equal 0 for all $0 \leq i \leq N$ at $j = 0$.
2. Use Equations (56), (58), and (59) to obtain N-1 equations in the N-1 unknowns $x_1, x_2, \ldots, x_{N-1}$ at $(j+1) = 1$.
3. Solve the N-1 equations. The method used here is Gaussian elimination (Hornbeck, 1975).
4. From Equations (58) and (59), obtain x_0 and x_N.
5. Calculate the solid loading profile at $(j+1) = 1$ using Equation (57) for $0 \leq i \leq N$.
6. Repeat steps 2 through 5 setting j equal to the previous value of $(j+1)$ until the desired value of j, or $\Theta_j = j(\Delta\Theta)$, is reached.

A FORTRAN program that employs this solution method for a given set of parameters (ε, T_b, ρ_B, κ, q_m, D, S, k, A, V, and T_a) is given in Appendix A.

V. EXPERIMENTAL PROGRAM

Materials and Apparatus

A schematic of the experimental system is shown in Figure 3. The system was designed by P. W. Fisher at the Oak Ridge National Laboratory. Gas flows from a pressurized cylinder through either of two stainless steel leaks connected in parallel; the leaks were manufactured by Huntington Mechanical Laboratories. The leak rate through the orifices is determined by the pressure maintained in the feed line. For nitrogen, leak rates of 2.7×10^{-9} to 3.6×10^{-8} mol/s result as the pressure is increased from 10 to 100 psig; for carbon dioxide, the corresponding range is 3.0×10^{-9} to 3.9×10^{-8} mol/s.

From the leaks, gas is directed to one of two bed holders. The holder shown on the left was used in preliminary experiments but not in the runs reported here. When directed to the right, gas flows both to the bed section and to tubing to which five differential pressure cells and two absolute pressure sensors are attached. All of the gauges were manufactured by MKS Instruments, Inc. The five differential pressure transducers are type 223BH; the two absolute gauges are models 310CHS and 310CH. The bed section is a 21-cm piece of 0.77-cm-ID stainless steel tubing. The ends are covered with fine-mesh screen to prevent the escape of molecular sieves from the bed. Five 0.16-cm-OD tubes connect the holder to the differential pressure cells to allow measurement of the pressure drop across the bed at various points.

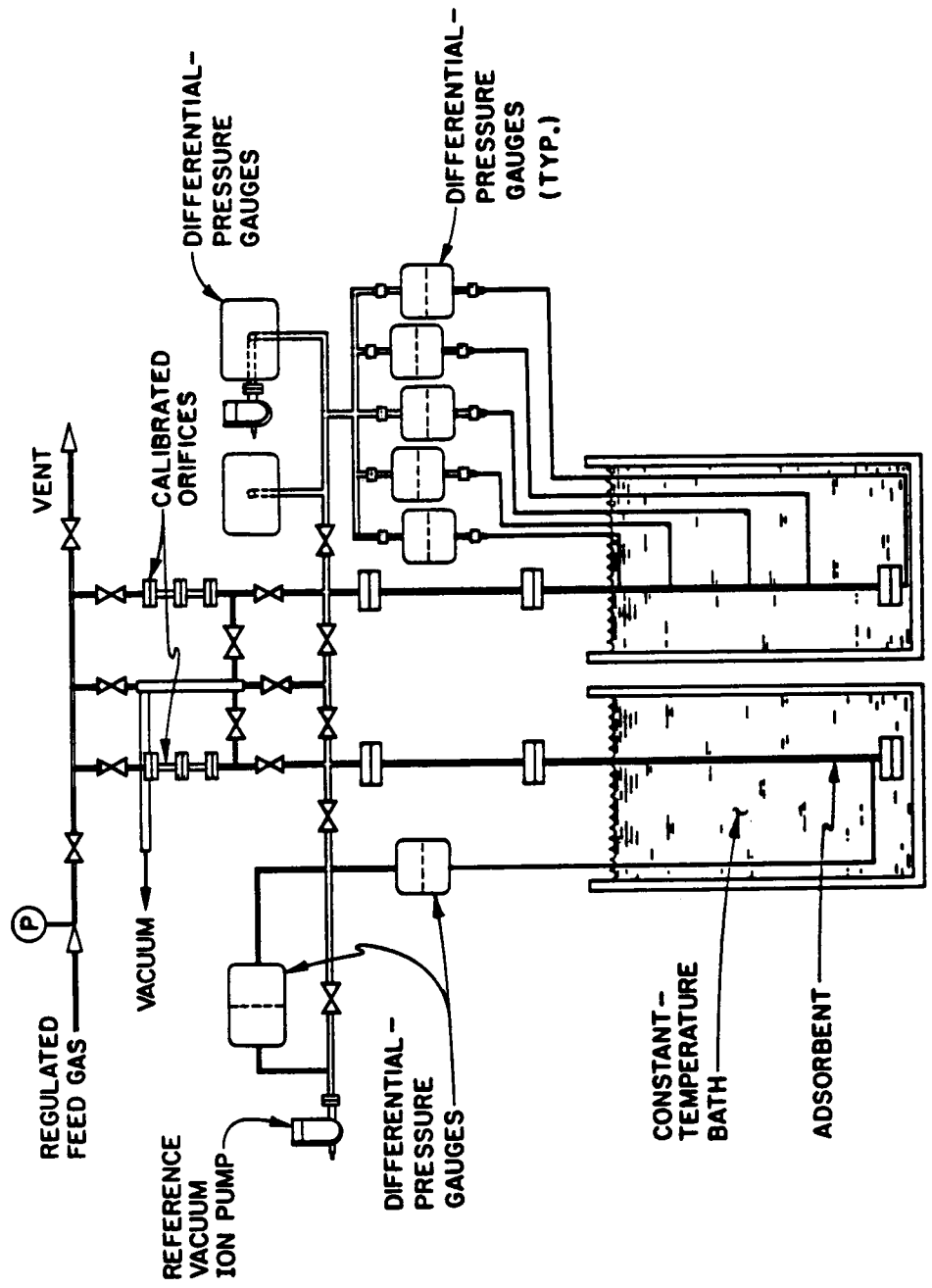

Figure 3. Schematic of experimental sorption pumping apparatus.

The seven capacitance manometers are connected to electronics and digital-readout units that feed to an Apple-II-plus microcomputer. For the absolute pressure gauges, the electronics units are MKS types 170M-27D and 170M-27E, and the digital-readout units are both model 170M-6B. The combined unit for the differential transducers is MKS type PDR-5B. Computer code was developed to record the absolute pressure in the system above the bed as well as the pressure drops across the bed at regular time increments. A vacuum of about 10^{-3} torr can be maintained in this system.

The sorbent was a type 4A artificial zeolite molecular sieve obtained from the Davison Chemical Division of W. R. Grace and Co. A batch of 14-to-40-mesh spherical sieves was separated into various sized cuts using wire mesh sieves. In two series of runs, particles with diameters ranging from 0.50 to 0.60 mm (30 to 35 mesh) and from 0.60 to 0.85 mm (20 to 30 mesh) were used.

Although the sieves are described as spherical, in a given sample pellets may be round, oblong, or broken into irregular shapes. Electron microscope photographs of a sample of crushed pellets, Figure 4, illustrates well the makeup of the particles. Zeolite crystals of various sizes and shapes are held together by an inert binder. From such photographs, determinations were made of the crystal size distribution; the results for Sample A shown in Figure 4 are listed in Table 1.

ORNL PHOTO 3778-84

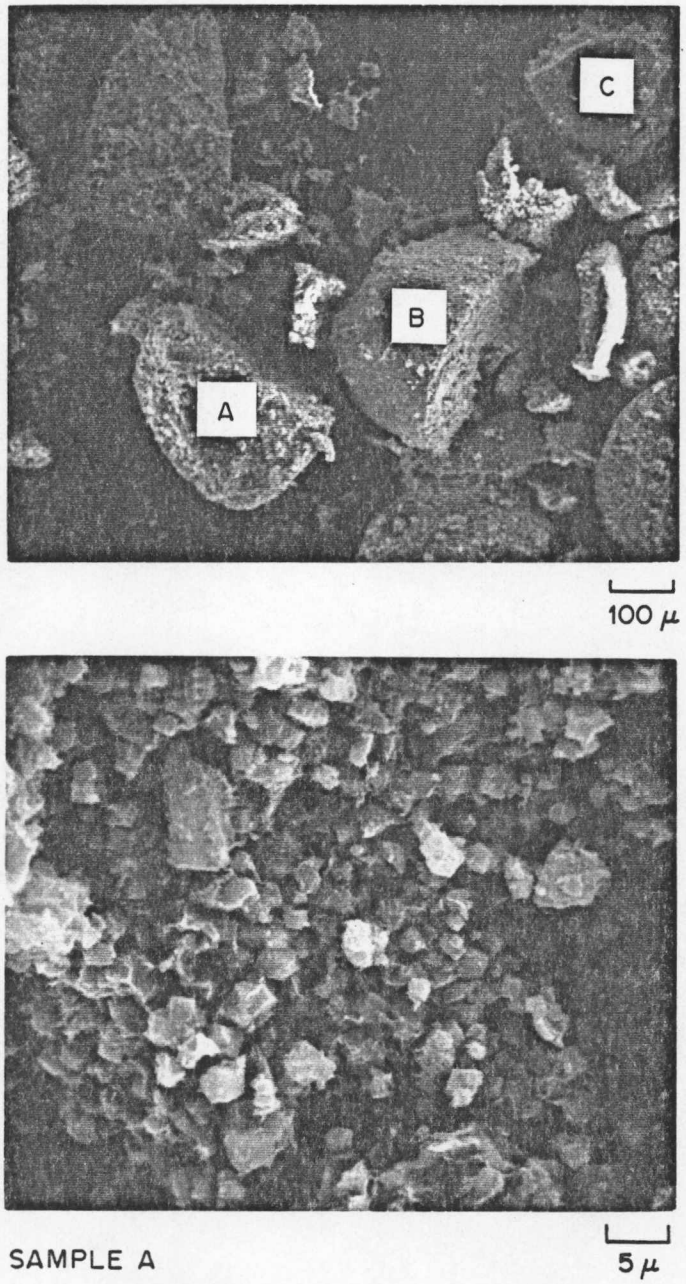

Figure 4. Electron microscope photographs of crushed Davison 4A zeolite molecular sieves.

Table 1. Crystal size distribution in sample of Davison 4A molecular sieves

Particle size (μm)	Number of particles	Particle size (μm)	Number of particles
<0.44	24	2.86	21
0.51	20	3.00	9
0.65	16	3.13	11
0.79	26	3.27	2
0.93	20	3.41	2
1.06	18	3.55	11
1.20	27	3.69	2
1.34	23	3.82	5
1.48	33	3.96	5
1.62	31	4.10	3
1.78	35	4.38	2
1.89	32	4.51	1
2.03	39	4.93	1
2.17	29	5.20	1
2.31	24	5.48	1
2.44	20	6.03	1
2.58	11	6.19	1
2.72	14	6.86	1

Procedure

The experimental objective was to obtain pressure measurements as gas was leaked into the evacuated system and pumped into the bed. An experimental run included the following steps:

1. Bed preparation.
2. Pumpdown of the system.
3. Data collection.
4. System recovery.

Before a series of runs, molecular sieves of a specified type and size were dried by heating at 300°C, weighed, and loaded into the bed holder to the desired depth.

To begin a run, the bed section was heated at 300°C for about 24 h to ensure that the sieves were clean and dry; the system was rough pumped during this time using an external pump. The bed was then cooled to room temperature and submerged in a liquid coolant. Finally, the system was isolated from the external pump.

After about 1 h, when the system pressure steadied (at about 10^{-3} torr), the valve from the gas cylinder to the bed was opened and data collection begun. Data were collected until the bed was saturated with gas, as indicated by a sharp increase in system pressure and decrease in pressure drop across the bed, or until the system pressure reached 1 torr. The system was then returned to room temperature using the external pump to evacuate the desorbing gas.

Difficulties

One difficulty was in obtaining accurate pressure measurements using the computer system for data collection. As described before, the seven MKS capacitance manometers connect to digital-readout electronics boards. The absolute error in the measurements printed out on the boards should be small. For the manometers, the manufacturer's literature lists errors of <0.25% of full scale (±1 torr) for the small gauges used for the differential pressure measurements and <0.05% of full scale (1 torr) for the gauges used to measure the absolute pressure above the bed. The electronics units are connected next to an analog-to-digital converter board manufactured by Interactive Microware, Inc. This in turn is connected to the Apple-II-plus computer.

Comparison of the pressure measurements recorded by the computer with those given by the electronics units indicates that there is random noise in the signals received by the computer. The magnitude of the error depends on the gain used in converting the analog signal to a pressure measurement. For the five differential pressure readings, the difference between the board values and computer values is about ±0.002 torr. For the two absolute pressure readings, the difference ranges to ±0.005 torr. The errors are potentially significant only during the first part of an experimental run, when the differential and absolute pressures are of the order 10^{-2} torr. As shown in the next section, the experimental runs are very reproducible; thus it was concluded that the random errors did not adversely affect the overall results.

Another potential problem in measuring pressures at low temperatures results from a phenomenon called thermal transpiration. For two chambers at different temperatures connected by a tube or orifice, the condition that holds at equilibrium is that the flux from one chamber equals that from the other. For molecular flow, theory predicts (O'Hanlon, 1980, p. 20) that the pressures in the chambers are related by

$$\frac{P_1}{P_2} = \left(\frac{T_1}{T_2}\right)^{1/2}. \tag{61}$$

Thus in trying to measure the pressure (P_1) at a low temperature (T_1) using a gauge at ambient temperature (T_2), Equation (61) indicates that the pressure at the gauge (P_2) will differ from the actual low-temperature pressure by the given ratio. The ratio of P_1 to P_2 is referred to as the thermal transpiration ratio, and the phenomenon that temperature gradients cause pressure gradients is called thermal transpiration.

Experimental work has shown that the predicted ratio is approached only under limited conditions (Siu, 1973; Hobson, 1969; Hobson, Edmonds, and Verreault, 1963; Podgurski and Davis, 1961). The ratio P_1/P_2 ranges from the theoretical value to 1 and depends on the pressures and temperatures in the system, the gas, and the physical properties of the tubing connecting the two chambers. Most significantly, the theoretical ratio is approached only at extremely low pressures, or, in other words, only when the mean free path of the gas molecules is much greater than the tube diameter.

In the work conducted here, potential for this problem occurred in trying to measure the pressure profile along the bed. Five 0.16-cm-OD tubes lead from the cooled bed to differential pressure gauges at ambient temperature. If thermal transpiration occurred along the connecting tubes, then the recorded differential pressures would be inaccurate. Thus the attempt was made to determine what correction, if any, was needed to account for this phenomenon.

Consider again the experimental apparatus shown in Figure 3, p. 30. A test was conducted in which there were no sieves in the bed section. The empty system was evacuated to a pressure of about 10^{-3} torr, and the bed section and five tubes leading to the differential pressure gauges were cooled to 77 K with a liquid nitrogen bath as shown. Nitrogen was leaked into the empty system at a rate of 5.3 x 10^{-9} mol/s until the pressure measured above the section reached 1 torr. Because of the relatively large diameter (0.77 cm ID) of the tubing and the very low flow rate, pressure drop through the tubing should have been negligible and the pressure uniform throughout the system at any time.

For no thermal transpiration along the small tubes, the pressure at the gauge end would equal the pressure at the cold end and throughout the system. The five gauges would record no pressure difference in the pressures above and in the cold section. However, if the temperature gradient does cause a pressure gradient, then the pressure at the gauge would be greater than the pressure at the cold end. In this case, the gauges would indicate that the pressure in the cold section was greater than that above. The fact that the differential pressure

measurements, which were about the same for all five gauges, were indeed positive relative to the absolute pressure measurements indicates that thermal transpiration did occur.

To obtain values of P_2, the pressure at the gauge end of the tube, the differential pressure measurements were added to the pressures measured above the bed using the two absolute gauges. The pressure above the bed was assumed to be the actual pressure in the cold section, P_1. Comparing P_1 to P_2 at various values of P_2 yielded values of the thermal transpiration ratio.

Figure 5 shows that the ratio P_1/P_2 ranged from 0.80 to 1 as P_2 ranged from 6×10^{-2} to 1 torr. This finding agrees well with the data of Hobson (1969); Hobson, Edmonds, and Verreault (1963); and Podgurski and Davis (1961). Their results show that the theoretical value of 0.51 for T_1 of 77 K and T_2 of 300 K is approached only for P_2 less than about 10^{-2} torr and that the ratio jumps sharply to 1 as the pressure increases to 10^{-1} torr. In subsequent tests in which T_1 was 198 K, the ratio was essentially equal to 1.

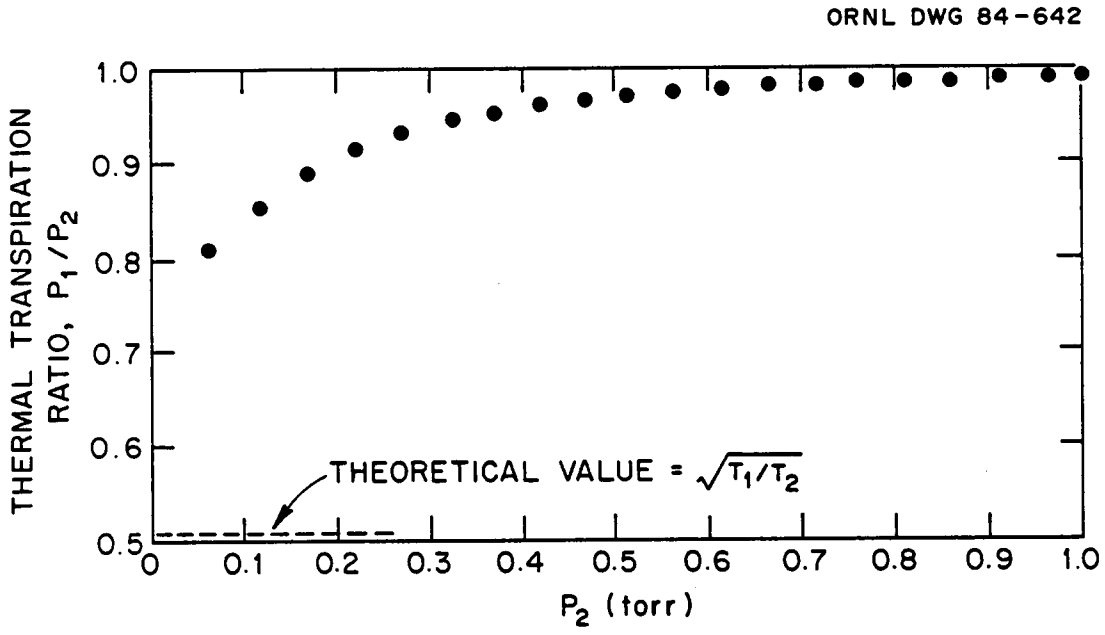

Figure 5. Experimentally estimated values of the thermal transpiration ratio for P_1 at T_1 = 77 K and P_2 at T_2 = 300 K.

VI. RESULTS

Presentation

Four series of experimental runs were conducted with nitrogen and carbon dioxide in which the major variables were the flow rate of gas into the system and the sorbent particle size. Figures 6 through 13 present the results of runs with N_2 in which the leak rates were 1.2, 2.5, and 3.0 x 10^{-8} mol/s and the average particle diameter was either 0.55 or 0.72 mm; the bed was cooled with liquid N_2 to 77 K. Figures 14 through 21 show data obtained sorbing CO_2 on similar beds at flow rates of 3.3 and 3.9 x 10^{-8} mol/s and a bed temperature of 198 K maintained using dry ice in acetone. To illustrate the reproducibility of the data, the results of two identical runs are compared in Figure 22. Table 2 summarizes the run conditions. Appendix B contains tables of the experimental data.

Figures 6 and 7 plot the experimental values of the pressure in the ambient-temperature void above the sorbent bed as a function of time for the six N_2 runs. Figure 6 compares the three runs conducted using the 0.55-mm sieves and Figure 7 the three runs using the 0.72-mm sieves. The pressure-vs-time profiles are similar for all the runs. The first portion shows a linear increase in the void pressure as gas is pumped into the bed at a constant rate. As the bed begins to become saturated, flow into the bed decreases and the pressure increases rapidly.

The pressure profiles for the runs conducted with N_2 are again shown in Figures 8 through 13 along with measurements of the absolute

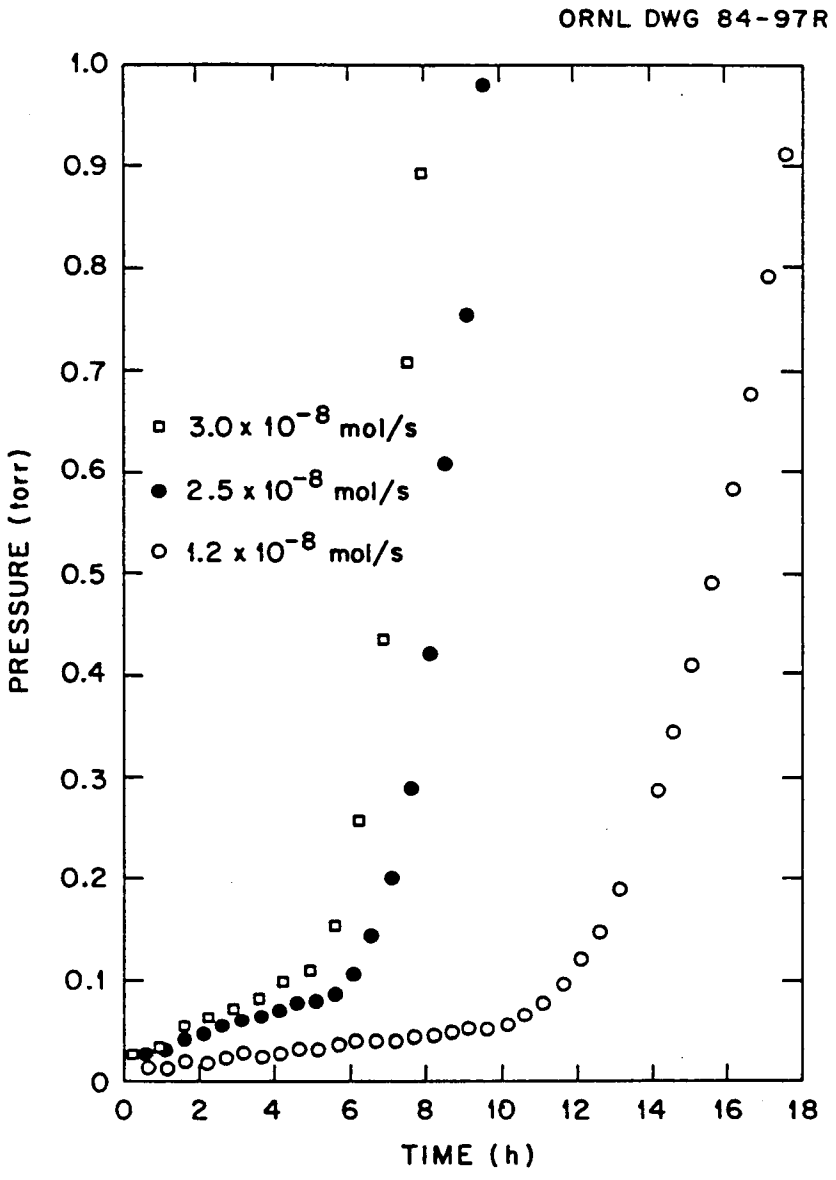

Figure 6. Sorption pumping of N_2 on 5.06 g of 0.55-mm Davison 4A molecular sieves at 77 K.

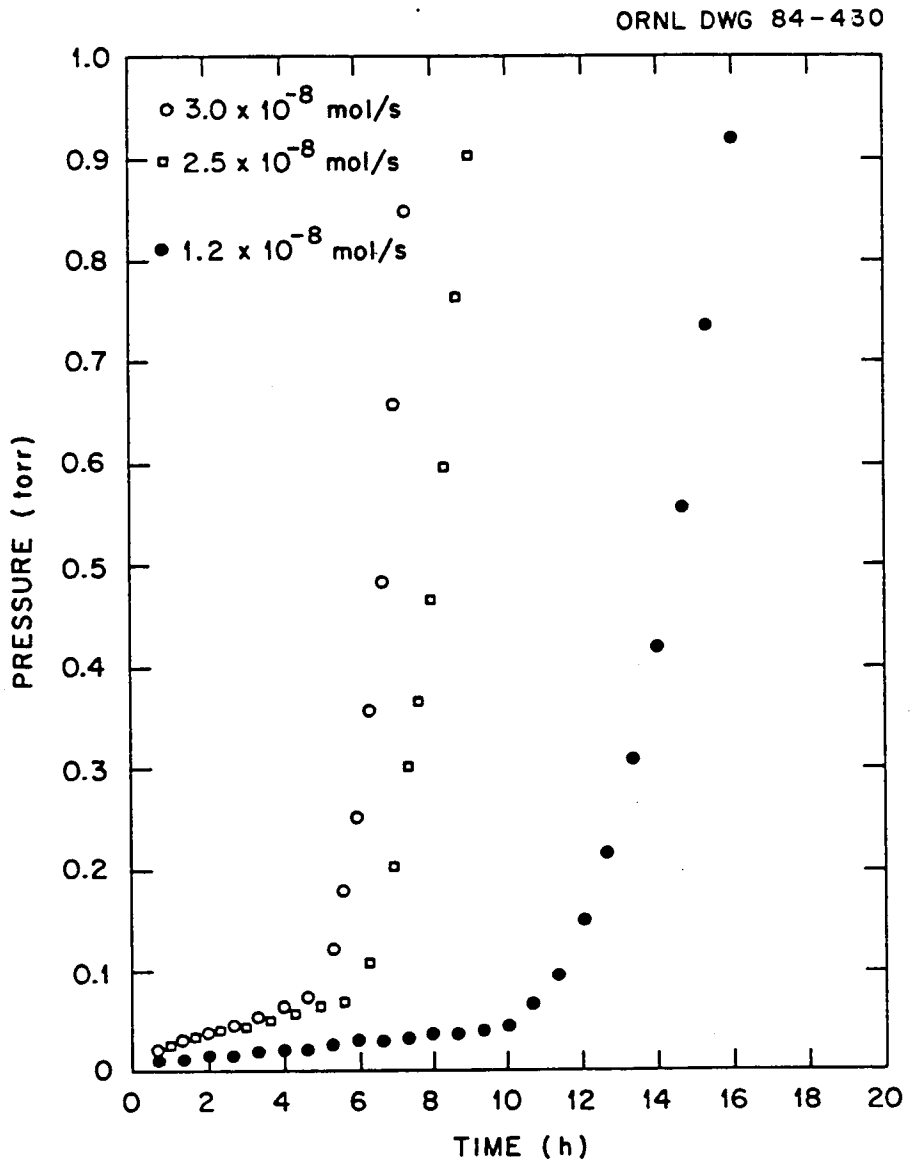

Figure 7. Sorption pumping of N_2 on 4.12 g of 0.72-mm Davison 4A molecular sieves at 77 K.

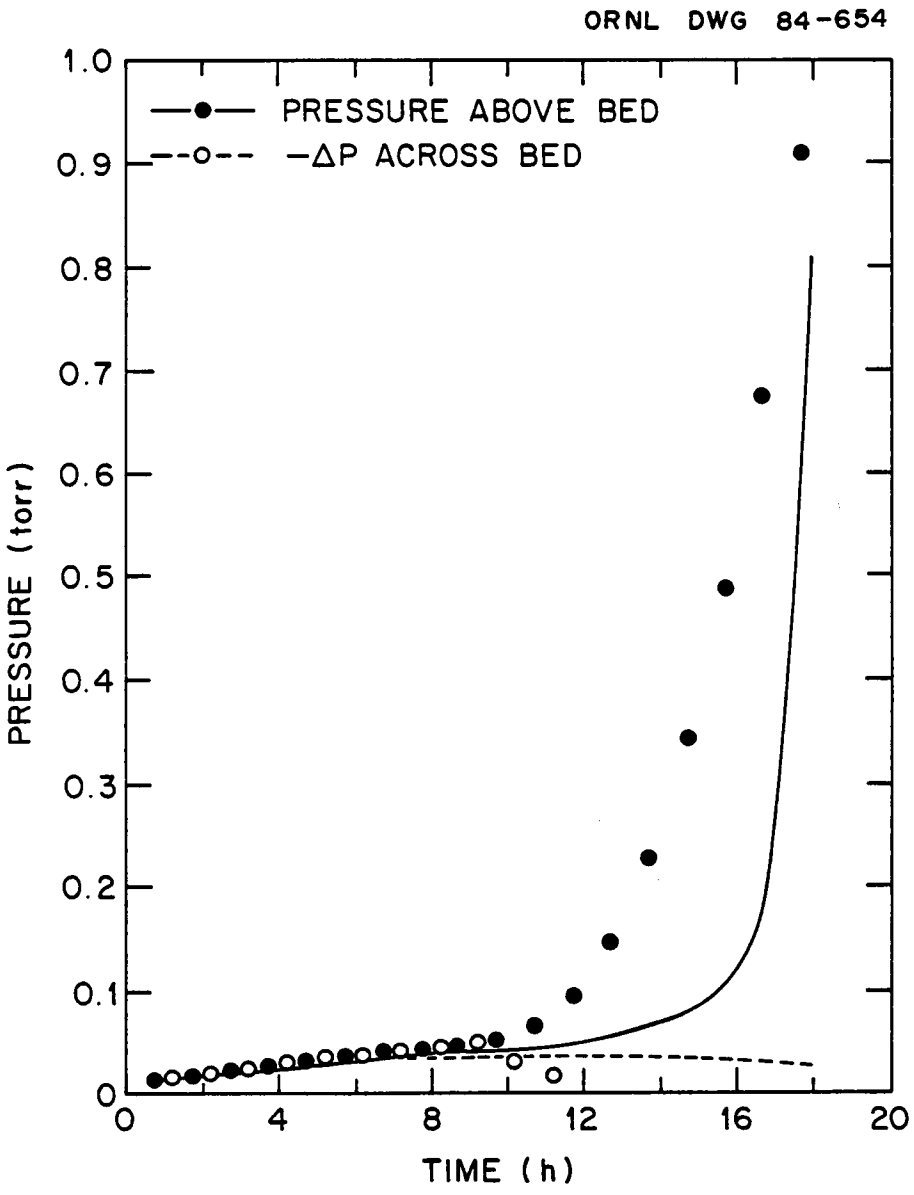

Figure 8. Comparison of experimental pressure and pressure drop data with theoretical curves for Run 206. Table 2, p. 58, details experimental conditions; Table 3, p. 60, lists parameters used to calculate theoretical curves.

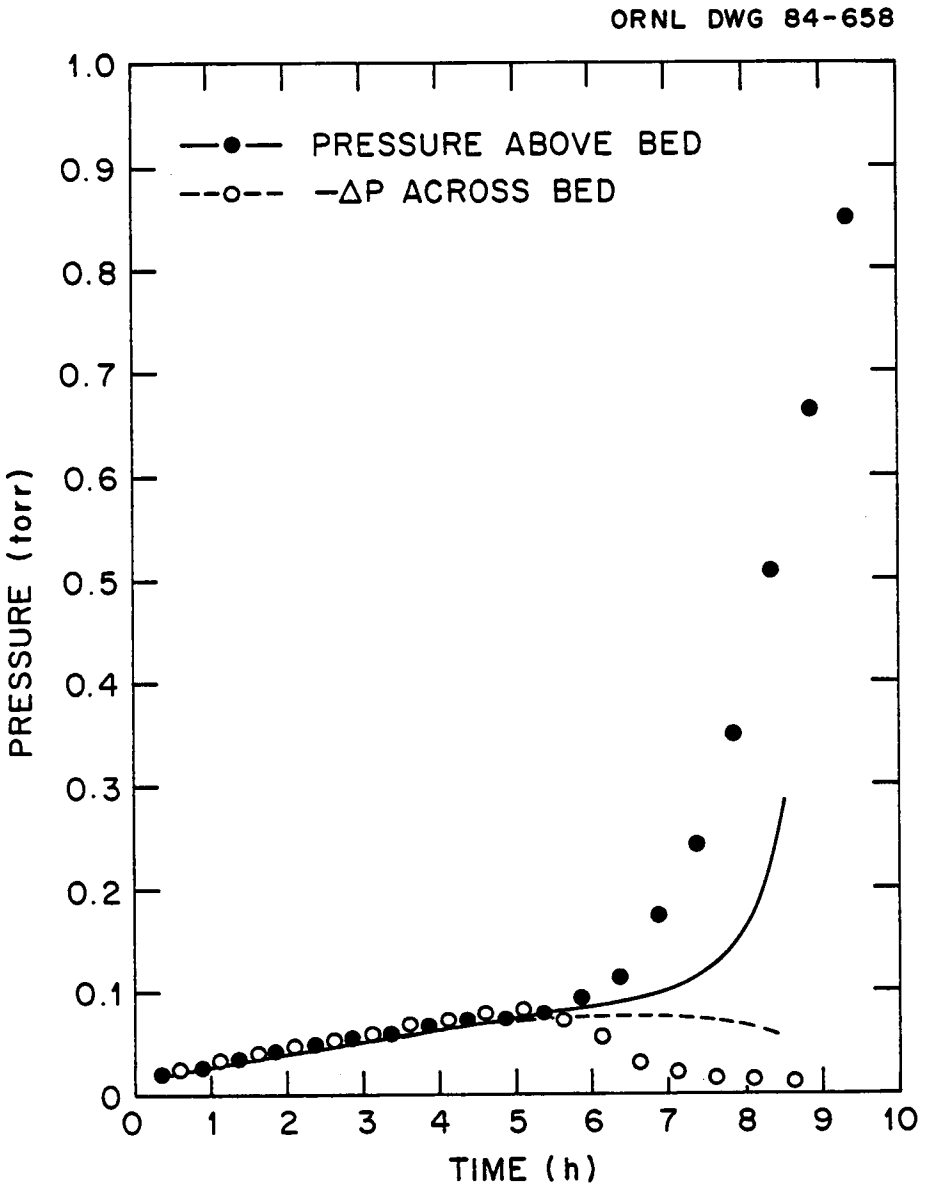

Figure 9. Comparison of experimental pressure and pressure drop data with theoretical curves for Run 205. Table 2, p. 58, details experimental conditions; Table 3, p. 60, lists parameters used to calculate theoretical curves.

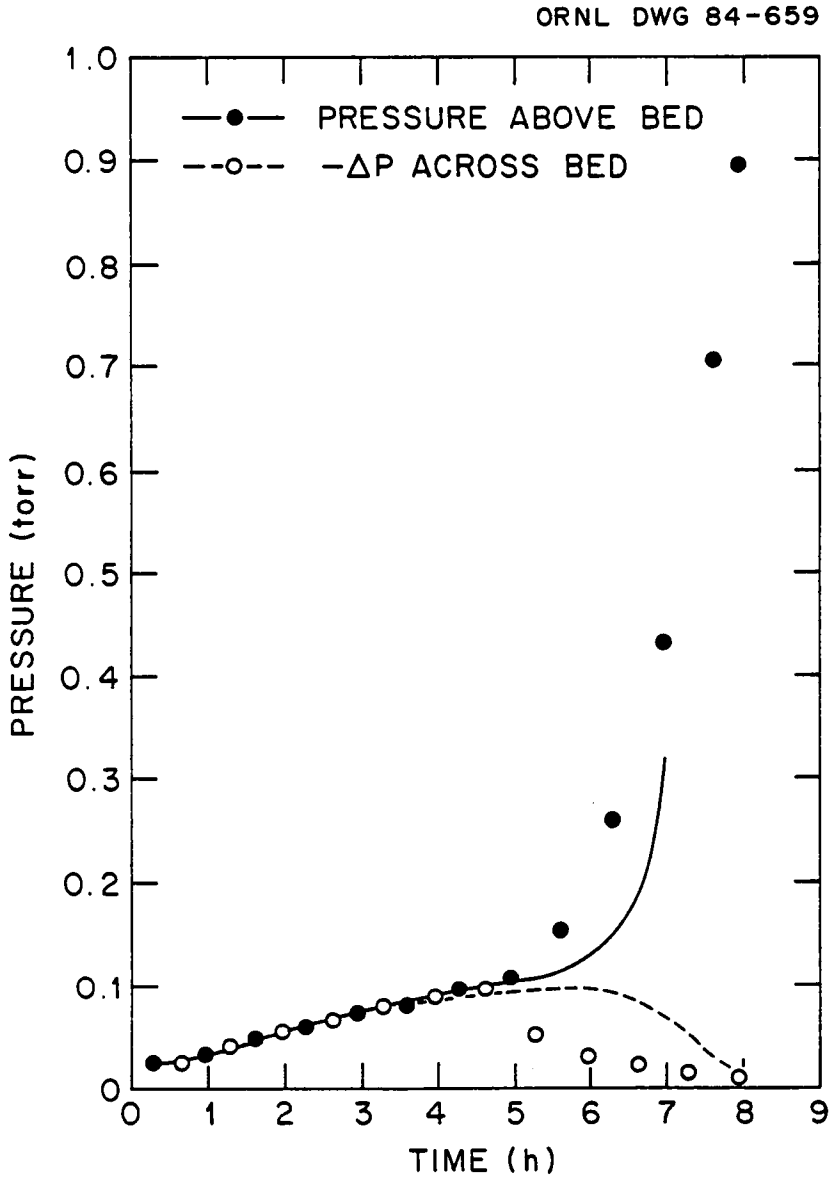

Figure 10. Comparison of experimental pressure and pressure drop data with theoretical curves for Run 208. Table 2, p. 58, details experimental conditions; Table 3, p. 60, lists parameters used to calculate theoretical curves.

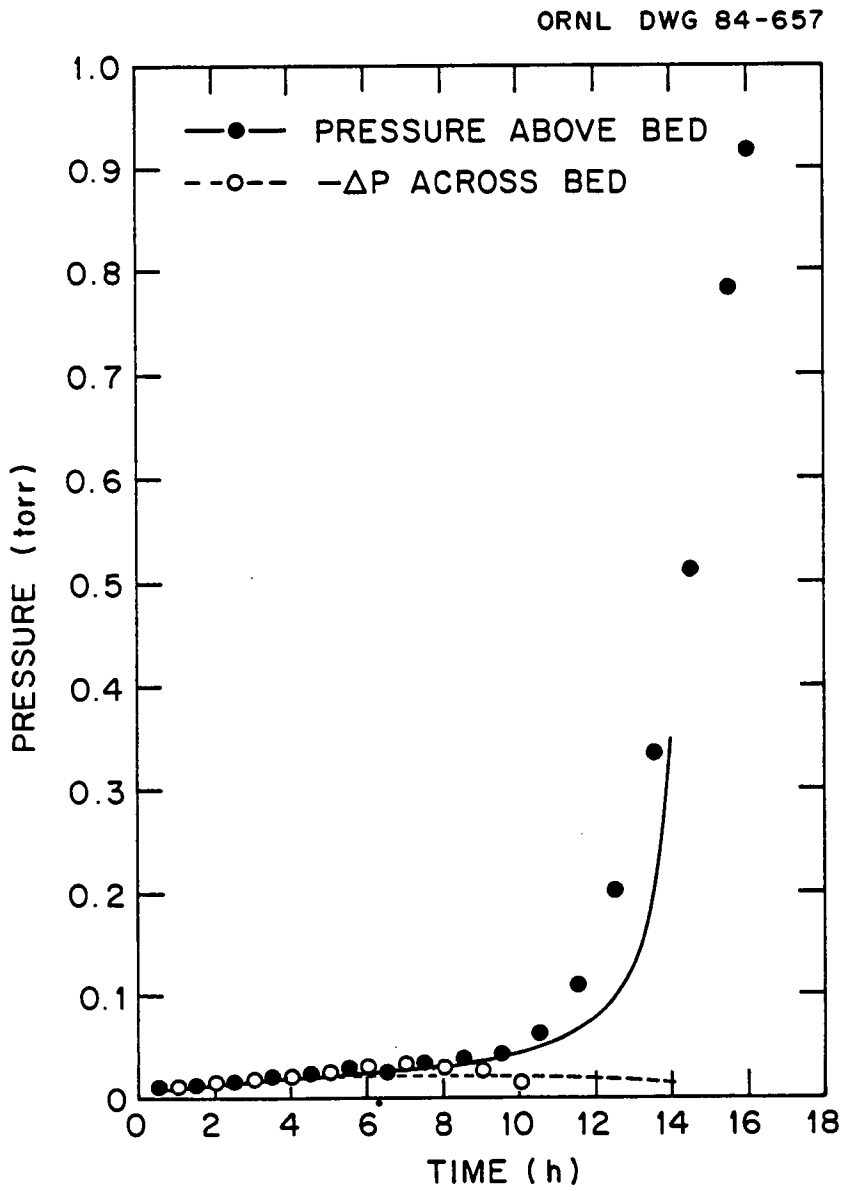

Figure 11. Comparison of experimental pressure and pressure drop data with theoretical curves for Run 238. Table 2, p. 58, details experimental conditions; Table 3, p. 60, lists parameters used to calculate theoretical curves.

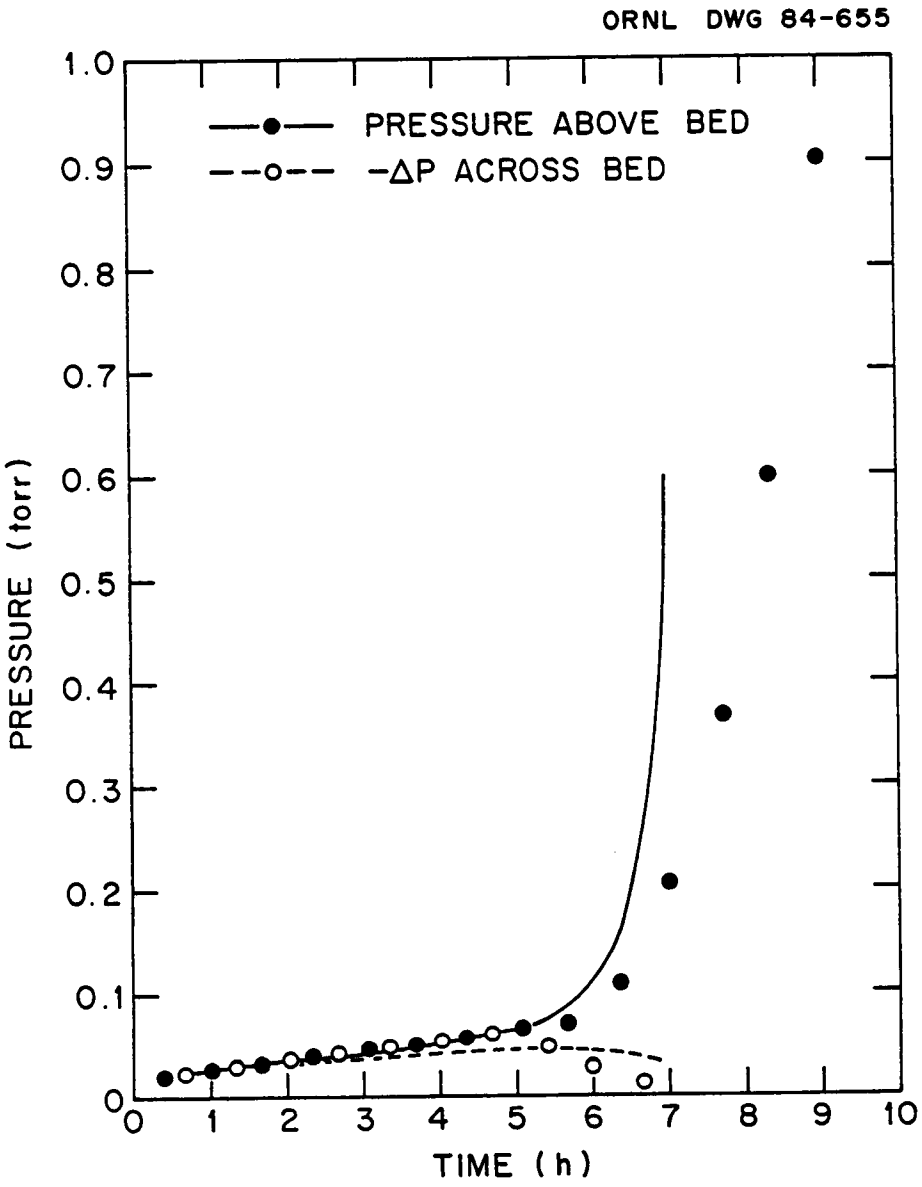

Figure 12. Comparison of experimental pressure and pressure drop data with theoretical curves for Run 237. Table 2, p. 58, details experimental conditions; Table 3, p. 60, lists parameters used to calculate theoretical curves.

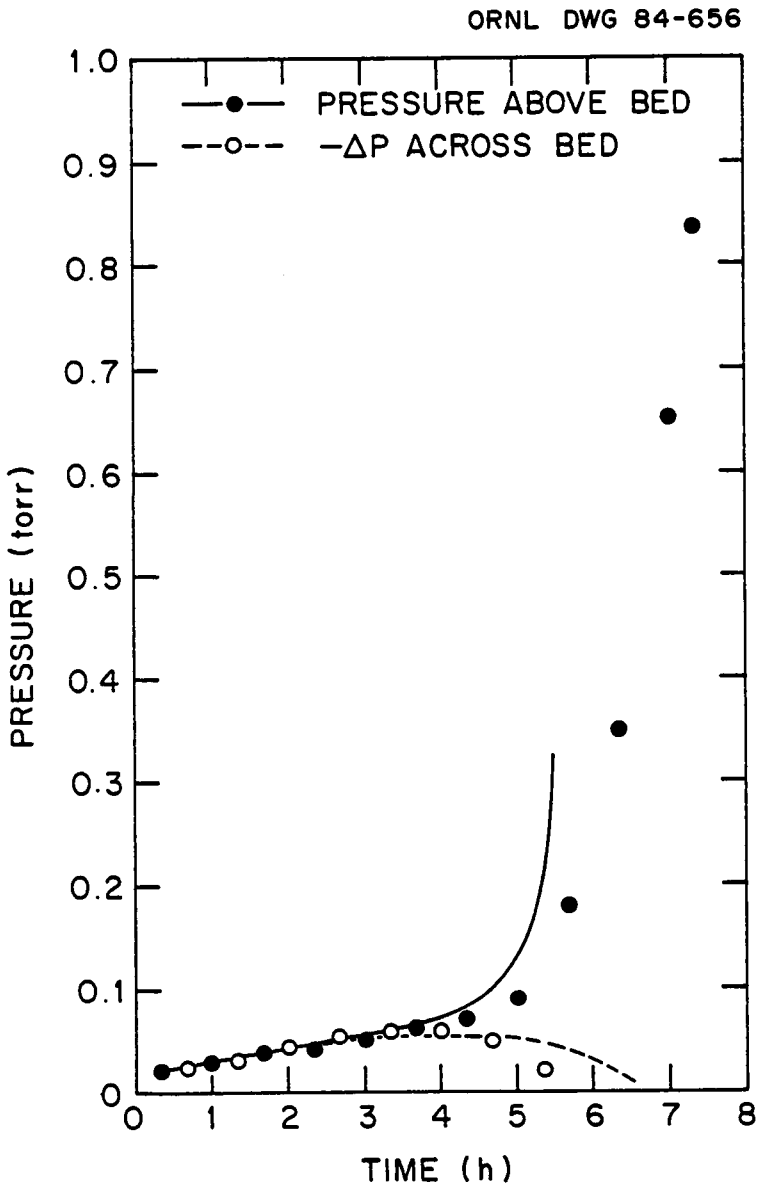

Figure 13. Comparison of experimental pressure and pressure drop data with theoretical curves for Run 233. Table 2, p. 58, details experimental conditions; Table 3, p. 60, lists parameters used to calculate theoretical curves.

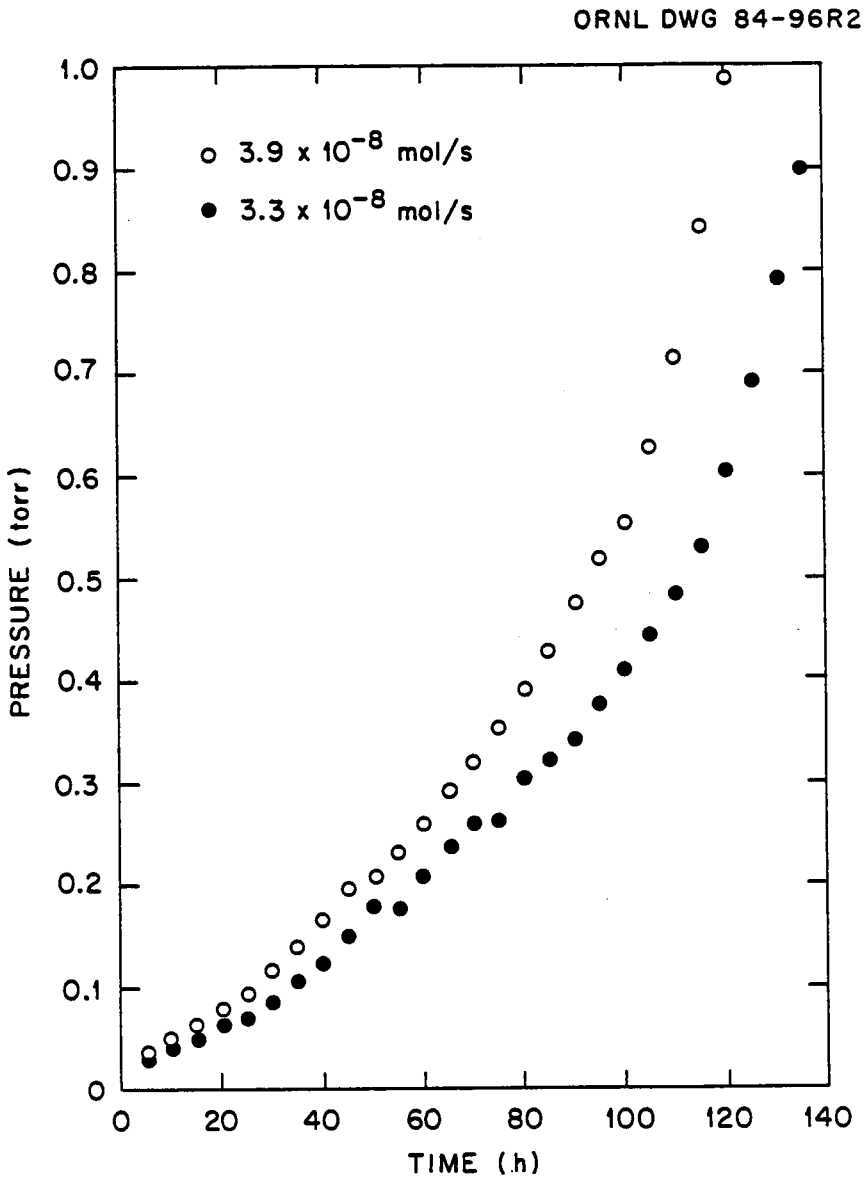

Figure 14. Sorption pumping of CO_2 on 4.69 g of 0.55-mm Davison 4A molecular sieves at 198 K.

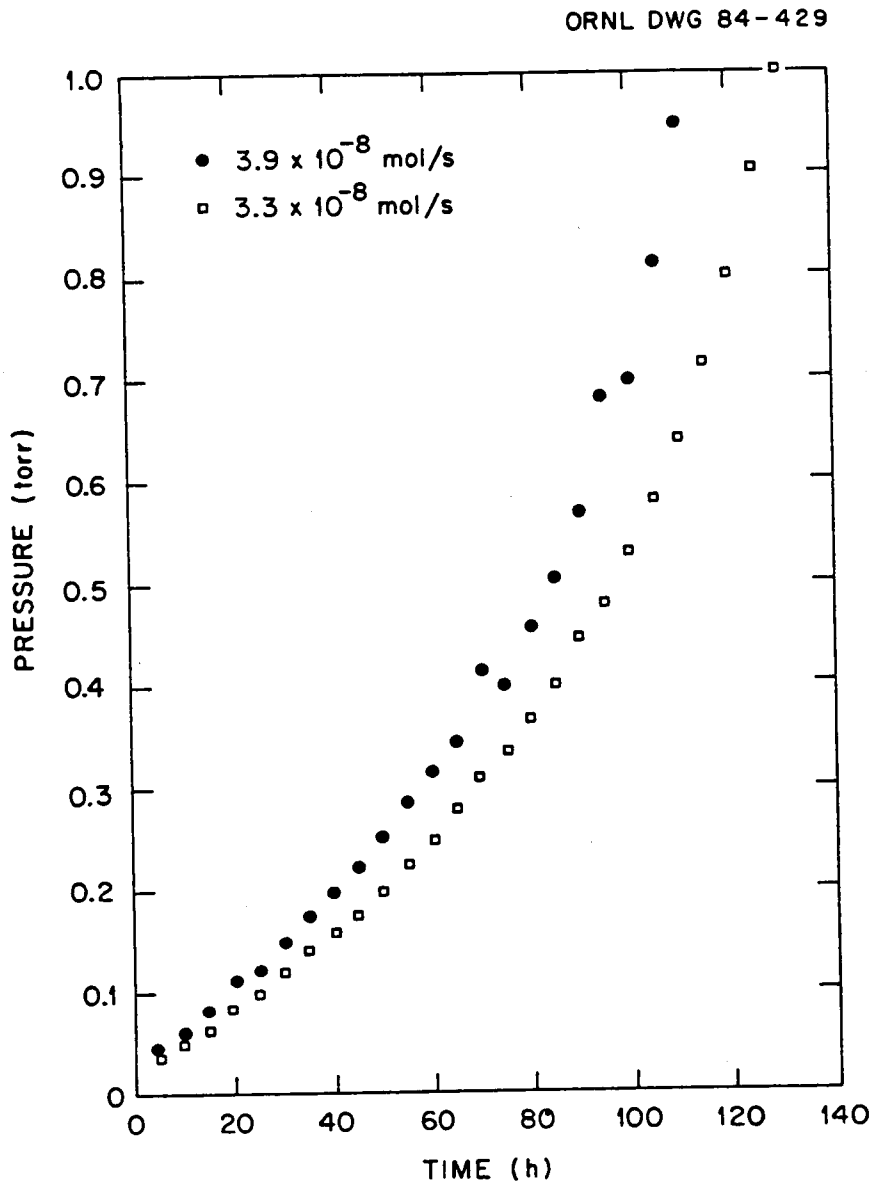

Figure 15. Sorption pumping of CO_2 on 4.33 g of 0.72-mm Davison 4A molecular sieves at 198 K.

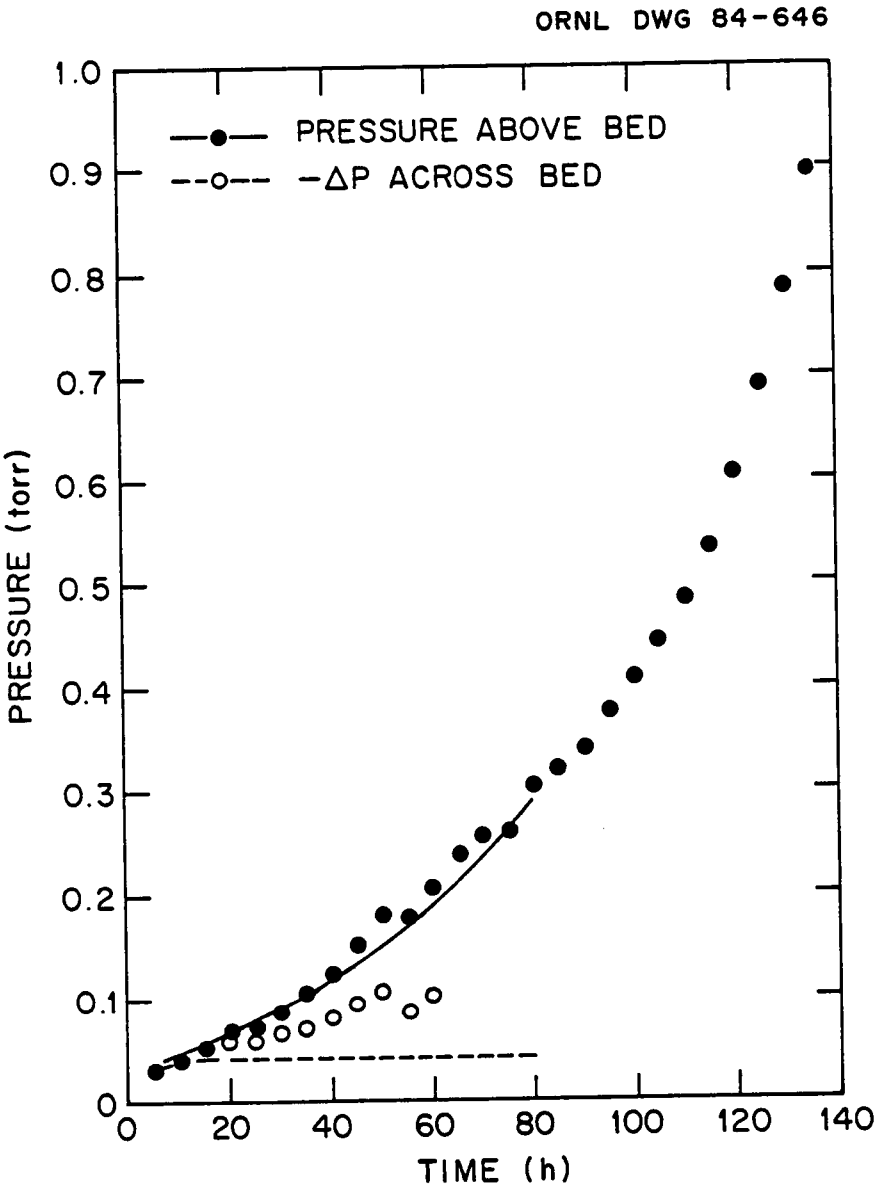

Figure 16. Comparison of experimental pressure and pressure drop data with theoretical curves for Run 217. Table 2, p. 58, details experimental conditions; Table 3, p. 60, lists parameters used to calculate theoretical curves.

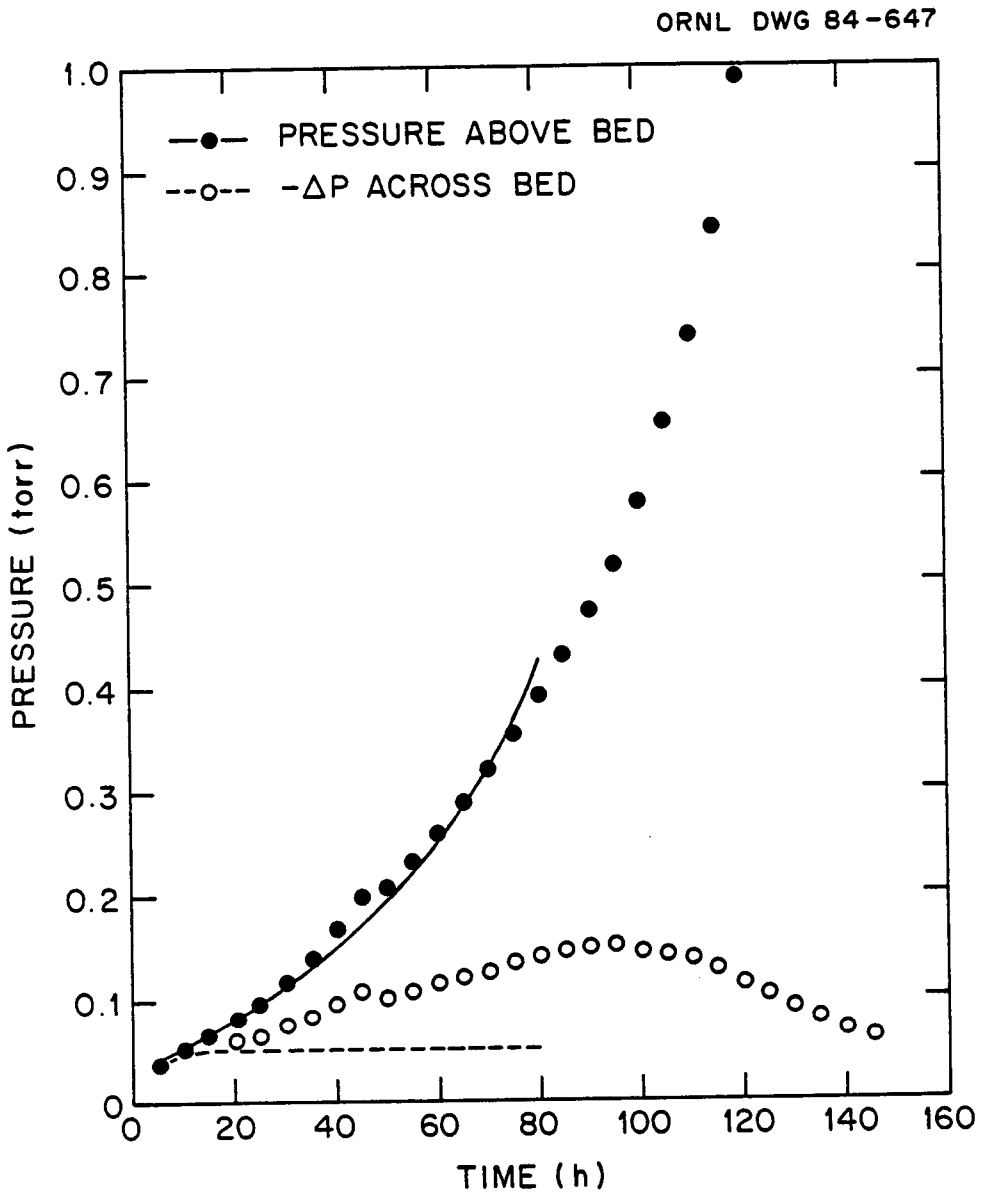

Figure 17. Comparison of experimental pressure and pressure drop data with theoretical curves for Run 218. Table 2, p. 58, details experimental conditions; Table 3, p. 60, lists parameters used to calculate theoretical curves.

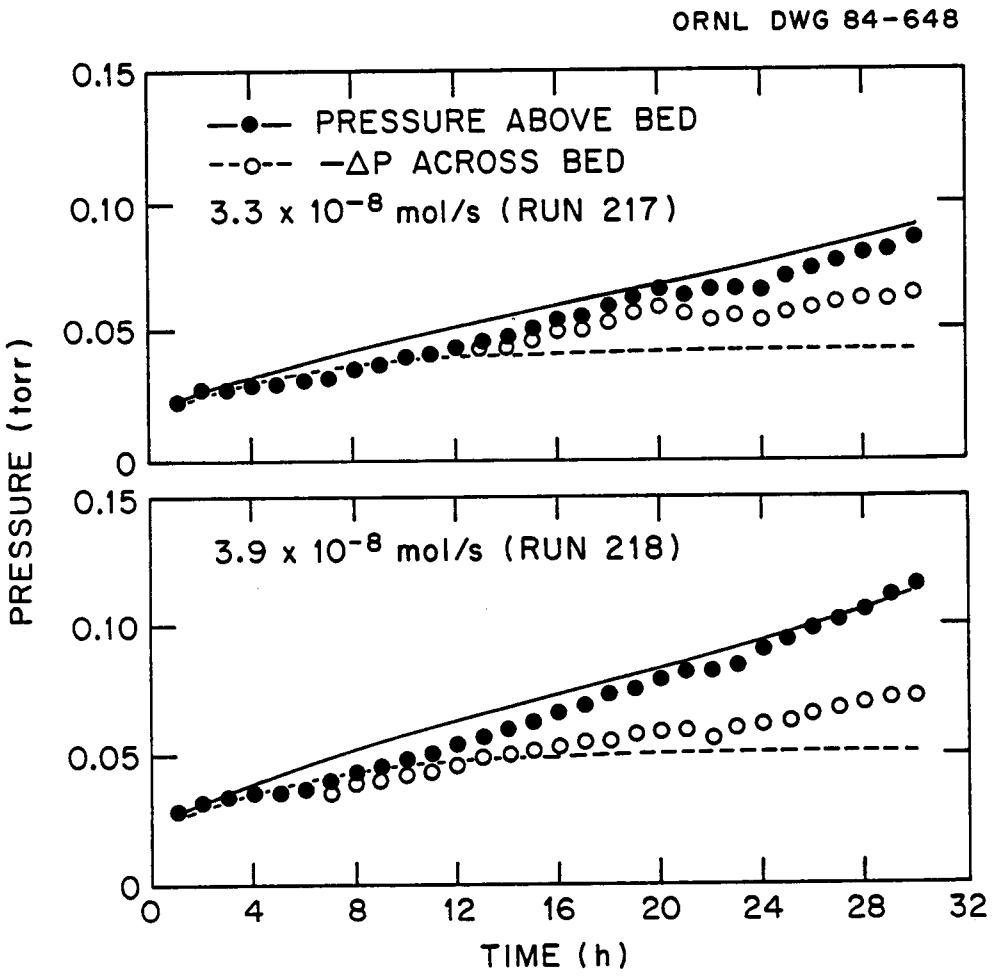

Figure 18. Comparison of short-time experimental pressure and pressure drop data with theoretical curves for Runs 217 and 218. Table 2, p. 58, details experimental conditions; Table 3, p. 60, lists parameters used to calculate theoretical curves.

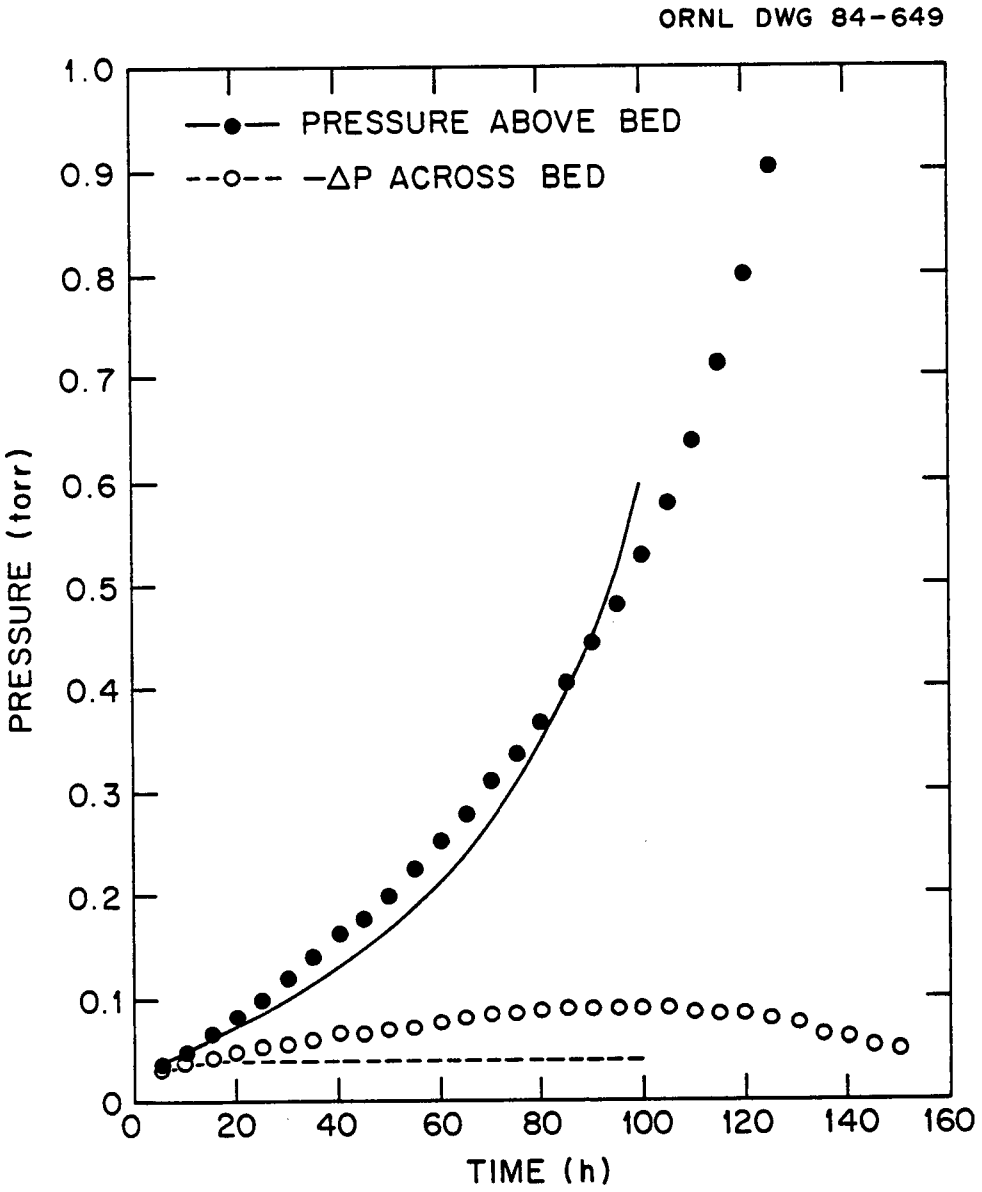

Figure 19. Comparison of experimental pressure and pressure drop data with theoretical curves for Run 227. Table 2, p. 58, details experimental conditions; Table 3, p. 60, lists parameters used to calculate theoretical curves.

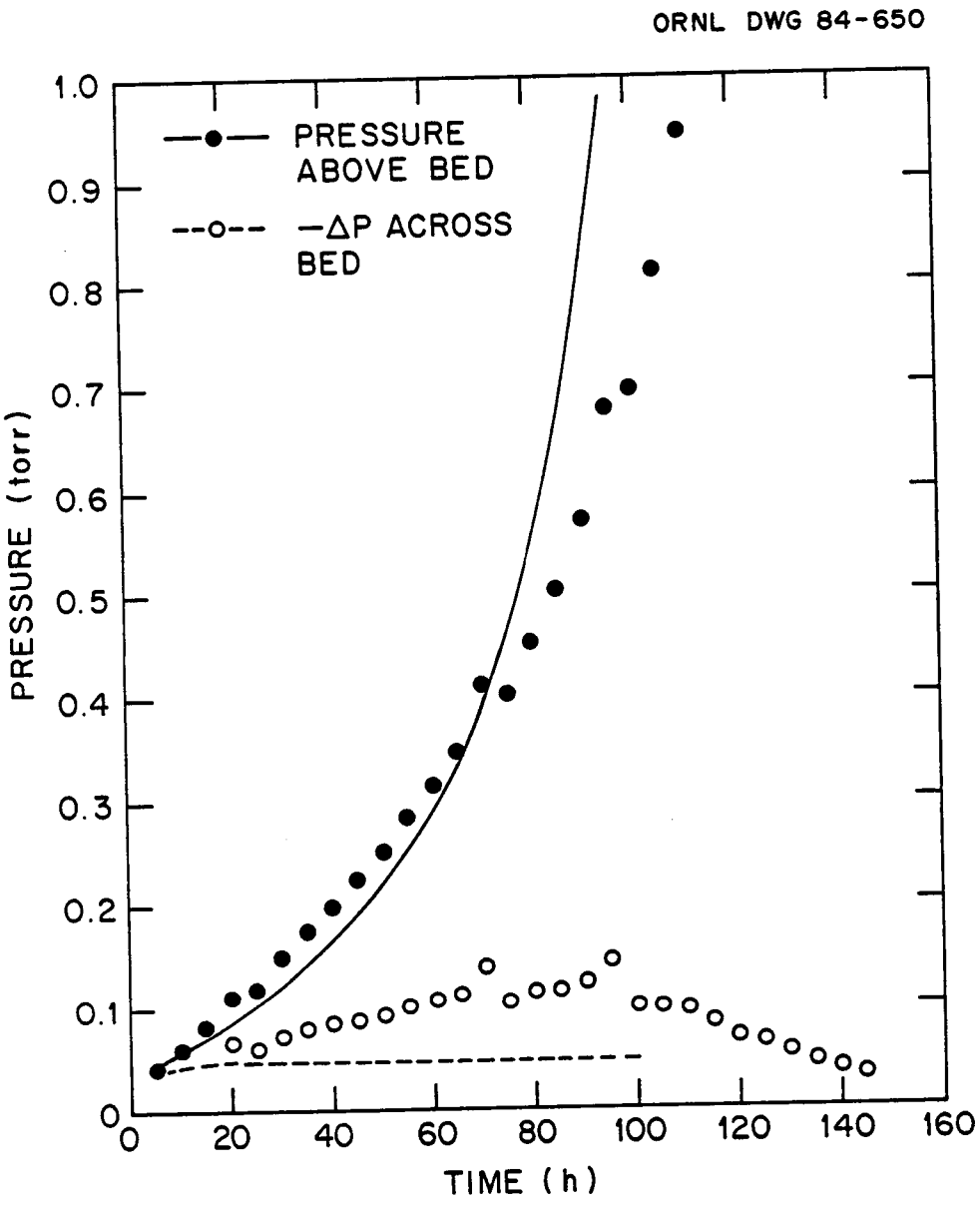

Figure 20. Comparison of experimental pressure and pressure drop data with theoretical curves for Run 225. Table 2, p. 58, details experimental conditions; Table 3, p. 60, lists parameters used to calculate theoretical curves.

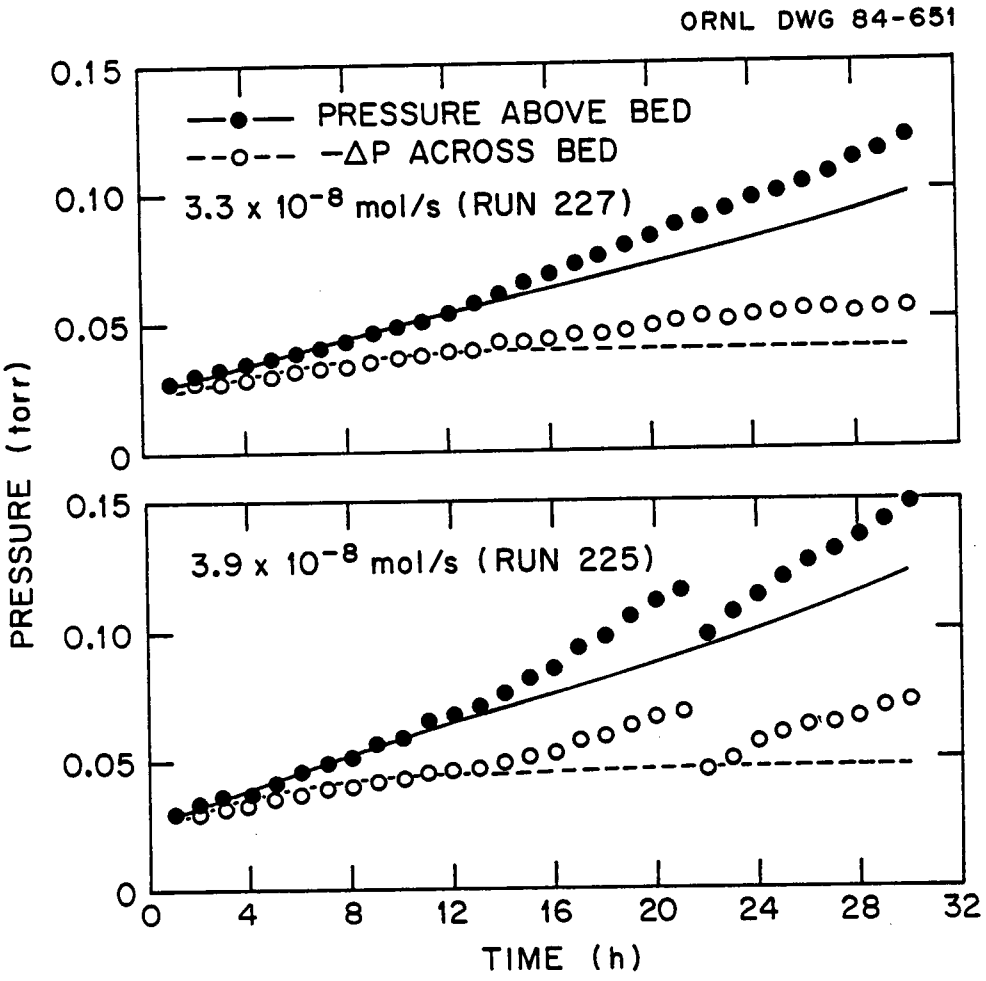

Figure 21. Comparison of short-time experimental pressure and pressure drop data with theoretical curves for Runs 225 and 227. Table 2, p. 58, details experimental conditions; Table 3, p. 60, lists parameters used to calculate theoretical curves.

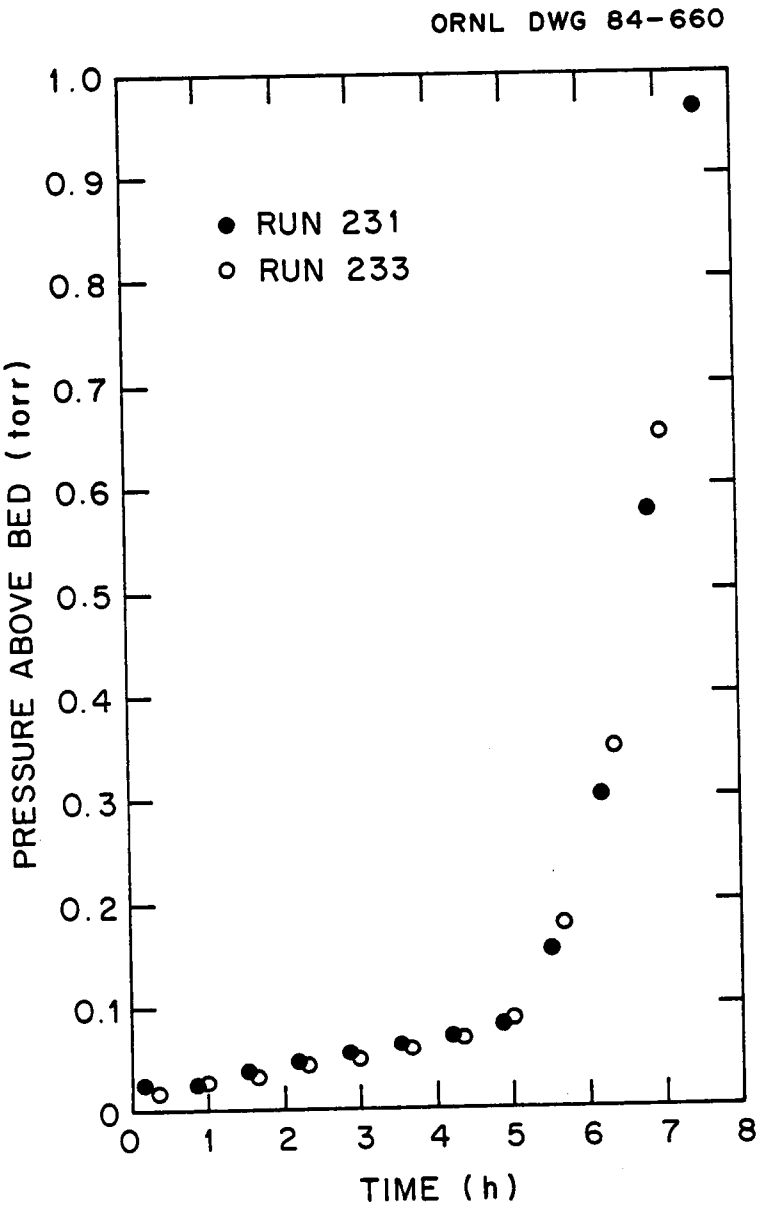

Figure 22. Comparison of pressure data from two identical sorption pumping experiments. Table 2, p. 58, details experimental conditions.

Table 2. Summary of experimental conditions for sorption pumping of N_2 and CO_2 on Davison 4A sieves

Run	Sorbent bed: Particle diameter (mm)	Sorbent bed: Weight (gm)	Sorbent bed: Height (cm)	Coolant temperature (K)	Flow rate of gas into void above bed (x 10^{-8} mol/s)
			N_2		
205	0.50–0.60	5.06	11.6	77	2.5
206	0.50–0.60	5.06	11.6	77	1.2
208	0.50–0.60	5.06	11.6	77	3.0
231	0.60–0.80	4.12	9.5	77	3.0
233	0.60–0.80	4.12	9.5	77	3.0
237	0.60–0.80	4.12	9.5	77	2.5
238	0.60–0.80	4.12	9.5	77	1.2
			CO_2		
217	0.50–0.60	4.69	10.8	198	3.3
218	0.50–0.60	4.69	10.8	198	3.9
225	0.60–0.80	4.33	10.0	198	3.9
227	0.60–0.80	4.33	10.0	198	3.3

value of the pressure drop through the bed ($-\Delta p$). For the period of linear pressure increase, very little gas penetrates to the bottom of the bed, and the pressure drop is high. By the time gas reaches the bottom, the bed is close to saturation. The pressure drop decreases rapidly as flow into the bed slows and the pressure equalizes throughout the system and begins its sharp rise.

Figures 8 through 13 also show the pressure and pressure drop curves generated using the numerical solution of the theoretical model. The model requires values of the following previously defined parameters: ε, ρ_B, T_a, T_b, S, L, V, I, κ, D, q_m, and k. Table 3 lists the values used to calculate the curves shown.

The experimental pressure-vs-time profiles from the two series of runs conducted with CO_2 are compared in Figures 14 and 15. The major difference between the sorption pumping behavior of N_2 and that of CO_2 is that the sieves have a much greater capacity to adsorb CO_2. Where the pressure above the sorbent bed reached 1 torr in about 7-1/2 h when sorbing N_2 at a flow rate of 3.0×10^{-8} mol/s, over 135 h were required to reach 1 torr when sorbing CO_2 at 3.3×10^{-8} mol/s. With CO_2 the pressure rises at a gradually but steadily increasing rate without the period of linear pressure increase characteristic of the N_2 curves.

Figures 16 through 21 again show the CO_2 profiles along with the pressure drop data. Almost from the outset, as well illustrated by Figures 18 and 21, the absolute value of the pressure drop is less than the total pressure above the bed, indicating that some CO_2 penetrates to the bottom. The pressure drop increases steadily until the bed

Table 3. Values of parameters used to calculate theoretical pressure and pressure drop curves shown in Figures 8 through 13 and 16 through 21[a]

Run	T_b (K)	D (cm^2/s)	k ($torr^{-1}$)	q_m (mol/g)	κ (cm^2/s)	S (cm)	L (cm)	I (x 10^{-8} mol/s)
				N_2				
All	77	5×10^{-8}	80	1.6×10^{-4}				
205, 206, 208					80	0.027	11.65	
205								2.5
206								1.2
208								3.0
233, 237, 238					105	0.036	9.49	
233								3.0
237								2.5
238								1.2
				CO_2				
All	198	1×10^{-8}	4	4×10^{-3}	350			
217, 218						0.027	10.80	
217								3.3
218								3.9
225, 227						0.036	9.97	
225								3.9
227								3.3

[a]For all runs, $\varepsilon = 0.35$ cm^3 void/cm^3 bed, $\rho_B = 0.92$ g/cm^3 bed, $T_a = 300$ K, and $V = 200$ cm^3.

begins to saturate at 0.5 to 0.6 torr. Along with the experimental data, Figures 16 through 21 show the theoretical curves obtained using the parameter values given in Table 3.

Discussion

Before delving into a detailed discussion comparing the experimental and theoretical results, a couple of questions need to be raised and answered. First, in developing the theoretical model describing mass transfer in the sorption pump, a basic assumption was that the hydrodynamic flow through the bed interstices could be characterized as molecular flow. The question arises of whether molecular flow does actually occur for the experimental conditions. A second issue, which was introduced in Section V, is whether the phenomenon of thermal transpiration significantly affects the experimental data.

To begin with the first question, recall that molecular flow occurs when the mean free path of a molecule, λ, is greater than the diameter of the channel through which it is moving, D_c, that is, when $\lambda/D_c > 1$. The mean free path is a function of temperature, pressure, and molecular diameter, d:

$$\lambda = \frac{k_B T}{\sqrt{2}\,\pi d^2 p}\,, \tag{62}$$

where k_B is the Boltzmann constant. Another look at the experimental data reveals that for a given run the pressure ranges from about 0.01 to 1 torr; consequently, λ decreases by a factor of 100 through the

course of a run. Does molecular flow occur over the whole pressure range?

Answering this question requires values of λ and D_c. Calculating λ by Equation (62) is straightforward. For N_2, T is 77 K and d is 3.75×10^{-8} cm (O'Hanlon, 1980, p. 357). For CO_2, T is 198 K and d is 4.59×10^{-8} cm (O'Hanlon, 1980, p. 357). Table 4 lists values calculated for pressures of interest.

Estimating D_c, the diameter of the channel through the bed interstices, requires a bit more ingenuity. Assume that the spherical sorbent particles pack in the closest possible arrangement. In two dimensions, they would form a triangle as shown in Figure 23. Calculating the hydraulic diameter of the void thus formed is fairly easy and is outlined in the figure. For a bed of 0.55-mm-diameter sieves, the S of Figure 23 is 0.27 mm and D_H is 0.055 mm. With an S of 0.36 mm for the 0.72-mm sieves, D_H is 0.074 mm. Averaging the two yields a very rough estimate of about 0.064 mm for the minimum D_c.

Comparing this estimate of D_c with the values of λ listed in Table 4 reveals that molecular flow should occur for N_2 at pressures below about 0.2 torr and for CO_2 below at least 0.3 torr. Although the estimate of D_c is very approximate, it appears safe to assume that molecular flow does occur in the bed interstices at least at the lower pressures encountered in an experimental run and that the theoretical model should apply.

To address the second issue, recall that in Section V it was shown that, for runs conducted at 77 K, measurements of the pressure drop across the bed are not accurate when the pressure at the bottom of the

Table 4. Mean free path of N_2 at 77 K and CO_2 at 198 K from 0.01 to 1 torr

Pressure (torr)	Mean free path, mm	
	N_2 at 77 K	CO_2 at 198 K
0.01	1.28	2.19
0.05	0.255	0.438
0.1	0.128	0.219
0.2	0.0638	0.109
0.3	0.0425	0.0730
0.4	0.0319	0.0547
0.5	0.0255	0.0438
1	0.0128	0.0219

ORNL DWG 84-641R

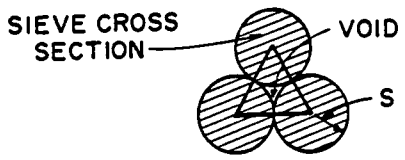

$$\text{HYDRAULIC DIAMETER, } D_H = 4\left(\frac{\text{VOID AREA}}{\text{VOID PERIMETER}}\right)$$

$$\text{VOID AREA} = \text{TRIANGLE AREA} - \text{AREA OF CIRCLES IN TRIANGLE}$$
$$= S\left(\sqrt{4S^2 - S^2}\right) - 3\left(\pi \frac{S^2}{6}\right)$$

$$\text{VOID PERIMETER} = \text{LENGTH OF CIRCUMFERENCE OF CIRCLES IN TRIANGLE}$$
$$= 3\left(\pi \frac{S}{3}\right)$$

$$\therefore D_H = 4\frac{S}{\pi}\left(\sqrt{3} - \frac{\pi}{2}\right)$$

Figure 23. Estimation of hydraulic diameter of channel through bed interstices.

bed is very low. The temperature gradient along the tube leading from the bottom of the bed at 77 K to the ambient-temperature differential pressure gauge produces a pressure gradient. Consequently, the pressure at the gauge end of the tube is greater than the pressure at the cold end of the tube, which is the value of interest. As the pressure at the gauge ranges from 0.06 to 1 torr, the ratio of the low-temperature pressure to the high ranges from 0.80 to 1. The question is whether to attempt to correct the experimental data to account for this phenomenon, which is termed thermal transpiration.

Looking again at the experimental pressure and pressure drop profiles obtained sorbing N_2 at 77 K provides an answer. During the first part of the runs, when the pressure increases linearly, the measured pressure drop across the bed essentially equals the pressure above the bed. In other words, the pressure measured at the gauge end of the tube leading from the bottom of the bed is about zero. Correcting a pressure close to zero for thermal transpiration still yields a value close to zero. Once gas does reach the bottom of the bed, the sieves are close to saturation and flow into the bed slows. The pressure at the bottom of the bed quickly approaches the pressure above the bed, and the pressure drop through the bed becomes immeasurably small. For most of a run, then, the pressure drop across the bed either about equals the pressure above the bed or is almost zero. Thus correcting the measured values for thermal transpiration is really not necessary, and corrections have not been made to the experimental data shown in Figures 6 through 13, pp. 41 through 48, and in Figure 22, p. 57.

With the previous discussion assuring that the experimental data are reasonably accurate despite thermal transpiration and that the theoretical model as derived for molecular flow should fit the data, attention can be turned to analyzing and comparing the experimental and theoretical results. Generating pressure and pressure drop curves using the numerical solution of the theoretical model requires values of twelve parameters. Eight of these parameters, ϵ, ρ_B, T_a, T_b, V, S, L, and I, are either properties of the sorbent or experimental conditions that can be readily measured or estimated. However, accurate values of D, k, q_m, and κ are not easily obtained.

The solid-phase diffusivity, D, for gas-zeolite systems is related to temperature through an Arrhenius equation (Ruthven and Derrah, 1975):

$$D = D^* \exp(-E/RT) \ . \tag{63}$$

Several sets of values of the preexponential factor, D*, and the activation energy, E, are available in the literature for N_2 and CO_2 in 4A sieves. Table 5 lists these values along with the corresponding diffusivities calculated from Equation (63) for N_2 at 77 K and CO_2 at 198 K. For N_2, the calculated values range from 1.2×10^{-26} to 5.3×10^{-21} cm^2/s and for CO_2, the values are 7.7×10^{-12} and 1.2×10^{-13} cm^2/s.

In trying to use these diffusivities to model the experimental data, several points must be considered. First, for N_2 the values of D* and E listed in Table 5 were developed from experimental data obtained at much higher temperatures (about 200 to 300 K) than the temperature of interest here (77 K). Extrapolating over such a wide range could be inaccurate. Second, as discussed in Section III, two

Table 5. Literature diffusivity data and calculated coefficients for N_2 at 77 K and CO_2 at 198 K in 4A zeolite crystals

Literature Arrhenius equation constants		Calculated D (cm^2/s)
D* (cm^2/s)	E (kcal/mol)	
	N_2[a]	
4.3×10^{-3}	8.3	1.2×10^{-26}
9.6×10^{-7}	6.1	4.7×10^{-24}
2.3×10^{-9}	4.1	5.3×10^{-21}
	CO_2[b]	
9.3×10^{-6}	5.5	7.7×10^{-12}
2.5×10^{-8}	4.8	1.2×10^{-13}

[a]As reported by R. M. Barrer, Zeolites and Clay Minerals as Sorbents and Molecular Sieves, Academic Press, London, 1978, p. 292.

[b]H. Yucel and D. M. Ruthven, "Diffusion of CO_2 in 4A and 5A Zeolite Crystals," J. Coll. Int. Sci., 74, 186 (1980).

diffusive processes occur in commercial molecular sieve pellets: diffusion through the macrovoids between crystals and diffusion within the crystal microvoids. The model assumes that one of these processes controls. The diffusion coefficients calculated from the literature data apply to diffusion of gas in the microvoids.

Searching the literature for estimates of k and q_m, the constants required in the Langmuir adsorption isotherm equation, reveals very little data for the N_2-4A system at low temperatures. To estimate k and q_m, experimental measurements were made of the amount of N_2 adsorbed from mixtures of N_2 and helium on a sample of 4A sieves at various partial pressures of N_2. The instrument used was a Quantasorb manufactured by Quantachrome Corporation. The times allowed for sorption were on the order of minutes. Appendix C briefly describes the experiments, plots the data obtained, and shows how k and q_m were estimated from the data.

Two problems were encountered. Data could not be obtained for partial N_2 pressures lower than about 6 torr, which is well above the upper limit of 1 torr attained in the sorption pumping experiments. Also, the data do not fit the Langmuir equation particularly well. The estimated values of k and q_m are 1 $torr^{-1}$ and 3 x 10^{-4} mol/g.

Equilibrium adsorption data for CO_2 on 4A sieves at 198 K were provided by the manufacturer over the range 2 to 400 torr. The data from 2 to 10 torr were used to estimate k and q_m; the estimated values are 4 $torr^{-1}$ and 0.004 mol/g. Details are presented in Appendix C.

In Section III, the following expression was derived for κ, the interstitial mass transfer coefficient:

$$\kappa = \frac{4}{3} \frac{v_m}{\left(\frac{H}{A}\right)_{avg}} \quad . \tag{64}$$

The average molecular velocity, v_m, a function of temperature and molecular weight, is given by

$$v_m = \left(\frac{8\ k_B\ T}{\pi m} \right)^{1/2} \quad , \tag{65}$$

where m is mass per molecule. The ratio of the channel perimeter to channel area, $(H/A)_{avg}$, is determined by the channel geometry. To obtain a very gross estimate of $(H/A)_{avg}$, consider again Figure 23, p. 64. By definition,

$$\frac{H}{A} = \frac{4}{D_H} \quad , \tag{66}$$

and for the geometry shown,

$$\frac{H}{A} = \frac{\pi}{S} \left(\sqrt{3} - \frac{\pi}{2} \right)^{-1} \quad . \tag{67}$$

For N_2 at 77 K, v_m is 2.41 x 10^4 cm/s and for CO_2 at 198 K, v_m is 3.09 x 10^4 cm/s. Using Equation (67) in Equation (64) yields estimates of κ of 44 and 59 cm^2/s for N_2 on beds of 0.55-mm and 0.72-mm sieves. For CO_2, the values are 57 cm^2/s for the smaller sieves and 76 cm^2/s for the larger. Because the geometry shown is of the closest possible packing, the calculated values should be considered minimum estimates.

Of more interest than these very crude estimates are the relationships Equations (64) and (67) predict between κ's at various conditions. For two runs conducted using the same bed but different gases, $(H/A)_{avg}$ will not vary, and from Equation (64) the κ's are related by

$$\frac{\kappa_1}{\kappa_2} = \frac{v_{m,1}}{v_{m,2}} \cdot \tag{68}$$

For N_2 at 77 K and CO_2 at 198 K,

$$\kappa_{CO_2} = 1.3\ \kappa_{N_2} \cdot \tag{69}$$

If two different beds were used in sorbing the same gas, Equations (64) and (67) predict that the κ's will be related by

$$\frac{\kappa_1}{\kappa_2} = \frac{S_1}{S_2} \cdot \tag{70}$$

For beds with 0.55-mm and 0.72-mm particles,

$$\kappa_{0.72} = 1.3\ \kappa_{0.55} \cdot \tag{71}$$

In trying to fit the pressure and pressure drop profiles generated by the numerical solution of the theoretical model to the experimental data, these rough estimates of D, k, q_m, and κ were used as initial guesses. The values were then adjusted through trial and error to find the sets that yielded the best fits of the experimental data. Figures 6 through 13, pp. 41 through 48, and 16 through 21, pp. 51 through 56, show the experimental data and the best theoretical curves. Table 3, p. 60, lists the values of D, k, q_m, and κ used to generate the curves.

Consider first the results for the N_2 runs. Figures 8 through 10, pp. 43 through 45, show the profiles obtained using the 0.55-mm-diameter sieves, and Figures 11 through 13, pp. 46 through 48, show the results from runs using 0.72-mm-diameter sieves. For both sets, the values of D, k, and q_m used to fit the experimental data are 5×10^{-8} cm^2/s, 80 $torr^{-1}$, and 1.6×10^{-4} mol/g. For the smaller sieves, κ is 80 cm^2/s and for the larger, it is 105 cm^2/s.

The theoretical curves predict well the behavior of the pump for the first part of the runs. Two values that characterize the data up to the time when the bed begins to saturate are the rate of linear pressure increase and the maximum pressure drop across the bed. Table 6 lists these values for both the experimental data and theoretical curves. The slope and the pressure drop are greater at higher flow rates for a given bed and are greater for the smaller sieves than for the larger. The theoretical curves accurately predict these overall trends and provide fairly good estimates of the actual values of the slopes and pressure drops.

Where the model breaks down somewhat is in trying to predict what happens once gas reaches the bottom of the bed. The experimental data show that once gas penetrates to the bottom, the bed is almost saturated; the pressure quickly equalizes throughout the system and begins to increase rapidly with the pressure drop falling to zero. The theoretical curves predict more gradual changes. When the gas reaches the bottom of the bed, the pressure drop decreases slowly as the pressure above the bed begins to rise at a gradually increasing rate.

Table 6. Characteristics of the N_2 experimental profiles and theoretical curves shown in Figures 8 through 13

Flow rate ($\times 10^{-8}$ mol/s)	Rate of linear pressure increase ($\times 10^{-4}$ torr/m)		Maximum pressure drop (torr)	
	Experimental	Theoretical	Experimental	Theoretical
	0.55-mm sieves			
1.2	0.89	0.59	0.047	0.037
2.5	2.3	2.0	0.084	0.079
3.0	3.1	2.9	0.097	0.097
	0.72-mm sieves			
1.2	0.58	0.50	0.033	0.021
2.5	1.6	1.6	0.054	0.044
3.0	2.0	2.2	0.059	0.055

Eventually the pressure does increase sharply with the pressure drop going to zero. These trends are more pronounced at lower flows.

Consider now how the values of D, k, q_m, and κ determined by fitting the theoretical curves to the experimental data compare with the previously discussed values estimated from literature data and other experiments. As shown in Table 5, p. 67, literature estimates of D for N_2 in 4A crystals range from 1.2×10^{-26} to 4.7×10^{-24} cm^2/s. If these values are even close to accurate, then essentially no N_2 diffuses into the crystal microvoids during the course of a run, and the controlling diffusive process is the movement of gas through the macrovoids of the manufactured pellets. Thus the value of D, 5×10^{-8} cm^2/s, estimated by the theoretical model applies to diffusion within the macrovoids. The conclusion that N_2 does not diffuse into the crystals is supported by the fact that the sieves adsorb very little N_2 at 77 K.

Independent work in which N_2 was sorbed on a sample of the 4A sieves at pressures from 6 to 107 torr yielded estimates for k and q_m of 1 $torr^{-1}$ and 3×10^{-4} mol/g. The value of k predicted by the theoretical model, 80 $torr^{-1}$, is significantly higher than that measured experimentally, whereas the value of q_m, 1.6×10^{-4} mol/g, although lower than the measured value, is of the same order of magnitude. Direct comparisons of the data are difficult because the experimental adsorption isotherm data were obtained at higher pressures than encountered in the sorption pumping runs and did not really fit the Langmuir form of equation used in the model.

In earlier discussions, κ for N_2 was roughly estimated as 44 cm^2/s for the bed of 0.55-mm sieves and as 59 cm^2/s for the 0.72-mm sieves.

It was also shown that κ is proportional to an average value of the hydraulic diameter of the channel through the bed interstices and that the channel diameter is in turn proportional to the diameter of the sorbent particles. Thus, $\kappa \approx (S_1/S_2)\ \kappa_2$, where S_1/S_2 is the ratio of particle radii. The values of κ obtained using the theoretical model, 80 and 105 cm^2/s, are higher than those estimated. This suggests that the channel through the interstices is larger than that estimated assuming the closest packed arrangement of Figure 23. However, the ratio of theoretical κ's does equal the ratio of the particle radii.

Choosing the values of D, k, q_m, and κ that best fit the theoretical curves to the experimental data is not as arbitrary as it might seem. Figures 24 through 27 illustrate the effects of varying each of the four parameters independently of the others. A change in any of the four has a marked effect on either the theoretical pressure or pressure drop curve. For example, D shifts the upturn in the pressure curve and determines the magnitude of the pressure jump occurring at the start of a run. The effect of decreasing D from 5×10^{-8} to 1×10^{-8} cm^2/s is shown in Figure 24. A change in k alters the slope of the linear portion of the pressure curve (Figure 25); q_m also affects when the pressure profile will break upward (Figure 26); and κ most significantly affects the magnitude of the pressure drop across the bed (Figure 27).

Figures 16 through 21, pp. 51 through 56, compare the theoretical curves and the experimental data for CO_2. Table 3, p. 60, lists the parameters used to obtain the curves; in particular, D is 1×10^{-8} cm^2/s; k, 4 $torr^{-1}$; q_m, 0.004 mol/g; and κ, 350 cm^2/s. The values of

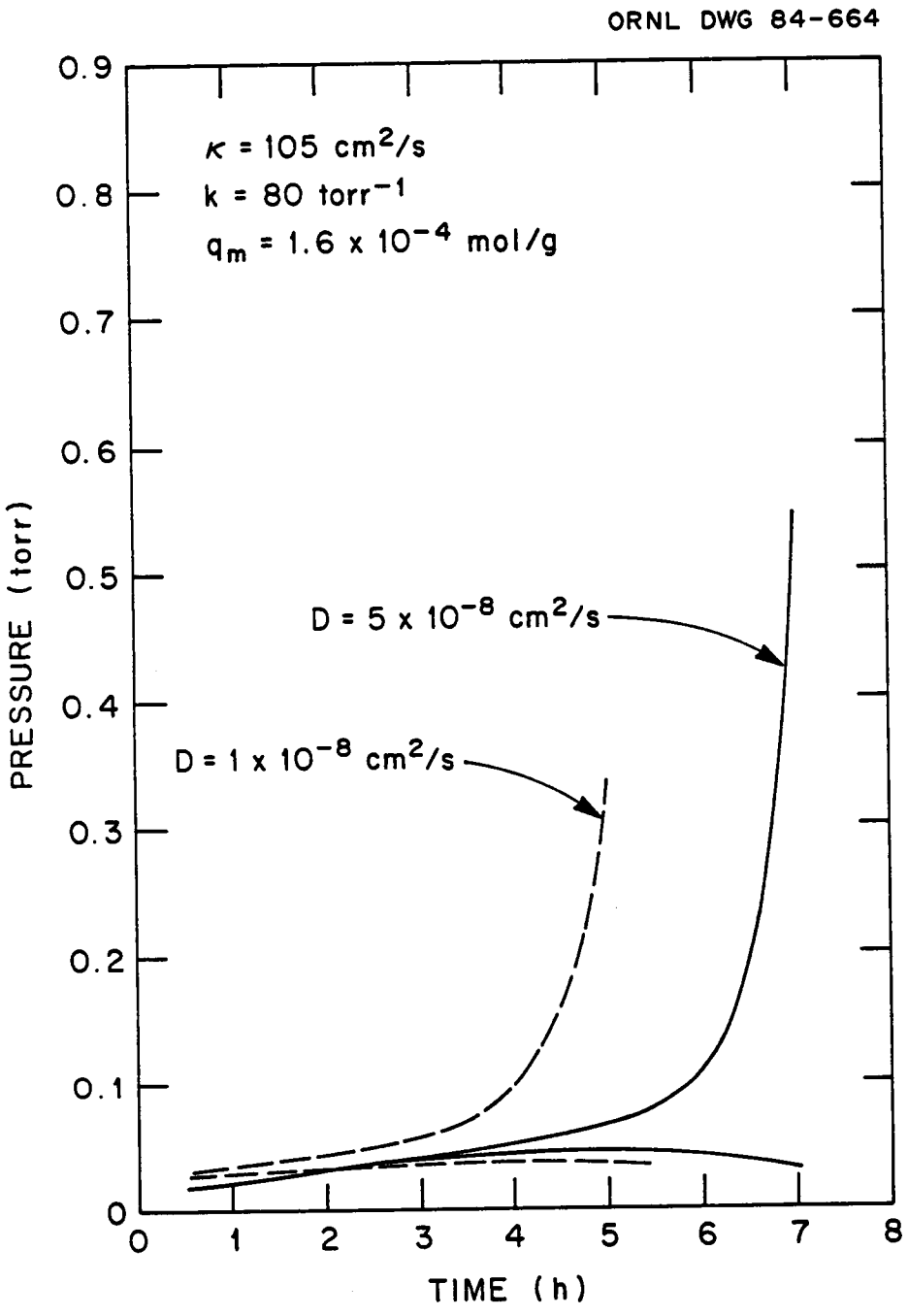

Figure 24. Effect of D on theoretical pressure and pressure drop curves. Parameters other than D used to calculate curves are those listed in Table 3, p. 60, for Run 236.

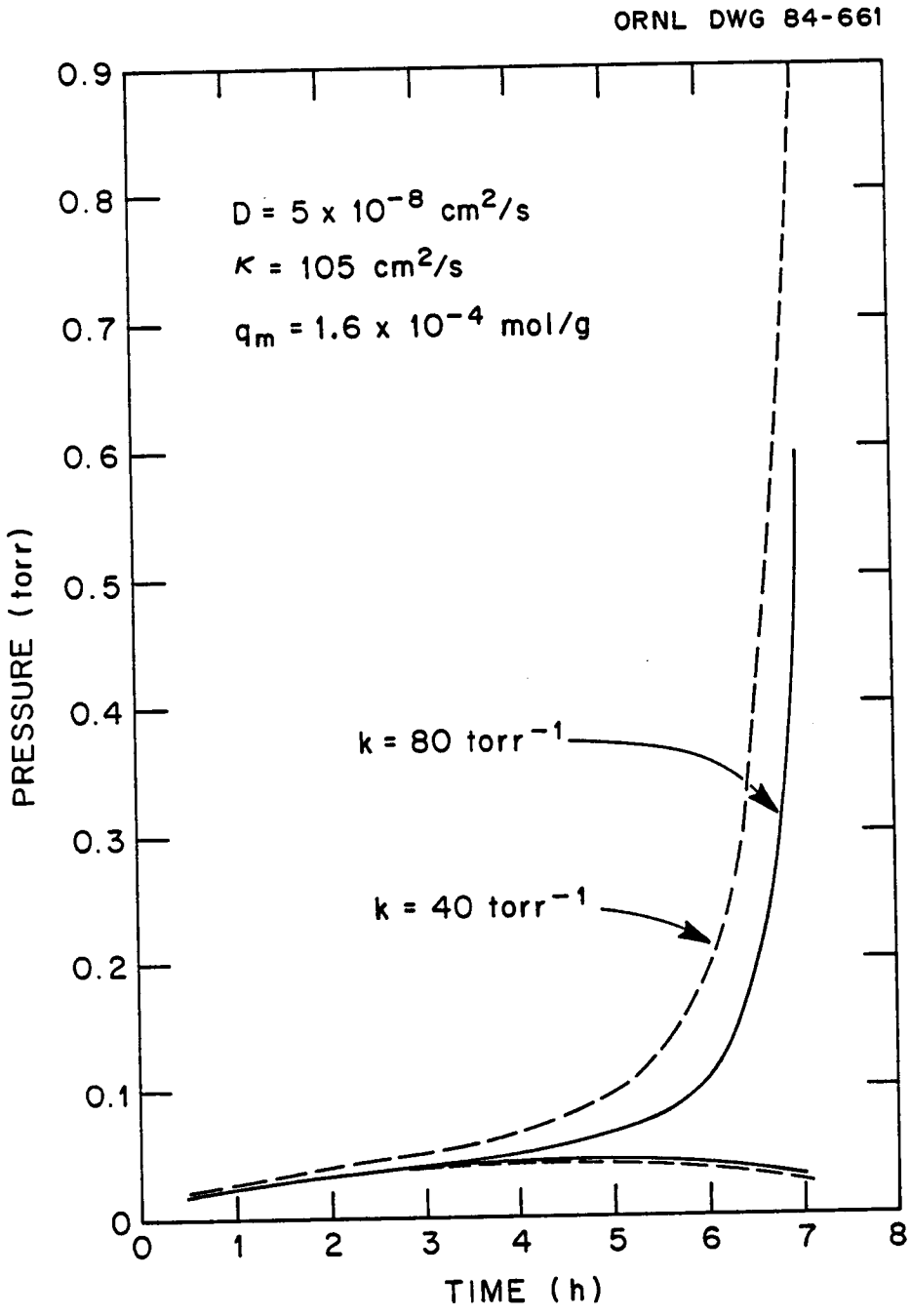

Figure 25. Effect of k on theoretical pressure and pressure drop curves. Parameters other than k used to calculate curves are those listed in Table 3, p. 60, for Run 236.

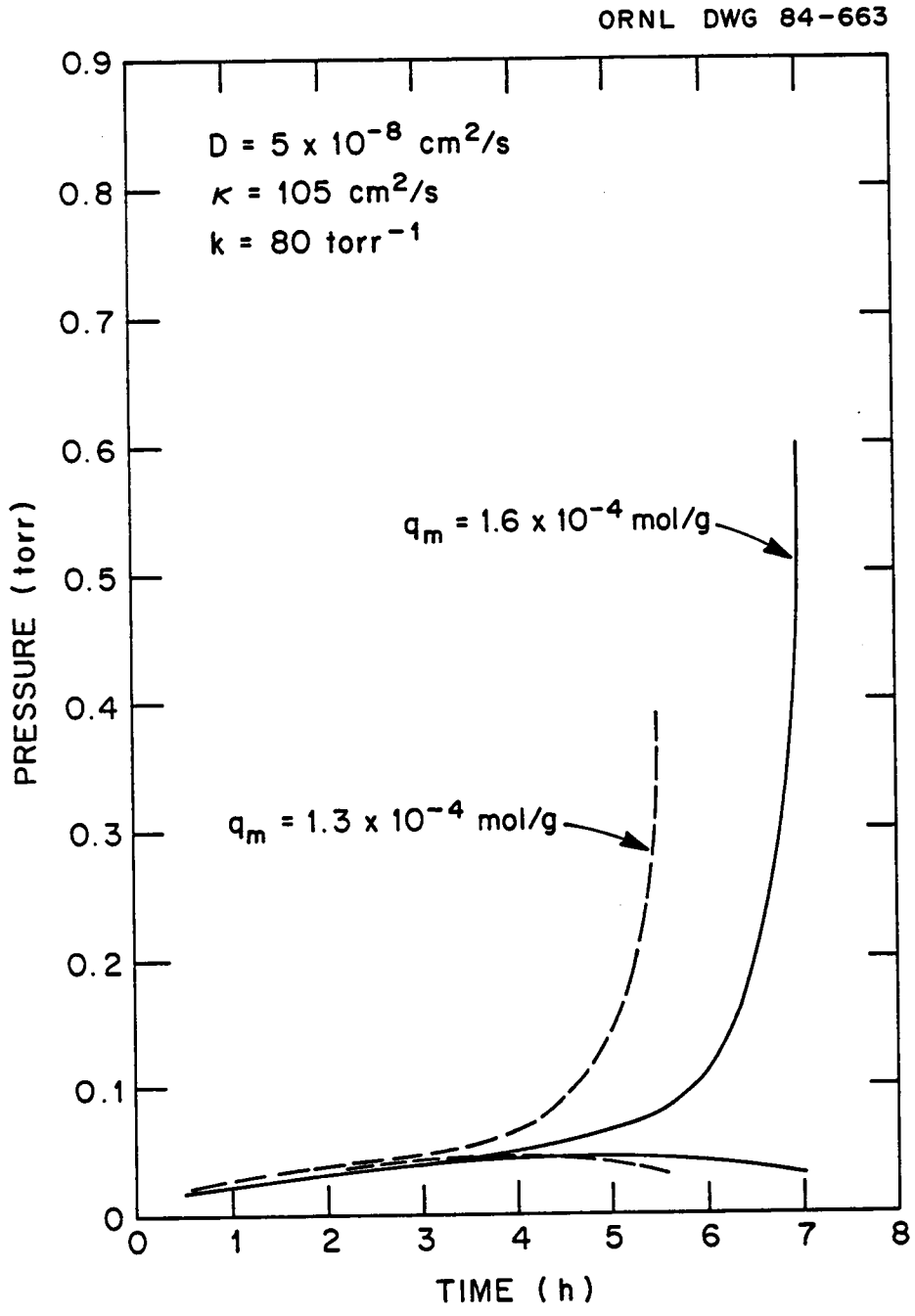

Figure 26. Effect of q_m on theoretical pressure and pressure drop curves. Parameters other than q_m used to calculate curves are those listed in Table 3, p. 60, for Run 236.

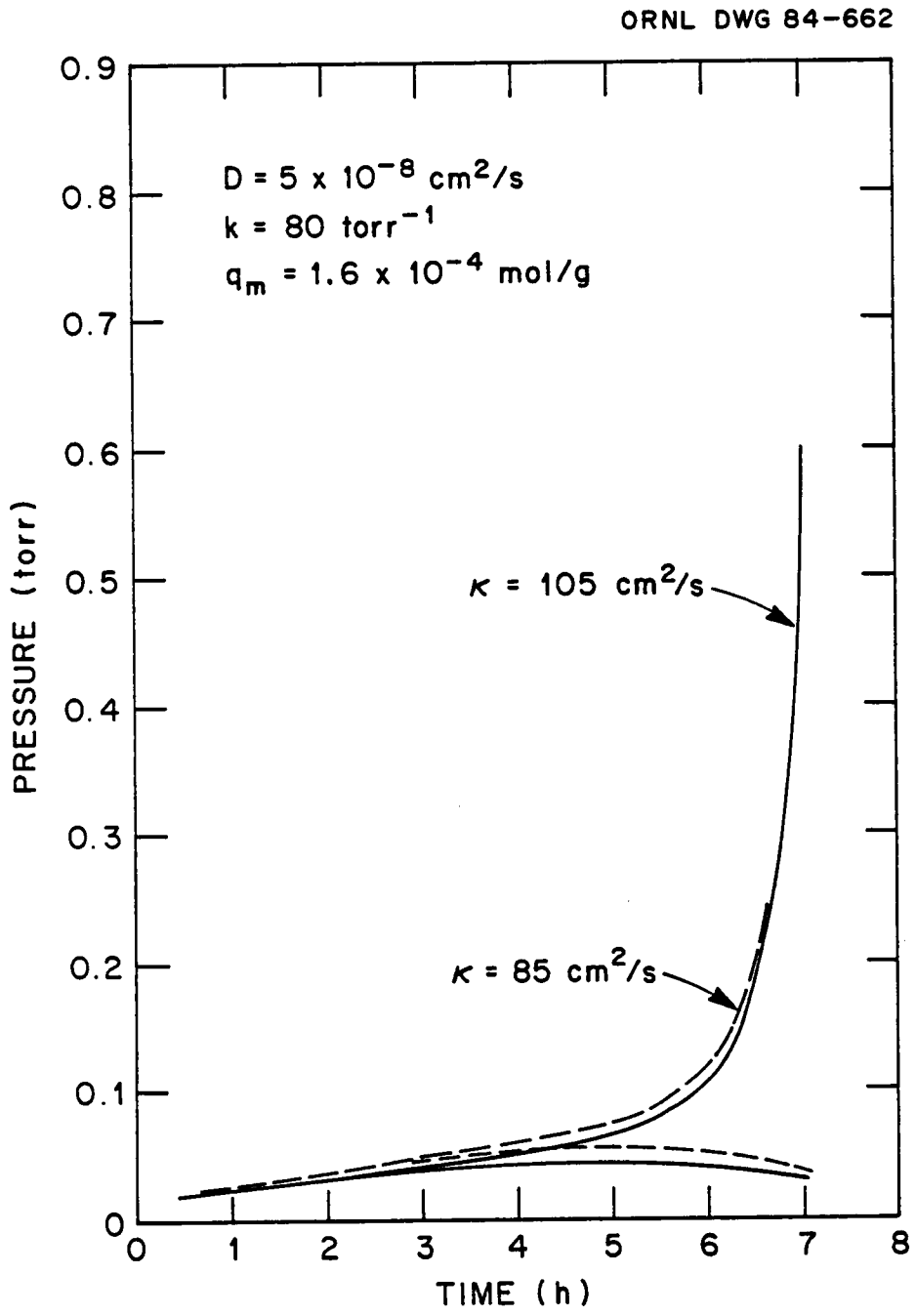

Figure 27. Effect of κ on theoretical pressure and pressure drop curves. Parameters other than κ used to calculate curves are those listed in Table 3, p. 60, for Run 236.

k and q_m are those estimated from fitting the manufacturer's equilibrium adsorption data (Appendix C); D and κ were obtained from the best fit of the curves to the experimental data.

The model predicts well the pressure above the bed. The theoretical profiles have more curvature than the experimental data and fall slightly above the data for short and long times and below it in between. Unfortunately, the model does not describe the pressure drop across the bed quite as well.

The experimental data show that the pressure drop increases steadily as the pressure above the bed climbs to about 0.5 torr. The bed then begins to saturate, the pressure above the bed increases at an ever higher rate, and the pressure drop decreases. The theoretical model predicts that the pressure drop quickly reaches a maximum value that is maintained at least through times up to saturation. In other words, the experimental data reveal that the pressure above the bed increases faster than the pressure at the bottom up to saturation, whereas the model predicts that, although a gradient is maintained, the pressure increases at the same rate throughout the bed for most of a run.

The values of k and q_m used to generate the curves in Figures 16 through 21, pp. 51 through 56, are those estimated from the manufacturer's equilibrium adsorption data. The value of D, 1×10^{-8} cm/s, differs significantly from the values 7.7×10^{-12} and 1.2×10^{-13} cm^2/s found in the literature. To understand why this could be, consider again the final equation derived to model diffusion within the solid:

$$\frac{\partial \bar{q}}{\partial t} = \frac{15D}{S^2} (q_S - \bar{q}) \quad . \tag{72}$$

This is the only equation in the model in which either D or S, the particle radius, appears. Thus the value of S is important in determining D.

In the case of N_2, because the literature diffusion coefficients are so low, it was concluded that the important diffusive process is movement through the macrovoids of the manufactured sorbent particles. Consequently, the appropriate estimate of S is the radius of the manufactured sorbent particles. For CO_2, however, the literature coefficients suggest that diffusion into the crystal microvoids will occur for the times required for the sorption experiments. For this case, if resistance to diffusion within the macrovoids can be assumed negligible, then the correct radius is that of the zeolite crystals.

Table 1, p. 33, shows that the bound crystals vary greatly in size; as a rough estimate, let S be 1 μm. The D of 1×10^{-8} cm^2/s for CO_2 was obtained using S equal to the particle radius, either 0.55 or 0.72 mm. With S equal to 1 μm, D is about 3×10^{-14} cm^2/s, which agrees much more closely with the literature values.

As demonstrated for N_2, κ determines the magnitude of the pressure drop across the bed. Table 7 lists the values of the maximum pressure drops measured experimentally for the CO_2 runs along with the values predicted theoretically using a κ of 350 cm^2/s. The theoretical values are much lower, suggesting that the estimate of 350 cm^2/s is too high. In earlier discussions, κ for CO_2 was roughly estimated as 57 or 76

Table 7. Maximum pressure drop across bed for CO_2 results shown in Figures 16 through 21

Flow rate ($\times 10^{-8}$ mol/s)	Maximum pressure drop, torr	
	Experimental	Theoretical
	0.55-mm sieves	
3.3	Not available	0.043
3.9	0.149	0.052
	0.72-mm sieves	
3.3	0.091	0.040
3.9	0.145	0.047

cm^2/s depending on sorbent particle size, and the ratio of κ for CO_2 to κ for N_2 was predicted to be 1.3. The ratio of 350 cm^2/s to 105 cm^2/s, the larger of the two estimated for N_2, is 3.3. With all these indications that 350 cm^2/s is too high, why was a smaller value not chosen?

The experimental data of Figures 19 and 21, pp. 54 and 56, are again plotted in Figures 28 and 29 along with theoretical curves generated by changing k from 4 to 5 $torr^{-1}$ and κ from 350 to 200 cm^2/s. The model still predicts the pressure profile well, and the maximum pressure drop calculated theoretically, 0.071 torr, more closely approaches the experimental value of 0.091 torr. The problem with using this lower κ becomes apparent on comparing Figures 21 and 29. While a κ of 200 cm^2/s does a better job predicting the maximum pressure drop than does a κ of 350 cm^2/s, it yields a poorer fit of the experimental data measured during the first hours of the run. The real problem is that the theoretical model does not accurately describe the shape of the experimental pressure drop profile regardless of the value of κ.

As discussed in Section III, the theoretical model was derived from many simplifying assumptions. Which assumption resulted in the model not accurately describing the pressure drop data for CO_2 is not obvious. Several assumptions, specifically, those of ideal gas behavior and an isothermal sorbent bed, are almost certainly valid. Others are known to be oversimplifications. For example, independent experimental work showed that the Langmuir isotherm used in the model does not accurately describe equilibrium adsorption for all the systems

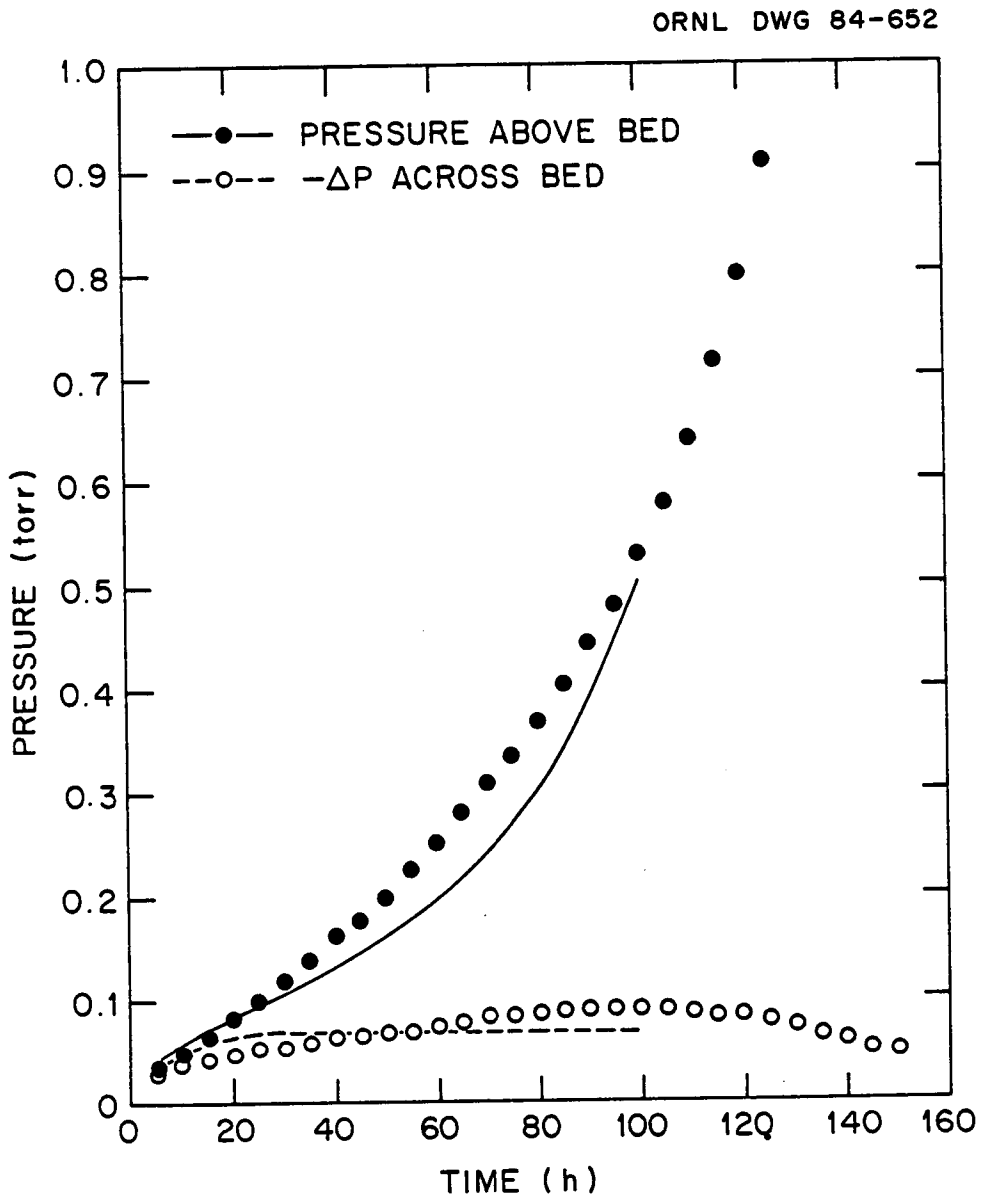

Figure 28. Comparison of experimental pressure and pressure drop data for Run 227 with theoretical curves for which κ = 200 cm^2/s and k = 5.0 $torr^{-1}$. Table 2, p. 58, details experimental conditions; Table 3, p. 60, lists parameters other than κ and k used to calculate theoretical curves.

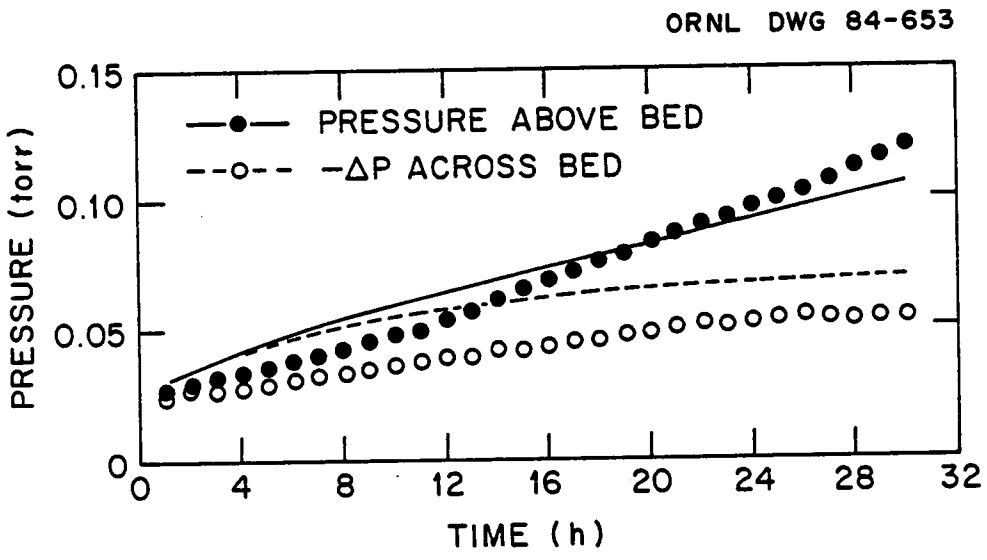

Figure 29. Comparison of short-time experimental pressure and pressure drop data for Run 227 with theoretical curves for which κ = 200 cm^2/s and k = 5.0 $torr^{-1}$. Table 2, p. 58, details experimental conditions; Table 3, p. 60, lists parameters other than κ and k used to calculate theoretical curves.

studied. Garg and Ruthven (1973a) assert that the solid-phase diffusivity is concentration dependent; the model assumes the diffusion coefficient is constant.

An important simplification that greatly affected the development of the model was the use of a parabolic profile for the solid-phase concentration across the sorbent particles. Simulating the concentration profile with a parabola has proven successful in obtaining a general solution to the equations modeling the kinetics of a fixed-bed absorber in response to a step change in feed concentration (Liaw et al., 1979). Whether the simplification applies to gas-zeolite systems specifically is not known. In developing a more rigorous model of the mass transfer processes considered here, this is the first simplification that should be eliminated.

Before ending the discussion of the theoretical results, a few comments need to be made about the finite difference solution of the equations comprising the theoretical model. The solution method is discussed in detail in Section IV, and the FORTRAN program implementing the solution is listed in Appendix A. The solution calculates pressure and solid loading along the sorbent bed at a set of discrete points evenly spaced through the bed after differential steps in time. Two necessary specifications are the number of points and the size of the time step.

For a given set of parameters D, k, q_m, κ, ε, etc., there is a maximum size for the time step. Using a step size greater than the maximum yields negative values for the pressures and solid loadings in the bed; using a smaller step size has no effect. The result of

changing the number of points in the bed is illustrated in Figure 30. It plots the pressure calculated at 1 h for a set of parameters D, k, q_m, etc.; a fixed time step; and an increasing number of bed increments (number of points = number of increments + 1). Note that the pressure scale is much larger than that used in previous figures. As the number of increments is increased the calculations approach a limiting value; of course, as the number of increments increases, so does the CPU time required to calculate the pressures and solid loadings up to a given time. Ten increments were used in calculating all of the theoretical curves. Generating the curves for N_2 using ten increments and the maximum time step required about 1/2 to 1-1/2 h of CPU time on a DEC PDP-10. For the CO_2 results, about 5 to 6 h were required.

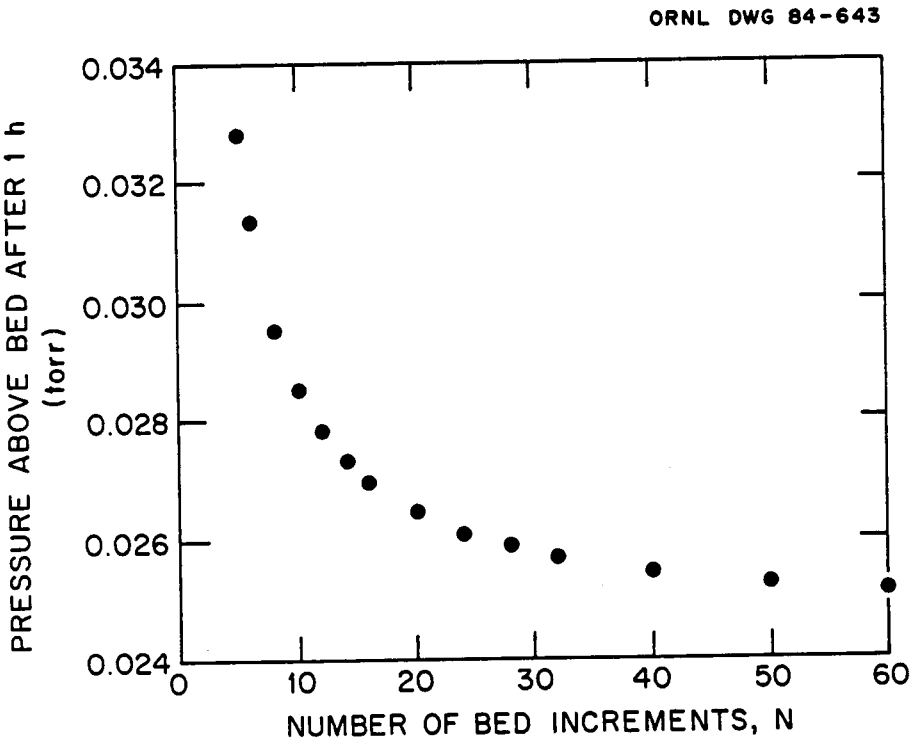

Figure 30. Effect of bed height step size on theoretical pressure calculations. Parameters used for calculations are those listed in Table 3, p. 60, for Run 233.

VII. SUMMARY AND CONCLUSIONS

The major objective of the work was to develop a mathematical model to quantitatively describe mass transfer in a deep bed cryosorption pump. Specifically, study was made of the hydrodynamic and diffusive processes involved in the vacuum sorption pumping of single-component gases on cylindrical sorbent beds. A set of equations describing these processes was derived from theory, and a numerical solution of the set was developed. For comparison with the theoretical model results, sorption pumping experiments were conducted using nitrogen and carbon dioxide on commercial 4A zeolite molecular sieves.

The theoretical model was developed from the following assumptions:

1. The fluid phase is an ideal gas under vacuum conditions.
2. The sorbent bed is isothermal for low flow rates and the consequent low adsorption fluxes.
3. Solid-phase mass transfer can be modeled as surface adsorption on a sphere followed by radial diffusion inward.
4. The solid-phase concentration across a sorbent particle is parabolic.
5. Equilibrium adsorption isotherms for pure gases in zeolite molecular sieves can be modeled by a Langmuir form of equation.
6. Either micropore (intracrystalline) or macropore (intercrystalline) diffusion controls in the manufactured sieves and is independent of concentration.

7. Hydrodynamic mass transfer can be characterized as flow through a long channel of regular geometry; specifically, the interstitial velocity can be related to the pressure gradient and pressure in the channel through an interstitial mass transfer coefficient, κ, which is a function of temperature, molecular weight of the flowing gas, and the channel geometry and which must be determined experimentally.

The model describes the pump performance in terms of the pressure above and through the bed and the solid-phase concentration. The experimentally measured values are the pressure above the bed and the pressure drop at five locations down the bed.

Comparisons of the experimental sorption pumping data obtained for N_2 and CO_2 with the theoretical model results lead to the following conclusions:

1. The theoretical model describes well the pump performance when sorbing N_2 on beds cooled to 77 K for times up to when the bed becomes saturated and pumping slows.
2. For a bed of 0.55-mm sieves, the value of κ that provides the best fit of experimental data obtained at flow rates from 1.2 to 3.0 x 10^{-8} mol/s is 80 cm^2/s; for a bed of 0.72-mm sieves and the same flow rates, the best κ is 105 cm^2/s.
3. The ratio of the κ's obtained for the N_2 runs with two different particle sizes equals the ratio of the particle diameters. Thus κ may be proportional to particle size.

4. For the low temperature (77 K) used here, essentially no N_2 diffuses into the crystal microvoids, and the important diffusive process is the movement of N_2 through the intercrystalline voids.
5. Equilibrium adsorption of N_2 on 4A sieves at 77 K does not fit the Langmuir isotherm well.
6. For CO_2, the theoretical model accurately predicts the pressures above the bed measured experimentally for runs at 3.3 and 3.9 x 10^{-8} mol/s on beds of 0.55-mm and 0.72-mm sieves at 198 K. However, the model does not describe the pressure drop data well.
7. Because the model does not fit the pressure drop data, it is difficult to decide what value of κ yields the best fit of the experimental data. A value of 350 cm^2/s provides a good fit of both the pressure and pressure drop data measured during the first hours of a run but predicts a maximum pressure drop much lower than that measured. A value of 200 cm^2/s can be used to obtain a better estimate of the maximum pressure drop but fails to describe the short-time data.
8. The ratio of κ for CO_2 to κ for N_2 predicted theoretically is 1.3; however, both 350 and 200 cm^2/s yield much higher values, 3.3 and 1.9 for the N_2 κ of 105 cm^2/s. A good fit of the experimental data could not be obtained using the κ for CO_2 of 137 cm^2/s predicted from the κ estimated for N_2

and the theoretical ratio. Thus κ may be affected by factors in addition to temperature, molecular weight, and channel geometry.

9. The important diffusive resistance for CO_2 occurs in the crystal microvoids.

10. The Langmuir equation adequately models equilibrium adsorption of CO_2 in 4A sieves at 198 K.

VIII. RECOMMENDATIONS

For the experiments with both nitrogen and carbon dioxide, one of the major problems in trying to determine the accuracy of the theoretical model was that too many parameters were unknown. Reliable estimates of D, k, q_m, and κ were not available from the literature for the systems studied and the experimental conditions. As discussed, κ must be estimated experimentally; however, D, k, and q_m could and should be determined in independent experiments. Only then could values of κ be estimated with confidence and the accuracy of the model be confirmed.

Another point to be considered is that the behavior of the pump in sorbing N_2 is drastically different from that when sorbing CO_2 because the 4A sieves adsorb much more CO_2 than N_2. Thus in comparing the results of the experiments, the comparison is between two extremes. It would perhaps be interesting to conduct runs with other gases — gases for which the sieves had either a large or small capacity. As for N_2, the model may provide a good fit of both the pressure and pressure drop data for gases for which the sieves have little capacity, or the model may fail to predict the pressure drop curve for all gases behaving like CO_2.

Also, comparisons between the κ's estimated for N_2 and CO_2 did not conclusively show whether the theoretically predicted relationship holds. Perhaps additional data obtained sorbing different gases would help resolve this question. If the model does in fact fail to describe the pressure drop profiles for many gases and if the relationships predicted theoretically between κ's do not hold, then the model should be reexamined and its shortcomings corrected.

From experiments in which N_2 and CO_2 were sorbed at the same flow rates on beds having different sorbent particle sizes, the maximum pressure drop across the bed was shown to decrease as the particle size increases. However, the effect of particle size on the other measure of pump performance, the pressure above the bed, could not easily be determined because different bed weights were used for different particle sizes. As particle size increases two things occur: the size of the interstitial channel increases and the ratio of particle surface area to volume, and consequently to weight, decreases. The first phenomenon allows gas to penetrate the bed more readily. From this, given two beds of equal weight but different particle size both sorbing gas at the same flow rate, one would expect the pressure above the bed of larger particles to be lower than that above the bed of smaller sieves. However, if having more surface area per unit weight of sieve increases the sorption rate, then one would expect the pressure above the bed of smaller sieves to be lower. To help resolve which factor has a greater effect on performance, two series of runs could be conducted with sieves of various sizes. One series would use equal bed weights; the other would use equal surface areas of sorbent per bed. The latter would of course be difficult because of variations in particle size, but nevertheless it should be attempted.

In addition to further experimental work, attention should be given to improving the numerical solution of the equations comprising the theoretical model. As discussed, using the current finite difference solution, there is a maximum allowable time step; using larger steps results in the calculation of negative pressures and solid

loadings. Consequently, long CPU times, about 1 to 6 h on a PDP-10, are required to generate the theoretical curves corresponding to the experimental data. Raghavan and Ruthven (1983) have recently shown that the method of orthogonal collocation can be used in modeling adsorption of a dilute component from a gas mixture in a fixed bed at standard conditions. For their model, orthogonal collocation requires very little CPU time on an IBM 3032. Thus orthogonal collocation should be examined as a possible solution method for the equation set derived here.

The above are only a few suggestions of further work that could be done in connection with the current model derived for single-component systems. Future work could include adapting the model to account for nonisothermal adsorption or to eliminate the assumption of a parabolic solid-phase concentration profile. Another logical step would be to study both theoretically and experimentally the sorption pumping of gas mixtures.

LIST OF REFERENCES

LIST OF REFERENCES

Barrer, R. M., Zeolites and Clay Minerals as Sorbents and Molecular Sieves, Academic Press, London, 1978.

Breck, D. W., Zeolite Molecular Sieves, Wiley, New York, 1974.

Conn, R. W., "Controlled Fusion and Reactors of the Tokamac Type," Adv. Nucl. Sci. Tech., 10, 405 (1977).

_____, "The Engineering of Magnetic Fusion Reactors," Sci. Am., 249, 60 (1983).

Dushman, S., Scientific Foundations of Vacuum Technique, Wiley, New York, 1949.

Fleck, Jr., R. D., D. J. Kirwan, and K. R. Hall, "Mixed-Resistance Diffusion Kinetics in Fixed-Bed Adsorption under Constant Pattern Conditions," Ind. Eng. Chem., Fundam., 12, 95 (1973).

Garg, D. R., and D. M. Ruthven, "The Effect of the Concentration Dependence of Diffusivity on Zeolite Sorption Curves," Chem. Eng. Sci., 27, 417 (1972).

_____, "Theoretical Prediction of Breakthrough Curves for Molecular Sieve Adsorption Columns - I. Asymptotic Solutions," Chem. Eng. Sci., 28, 791 (1973a).

_____, "Theoretical Prediction of Breakthrough Curves for Molecular Sieve Adsorption Columns - II. General Isothermal Solution for Micropore Diffusion Control," Chem. Eng. Sci., 28, 799 (1973b).

_____, "Theoretical Prediction of Breakthrough Curves for Molecular Sieve Adsorption Columns," Third International Conference on Molecular Sieves, Advances in Chemistry Series 121 (1973c).

_____, "The Performance of Molecular Sieve Adsorption Columns: Systems with Micropore Diffusion Control," Chem. Eng. Sci., 29, 571 (1974).

_____, "Linear Driving Force Approximations for Diffusion Controlled Adsorption in Molecular Sieve Columns," AIChE J., 21, 200 (1975a).

_____, "Performance of Molecular Sieve Adsorption Columns: Combined Effects of Mass Transfer and Longitudinal Diffusion," Chem. Eng. Sci., 30, 1192 (1975b).

Habgood, H. W., "The Kinetics of Molecular Sieve Action. Sorption of Nitrogen-Methane Mixtures by Linde Molecular Sieve 4A," Can. J. Chem., 36, 1384 (1958).

Hall, K. R., L. C. Eagleton, A. Acrivos, and T. Vermeulen, "Pore and Solid-Diffusion Kinetics in Fixed-Bed Adsorption under Constant-Pattern Conditions," Ind. Eng. Chem., Fundam., 5, 212 (1966).

Harper, R. J., G. R. Stifel, and R. B. Anderson, "Adsorption of Gases on 4A Synthetic Zeolite," Can. J. Chem., 47, 4661 (1969).

Hobson, J. P., "Surface Smoothness in Thermal Transpiration at Very Low Pressures," J. Vac. Sci. Technol., 6, 257 (1969).

Hobson, J. P., T. Edmonds, and R. Verreault, "Thermal Transpiration in Helium in the Pressure Range 10^{-8} to 20 Torr," Can. J. Phys., 41, 983 (1963).

Hornbeck, R. W., Numerical Methods, Quantum Publishers, Inc., New York, 1975.

Lee, L., and D. M. Ruthven, "Analysis of Thermal Effects in Adsorption Rate Measurements," J. Chem. Soc. Faraday Trans. I, 75, 2406 (1979).

Liaw, C. H., J. S. P. Wang, R. A. Greenkorn, and K. C. Chao, "Kinetics of Fixed-Bed Adsorption: A New Solution," AIChE J., 25, 376 (1979).

Loughlin, K. F., R. I. Derrah, and D. M. Ruthven, "On the Measurement of Zeolitic Diffusion Coefficients," Can. J. Chem. Eng., 49, 66 (1971).

O'Hanlon, J. F., A User's Guide to Vacuum Technology, Wiley, New York (1980).

Perona, J. J., K. S. Crabb, C. H. Byers, and J. S. Watson, "Vacuum Sorption Pumping Studies of Nitrogen on Molecular Sieves," AIChE Annual Meeting, Washington, D.C. (1983).

Podgurski, H. H., and F. N. Davis, "Thermal Transpiration at Low Pressure. The Vapor Pressure of Xenon Below 90°K," J. Phys. Chem., 65, 1343 (1961).

Raghavan, N. S., and D. M. Ruthven, "Numerical Solution of a Fixed-Bed Adsorption Column by the Method of Orthogonal Collocation," AIChE J., 29, 922 (1983).

Rosen, J. B., "Kinetics of a Fixed Bed System for Solid Diffusion into Spherical Particles," J. Chem. Phy., 20, 387 (1952).

Roth, A., Vacuum Technology, North-Holland, Amsterdam (1976).

Ruthven, D. M., and R. I. Derrah, "Diffusion of Monatomic and Diatomic Gases in 4A and 5A Zeolites," J. Chem. Soc. Faraday Trans. I, 71, 2031 (1975).

Ruthven, D. M., D. R. Garg, and R. M. Crawford, "The Performance of Molecular Sieve Adsorption Columns: Non-Isothermal Systems," Chem. Eng. Sci., 30, 803 (1975).

Ruthven, D. M., and L. Lee, "Kinetics of Nonisothermal Sorption: Systems with Bed Diffusion Control," AIChE J., 27, 654 (1981).

Ruthven, D. M., L. Lee, and H. Yucel, "Kinetics of Non-Isothermal Sorption in Molecular Sieve Crystals," 26, 16 (1980).

Ruthven, D. M., and K. F. Loughlin, "The Effect of Crystallite Shape and Size Distribution on Diffusion Measurements in Molecular Sieves," Chem. Eng. Sci., 26, 577 (1971).

_____, "The Measurement of Zeolite Diffusion Coefficients: Some Further Comments," Can. J. Chem. Eng., 50, 151 (1972a).

_____, "The Diffusional Resistance of Molecular Sieve Pellets," Can. J. Chem. Eng., 50, 550 (1972b).

Siu, M. C. I., "Equations for Thermal Transpiration," J. Vac. Sci. Technol., 10, 368 (1973).

Yucel, H., and D. M. Ruthven, "Diffusion of CO_2 in 4A and 5A Zeolite Crystals," J. Coll. Int. Sci., 74, 186 (1980).

APPENDICES

APPENDIX A

FORTRAN PROGRAM FOR CALCULATING NUMERICAL SOLUTION OF THEORETICAL MODEL

The following pages list the FORTRAN 77 program used to obtain solutions (on a DEC PDP-10) to the equations modeling mass transfer in the experimental sorption pumping system. Details of the theoretical model and the numerical solution method are given in the text in Sections III and IV. Incumbent to understanding the program is understanding the Gaussian elimination method of solving a tridiagonal matrix. A brief discussion of how this method can be systematically applied is given below in terms of the variables and constants used in the text and program.

As discussed previously, the program models the mass transfer phenomena occurring as gas flows into a sorbent bed for a given length of time. The goal of the program is to calculate the pressure and solid loading at N+1 evenly spaced points throughout the sorbent bed at specified times. The pressures at positions 2, 3, ..., N+1 (where 1 is at the top of the bed) are calculated at each time by solving a simultaneous set of fluid-phase material balance equations, given in matrix form in Figure 2, p. 27. In terms of the program variables and the constants of Figure 2, the equations are

$$\alpha X(2) + X(3) = R(2),$$

$$X(2) + \beta X(3) + X(4) = R(3), \ldots,$$

$$X(I) + \beta X(I+1) + X(I+2) = R(I+1), \ldots,$$

$$X(N) + \gamma X(N+1) = R(N+1), \qquad \text{(A-1)}$$

where α, β, and γ are constant and X(I) and R(I) are time dependent. Working through the details of solving the resultant matrix equation

by Gaussian elimination yields a simple and systematic solution method (Hornbeck, 1975).

First calculate

$$C(I) = \beta - \frac{1}{C(I-1)} \tag{A-2}$$

and

$$D(I) = \frac{R(I) - D(I-1)}{C(I)} , \tag{A-3}$$

for $2 \leq I \leq N+1$ where $C(2) = \alpha$ and $D(2) = R(2)/\alpha$. The values of X(I) can then be calculated from

$$X(N+1) = D(N+1) \tag{A-4}$$

and

$$X(I) = D(I) - \frac{X(I+1)}{C(I)} . \tag{A-5}$$

Once X(2) through X(N+1) are obtained, calculations of X(1) and Y(1) through Y(N+1) using Equation (58), p. 26, and Equation (57), p. 25, are straightforward.

```
C*************************************************************
C
C       FORTRAN PROGRAM FOR OBTAINING FINITE-DIFFERENCE
C       SOLUTION TO THEORETICAL MODEL OF MASS TRANSFER IN
C       VACUUM SORPTION PUMPING OF PURE GASES ON
C       MOLECULAR SIEVES
C
C*************************************************************
C
C       KATHERINE SAMUELS CRABB, 1984
C
C*************************************************************
C
C  VARIABLES
C
C       R      =COLUMN VECTOR CONTAINING RIGHT-HAND SIDES OF
C               MATERIAL BALANCE EQUATIONS
C       X      =COLUMN VECTOR CONTAINING DIMENSIONLESS
C               PRESSURES
C       OLDY,Y=COLUMN VECTORS CONTAINING DIMENSIONLESS
C               SOLID LOADINGS
C       Q      =COLUMN VECTOR CONTAINING DIMENSIONED
C               SOLID LOADINGS, MOL/G
C       C,D    =COLUMN VECTORS CONTAINING VALUES
C               NEEDED TO SOLVE MATERIAL BALANCE MATRIX
C               EQUATION; C'S ARE CONSTANT, D'S ARE TIME
C               DEPENDENT
C       VOID   =VOID FRACTION OF BED, CM**3 VOID/CM**3 BED
C       RGAS   =GAS CONSTANT, TORR-L/MOL-K
C       TBED   =BED TEMPERATURE, K
C       TAMB   =AMBIENT TEMPERATURE, K
C       DENS   =BULK DENSITY OF SORBENT, G/CM**3
C       AREA   =CROSS-SECTIONAL AREA OF BED, CM**2
C       PREF   =REFERENCE PRESSURE, TORR
C       DIFF   =EFFECTIVE SOLID-PHASE DIFFUSIVITY, CM**2/S
C       RAD    =SORBENT PARTICLE RADIUS, CM
C       KAPPA  =INTERSTITIAL MASS-TRANSFER COEFFICIENT,
C               CM**2/S
C       VOL    =VOLUME OF VOID ABOVE BED, CM**3
C       HGHT   =BED HEIGHT, CM
C       FLUX   =CONSTANT GAS FLUX INTO VOID ABOVE BED,
C               TORR-L/S
C       EQ,SAT=LANGMUIR ISOTHERM CONSTANTS, 1/TORR AND
C               MOL/G
C       DELTAP=PRESSURE DROP ACROSS BED, TORR
C       TIME   =TIME FROM START OF GAS FLOW INTO SYSTEM, MIN
C       N      =NUMBER OF BED INCREMENTS
C       DT     =DIMENSIONLESS TIME STEP
C       DZ     =DIMENSIONLESS BED INCREMENT SIZE, DZ=1/N
```

```
C        S      =NUMBER OF ITERATIONS PERFORMED BETWEEN
C                PRINTINGS OF PRESSURE AND SOLID LOADING
C                PROFILES
C        M      =NUMBER OF TIMES PRESSURE AND SOLID LOADING
C                PROFILES ARE PRINTED
C        AA,BB,=GROUPS OF CONSTANTS
C        CC,DD,
C        EE,FF,
C        GG
C
C  NOTES:
C
C        R,X,OLDY,Y,Q,C,D ARE OF DIMENSION N+1 OR GREATER.
C        IF PREF=1 TORR, THE DIMENSIONED PRESSURES EQUAL
C          THE DIMENSIONLESS VALUES AND NEED NOT BE
C          CALCULATED.
C
C*************************************************************
C
         DIMENSION R(100),X(100),Y(100),OLDY(100)
         DIMENSION C(100),D(100),Q(100)
         DOUBLE PRECISION AA,BB,CC,DD,EE,FF,GG
         DOUBLE PRECISION R,C,D,X,Y,OLDY,KAPPA
         INTEGER N,M,S
         DATA VOID/.35/,RGAS/62.361/,TBED/77./,TAMB/300./
         DATA DENS/.92/,AREA/.472/,PREF/1./
         DATA DIFF/5.0E-08/,RAD/.036/,KAPPA/105./,VOL/200./
         DATA HGHT/9.49/,FLUX/.000459 1/,EQ/80.0/,SAT/.00016/
         DATA N/10/,DT/.02/,DZ/.10/,M/18/,S/104930/
C
         AA=2.*(DZ**2.)/DT
         BB=(DENS*RGAS*1000.*TBED*EQ*SAT)/VOID
         CC=(FLUX*1000.*TBED*HGHT*DZ)/
     $        (VOID*TAMB*KAPPA*AREA*PREF)
         DD=(TBED*VOL*DZ)/(VOID*AREA*TAMB*DT*HGHT)
         EE=-2.-2.*(DZ**2.)/DT
         FF=-1.-2.*(DZ**2.)/DT
         GG=(15.*DT*DIFF*HGHT**2.)/(KAPPA*RAD**2.)
C
         J=N-1
         K=N+1
C
         C(2)=EE+1./(1.+DD)
C
         DO 10 I1=3,N
         C(I1)=EE-1./C(I1-1)
10       CONTINUE
C
         C(K)=FF-1./C(N)
```

```
C
      DO 20 I2=1,K
      X(I2)=0.
      Y(I2)=0.
      CLDY(I2)=0.
20    CONTINUE
C
C
C
      DO 200 I3=1,M
C
C
      DO 100 I4=1,S
C
      R(2)=AA*(Y(2)-OLDY(2))-(CC+DD*X(1))/(1.+DD)-X(1)
     $       -X(3)+(2.-AA)*X(2)
C
      DO 30 I5=3,N
      R(I5)=AA*(Y(I5)-OLDY(I5))-X(I5+1)+(2.-AA)*X(I5)
     $        -X(I5-1)
30    CONTINUE
C
      R(K)=(1.-AA)*X(K)-X(N)+AA*(Y(K)-OLDY(K))
C
      D(2)=R(2)/C(2)
C
      DO 40 I6=3,K
      D(I6)=(R(I6)-D(I6-1))/C(I6)
40    CONTINUE
C
      X(K)=D(K)
C
      DO 50 J3=1,J
      I7=K-J3
      X(I7)=D(I7)-X(I7+1)/C(I7)
50    CONTINUE
C
      X(1)=(CC+DD*X(1)+X(2))/(1.+DD)
C
      DO 60 I12=1,K
      OLDY(I12)=Y(I12)
      Y(I12)=(Y(I12)+GG*BB*X(I12)/(1.+EQ*PREF*X(I12)))/
     $          (1.+GG)
60    CONTINUE
C
100   CONTINUE
C
C
```

```
      DO 70 I8=1,K
      Q(I8)=Y(I8)*VOID*PREF/(DENS*RGAS*1000.*TBED)
70    CONTINUE
C
      TIME=(HGHT**2/KAPPA)*DT*S*I3/60
      DELTAP=X(1)-X(K)
C
      WRITE(5,14)TIME
      WRITE(5,15)X(1),X(2),X(K)
      WRITE(5,12)Q(1),Q(2),Q(K)
      WRITE(5,13)DELTAP
C
12    FORMAT(1X,'Q1= ',F15.10,2X,'Q2= ',F15.10,2X,'QN= ',
     $      F15.10)
13    FORMAT(1X,'DELTAP= ',F15.5)
14    FORMAT(1X,'TIME= ',F15.9,' MIN')
15    FORMAT(1X,'X1= ',F15.9,'  X2= ',F15.9,'  XN= ',
     $      F15.9)
C
200   CONTINUE
C
C
C
      STOP
      END
```

APPENDIX B

TABULATED DATA FROM SORPTION PUMPING EXPERIMENTS

Table B-1. Pressure and pressure drop data from Run 205: N_2 at 2.5×10^{-8} mol/s on 5.06 g of 0.55-mm sieves

Time (m)	Pressure above sorbent bed[a] (torr)	Total pressure drop across bed[a,b] (torr)
21	0.019	0.021
36	0.024	0.025
51	0.026	0.028
66	0.032	0.033
81	0.035	0.036
96	0.041	0.040
111	0.041	0.044
126	0.045	0.047
141	0.049	0.051
156	0.052	0.054
171	0.054	0.055
186	0.058	0.059
201	0.059	0.062
216	0.065	0.068
231	0.067	0.070
246	0.071	0.073
261	0.073	0.077
276	0.078	0.080
291	0.075	0.080
306	0.079	0.084
321	0.080	0.082
336	0.084	0.072
351	0.094	0.056
366	0.106	0.042
381	0.115	0.033
396	0.143	0.030
411	0.175	0.025
426	0.202	0.019
441	0.245	0.020
456	0.289	0.014
471	0.351	0.016
486	0.422	0.014
501	0.510	0.013
516	0.609	0.011
531	0.665	~0
546	0.752	~0
561	0.850	~0
576	0.981	~0
591	1.114	~0

[a]Data are accurate to ±0.005 torr.

[b]Pressure drop is greater than pressure above bed in some cases because of imprecise measurements.

Table B-2. Pressure and pressure drop data from Run 206: N_2 at 1.2×10^{-8} mol/s on 5.06 g of 0.55-mm sieves

Time (m)	Pressure above sorbent bed[a] (torr)	Total pressure drop across bed[a,b] (torr)
40	0.011	0.012
70	0.011	0.013
100	0.016	0.015
130	0.016	0.018
160	0.019	0.021
191	0.024	0.023
221	0.024	0.026
251	0.026	0.028
281	0.029	0.030
311	0.031	0.034
341	0.034	0.034
371	0.037	0.036
401	0.038	0.039
431	0.040	0.041
461	0.042	0.042
491	0.044	0.044
521	0.046	0.045
551	0.050	0.047
581	0.050	0.044
611	0.054	0.031
641	0.064	0.020
671	0.076	0.016
701	0.094	0.010
731	0.120	~0
761	0.146	~0
791	0.188	~0
821	0.228	~0
851	0.279	~0
881	0.343	~0
911	0.410	~0
942	0.488	~0
972	0.581	~0
1002	0.676	~0
1032	0.790	~0
1062	0.911	~0
1092	1.049	~0
1114	1.143	~0

[a]Data are accurate to ±0.005 torr.

[b]Pressure drop is greater than pressure above bed in some cases because of imprecise measurements.

Table B-3. Pressure and pressure drop data from Run 208: N_2 at 3.0 x 10^{-8} mol/s on 5.06 g of 0.55-mm sieves

Time (m)	Pressure above sorbent bed[a] (torr)	Total pressure drop across bed[a] (torr)
16	0.026	0.025
36	0.026	0.026
56	0.034	0.033
76	0.042	0.041
96	0.050	0.049
116	0.057	0.056
136	0.061	0.061
156	0.068	0.067
176	0.073	0.072
196	0.079	0.079
216	0.081	0.081
236	0.090	0.089
256	0.097	0.096
276	0.101	0.097
296	0.108	0.081
316	0.120	0.053
336	0.154	0.039
356	0.207	0.031
376	0.261	0.025
396	0.349	0.022
416	0.434	0.017
436	0.564	0.014
456	0.707	0.012
476	0.895	0.010
496	1.108	0.009

[a]Data are accurate to ±0.005 torr.

Table B-4. Pressure and pressure drop data from Run 217: CO_2 at 3.3×10^{-8} mol/s on 4.69 g of 0.55-mm sieves

Time (h)	Pressure above sorbent bed[a] (torr)	Total pressure drop across bed[a,b] (torr)
1	0.023	0.027
2	0.027	0.029
3	0.027	0.030
4	0.029	0.030
5	0.029	0.030
6	0.031	0.032
7	0.032	0.033
8	0.035	0.035
9	0.037	0.036
10	0.040	0.038
11	0.041	0.040
12	0.044	0.042
13	0.046	0.043
14	0.049	0.045
15	0.051	0.047
16	0.054	0.050
17	0.056	0.050
18	0.059	0.053
19	0.063	0.057
20	0.066	0.059
21	0.064	0.056
22	0.066	0.054
23	0.066	0.055
24	0.066	0.054
25	0.071	0.057
26	0.074	0.059
27	0.077	0.061
28	0.080	0.063
29	0.081	0.063
30	0.086	0.065
35	0.105	0.072
40	0.125	0.079
45	0.151	0.092
50	0.179	0.106
55	0.178	0.088
60	0.207	0.102
65	0.238	0.116
70	0.258	NA
75	0.261	NA
80	0.306	NA

Table B-4 (Continued)

Time (h)	Pressure above sorbent bed[a] (torr)	Total pressure drop across bed[a,b] (torr)
85	0.322	NA
90	0.342	NA
95	0.377	NA
100	0.409	NA
105	0.446	NA
110	0.485	NA
115	0.532	NA
120	0.606	NA
125	0.692	NA
130	0.786	NA
135	0.898	NA
140	1.034	0.116

[a]Data are accurate to ±0.005 torr.

[b]Pressure drop is greater than pressure above bed in some cases because of imprecise measurements; NA indicates that data are not available.

Table B-5. Pressure and pressure drop data from Run 218: CO_2 at 3.9 x 10^{-8} mol/s on 4.69 g of 0.55-mm sieves

Time (h)	Pressure above sorbent bed[a,b] (torr)	Total pressure drop across bed[a] (torr)
1	0.029	0.028
2	0.032	0.029
3	0.034	0.030
4	0.035	0.035
5	0.035	0.033
6	0.037	0.035
7	0.040	0.036
8	0.043	0.039
9	0.046	0.040
10	0.048	0.042
11	0.051	0.043
12	0.054	0.046
13	0.057	0.049
14	0.060	0.050
15	0.063	0.052
16	0.066	0.053
17	0.069	0.055
18	0.073	0.055
19	0.075	0.058
20	0.079	0.059
21	0.082	0.060
22	0.082	0.057
23	0.085	0.061
24	0.091	0.062
25	0.094	0.063
26	0.099	0.066
27	0.102	0.068
28	0.106	0.070
29	0.112	0.072
30	0.116	0.073
35	0.139	0.082
40	0.167	0.095
45	0.197	0.107
50	0.208	0.101
55	0.232	0.108
60	0.260	0.115
65	0.290	0.120
70	0.321	0.125
75	0.355	0.134
80	0.391	0.139

Table B-5 (Continued)

Time (h)	Pressure above sorbent bed[a,b] (torr)	Total pressure drop across bed[a] (torr)
85	0.429	0.145
90	0.473	0.148
95	0.519	0.149
100	0.577	0.146
105	0.654	0.142
110	0.741	0.138
115	0.843	0.129
120	0.990	0.114
125	1.147	0.103
130	NA	0.091
135	NA	0.081
140	NA	0.068
145	NA	0.060

[a]Data are accurate to ±0.005 torr.
[b]NA indicates that data are not available.

Table B-6. Pressure and pressure drop data from Run 225: CO_2 at 3.9×10^{-8} mol/s on 4.33 g of 0.72-mm sieves

Time (h)	Pressure above sorbent bed[a,b] (torr)	Total pressure drop across bed[a] (torr)
1	0.030	0.028
2	0.033	0.030
3	0.036	0.031
4	0.037	0.032
5	0.041	0.035
6	0.045	0.036
7	0.049	0.039
8	0.051	0.040
9	0.056	0.042
10	0.059	0.043
11	0.065	0.045
12	0.068	0.046
13	0.071	0.047
14	0.076	0.049
15	0.082	0.051
16	0.086	0.053
17	0.094	0.057
18	0.098	0.059
19	0.106	0.063
20	0.112	0.066
21	0.116	0.068
22	0.097	0.046
23	0.107	0.050
24	0.114	0.057
25	0.121	0.060
26	0.127	0.063
27	0.131	0.064
28	0.137	0.066
29	0.143	0.070
30	0.149	0.073
35	0.175	0.080
40	0.200	0.086
45	0.224	0.087
50	0.252	0.093
55	0.286	0.102
60	0.316	0.108
65	0.348	0.112
70	0.414	0.141
75	0.403	0.105
80	0.453	0.115

Table B-6 (Continued)

Time (h)	Pressure above sorbent bed[a,b] (torr)	Total pressure drop across bed[a] (torr)
85	0.506	0.117
90	0.572	0.125
95	0.681	0.145
100	0.697	0.099
105	0.814	0.101
110	0.947	0.098
115	1.095	0.084
120	NA	0.069
125	NA	0.066
130	NA	0.056
135	NA	0.045
140	NA	0.039
145	NA	0.032

[a]Data are accurate to ±0.005 torr.
[b]NA indicates that data are not available.

Table B-7. Pressure and pressure drop data from Run 227: CO_2 at 3.3×10^{-8} mol/s on 4.33 g of 0.72-mm sieves

Time (h)	Pressure above sorbent bed[a,b] (torr)	Total pressure drop across bed[a] (torr)
1	0.027	0.025
2	0.030	0.027
3	0.032	0.027
4	0.034	0.028
5	0.036	0.029
6	0.038	0.031
7	0.040	0.032
8	0.042	0.033
9	0.046	0.035
10	0.048	0.036
11	0.050	0.037
12	0.054	0.039
13	0.057	0.039
14	0.061	0.042
15	0.065	0.042
16	0.069	0.043
17	0.072	0.045
18	0.076	0.045
19	0.079	0.047
20	0.083	0.048
21	0.087	0.050
22	0.090	0.052
23	0.093	0.051
24	0.097	0.052
25	0.100	0.053
26	0.103	0.054
27	0.107	0.054
28	0.112	0.053
29	0.116	0.054
30	0.120	0.054
35	0.141	0.060
40	0.162	0.064
45	0.178	0.066
50	0.201	0.069
55	0.227	0.071
60	0.253	0.076
65	0.281	0.080
70	0.310	0.084
75	0.335	0.085
80	0.368	0.087

Table B-7 (Continued)

Time (h)	Pressure above sorbent bed[a,b] (torr)	Total pressure drop across bed[a] (torr)
85	0.404	0.090
90	0.445	0.090
95	0.482	0.091
100	0.529	0.089
105	0.579	0.090
110	0.641	0.088
115	0.714	0.084
120	0.800	0.085
125	0.906	0.080
130	1.016	0.075
135	1.152	0.066
140	NA	0.060
145	NA	0.053
150	NA	0.049

[a]Data are accurate to ±0.005 torr.
[b]NA indicates that data are not available.

Table B-8. Pressure and pressure drop data from Run 231: N_2 at 3.0 x 10^{-8} mol/s on 4.12 g of 0.72-mm sieves

Time (m)	Pressure above sorbent bed[a] (torr)	Total pressure drop across bed[a] (torr)
10	0.024	0.021
30	0.022	0.022
50	0.025	0.026
70	0.033	0.031
90	0.038	0.036
110	0.044	0.043
130	0.048	0.046
150	0.051	0.046
170	0.056	0.051
190	0.061	0.055
210	0.064	0.057
230	0.067	0.056
250	0.072	0.056
270	0.077	0.054
290	0.083	0.027
310	0.106	0.025
330	0.155	0.018
350	0.227	0.012
370	0.304	0.008
390	0.427	~0
410	0.578	~0
430	0.781	~0
450	0.965	~0

[a]Data are accurate to ±0.005 torr.

Table B-9. Pressure and pressure drop data from Run 233: N_2 at 3.0×10^{-8} mol/s on 4.12 g of 0.72-mm sieves

Time (m)	Pressure above sorbent bed[a] (torr)	Total pressure drop across bed[a,b] (torr)
20	0.018	0.018
40	0.022	0.023
60	0.027	0.025
80	0.031	0.029
100	0.034	0.037
120	0.037	0.042
140	0.041	0.046
160	0.045	0.052
180	0.050	0.054
200	0.054	0.058
220	0.059	0.059
240	0.064	0.057
260	0.069	0.054
280	0.073	0.048
300	0.089	0.029
320	0.122	0.019
340	0.181	0.012
360	0.253	~0
380	0.351	~0
400	0.502	~0
420	0.652	~0
440	0.836	~0
460	1.096	~0

[a]Data are accurate to ±0.005 torr.

[b]Pressure drop is greater than pressure above bed in some cases because of imprecise measurements.

Table B-10. Pressure and pressure drop data from Run 237: N_2 at 2.5 x 10^{-8} mol/s on 4.12 g of 0.72-mm sieves

Time (m)	Pressure above sorbent bed[a] (torr)	Total pressure drop across bed[a] (torr)
23	0.019	0.019
40	0.021	0.021
61	0.025	0.025
80	0.029	0.029
100	0.032	0.032
122	0.036	0.036
140	0.039	0.039
160	0.042	0.042
183	0.045	0.044
200	0.048	0.047
220	0.051	0.050
240	0.054	0.053
260	0.056	0.054
281	0.060	0.054
305	0.064	0.051
325	0.065	0.048
340	0.069	0.042
360	0.083	0.027
380	0.109	0.017
400	0.143	0.012
421	0.205	~0
447	0.303	~0
464	0.367	~0
481	0.468	~0
500	0.597	~0
520	0.763	~0
539	0.904	~0

[a]Data are accurate to ±0.005 torr.

Table B-11. Pressure and pressure drop data from Run 238: N_2 at 1.2×10^{-8} mol/s on 4.12 g of 0.72-mm sieves

Time (m)	Pressure above sorbent bed[a] (torr)	Total pressure drop across bed[a,b] (torr)
30	0.010	0.009
60	0.011	0.010
90	0.010	0.012
120	0.014	0.014
150	0.016	0.016
180	0.018	0.017
210	0.020	0.020
240	0.023	0.019
270	0.022	0.020
300	0.025	0.024
330	0.027	0.025
360	0.030	0.026
390	0.026	0.024
420	0.033	0.028
450	0.033	0.030
480	0.037	0.029
510	0.037	0.026
540	0.039	0.025
570	0.043	0.022
600	0.047	0.014
630	0.063	0.009
660	0.082	~0
690	0.111	~0
720	0.151	~0
750	0.202	~0
780	0.255	~0
810	0.334	~0
840	0.421	~0
870	0.513	~0
900	0.637	~0
930	0.786	~0
960	0.919	~0

[a]Data are accurate to ±0.005 torr.

[b]Pressure drop is greater than pressure above bed in some cases because of imprecise measurements.

APPENDIX C

ESTIMATION OF LANGMUIR ADSORPTION ISOTHERMS FOR NITROGEN AND CARBON DIOXIDE

The Langmuir adsorption isotherm relates surface solid loading to gas-phase concentration by

$$\frac{q}{q_m} = \frac{kp}{1 + kp} . \qquad \text{(C-1)}$$

This equation can be rearranged to yield

$$\frac{p}{q} = \frac{p}{q_m} + \frac{1}{kq_m} . \qquad \text{(C-2)}$$

Thus for gas-solid systems exhibiting Langmuir adsorption behavior, a plot of p/q as a function of p should yield a straight line having a slope of $1/q_m$ and a y-intercept of $1/(kq_m)$.

To obtain adsorption data for nitrogen, experiments were conducted using a Quantasorb manufactured by Quantachrome Corporation of Syosset, New York. With this instrument, measurements were made of the volumes of N_2 adsorbed from mixtures of helium and N_2 on a sample of the Davison 4A molecular sieves used in the sorption pumping experiments. The sample was cooled to 77 K using liquid N_2. By varying the concentration of N_2, the volumes adsorbed for a range of partial N_2 pressures could be measured; helium is not adsorbed by the sieves. Applying the word "equilibrium" to the data must be done carefully. The sieves were allowed to adsorb gas as long as the adsorbed quantity could be measured on a scale of minutes; the times for adsorption ranged up to an hour.

Figure C-1 plots the ratio of the partial N_2 pressures to the weight of N_2 adsorbed as a function of the partial pressure. As shown, the curve is not linear; thus N_2 on 4A sieves at 77 K does not truly

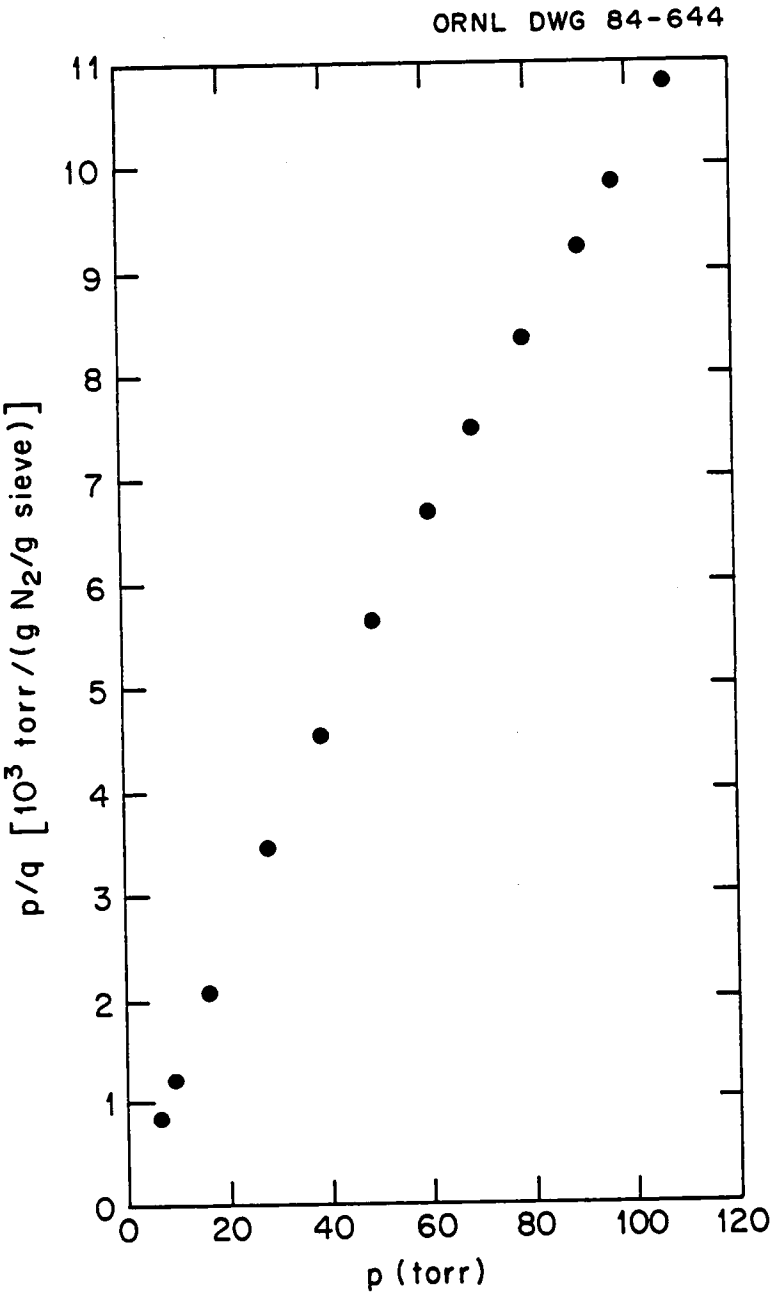

Figure C-1. Equilibrium adsorption data for N_2 on Davison 4A molecular sieves at 77 K.

fit the Langmuir isotherm. Linear regression using all the points shown from 6 to 107 torr estimates k as 0.17 $torr^{-1}$ and q_m as 3.6 x 10^{-4} mol/g. From the first four points, k is estimated as 0.82 $torr^{-1}$ and q_m as 3.0 x 10^{-4} mol/g; the first two points yield a k of 0.86 $torr^{-1}$ and q_m of 3.0 x 10^{-4} mol/g. Because the low pressure range is the range of interest, k is estimated as 1 $torr^{-1}$ and q_m as 3 x 10^{-4} mol/g for comparison with the results of the sorption pumping experiments.

Literature provided by the molecular sieve manufacturer included an adsorption isotherm for carbon dioxide at 198 K. Figure C-2 plots the data in terms of the ratio p/q and p. Linear regression of the nine points from 2 to 10 torr yields a k of 1.9 $torr^{-1}$ and a q_m of 0.004 mol/g. From the first four points, k is estimated as 3.2 $torr^{-1}$ and q_m as 0.004 mol/g. If only the first two points are used, k is 5.1 $torr^{-1}$ and q_m is 0.004 mol/g. The estimates of q_m are the same, but k varies depending on which points are used. In modeling the sorption pumping experiments, a value of 4 $torr^{-1}$ is assigned to k and 0.004 mol/g to q_m.

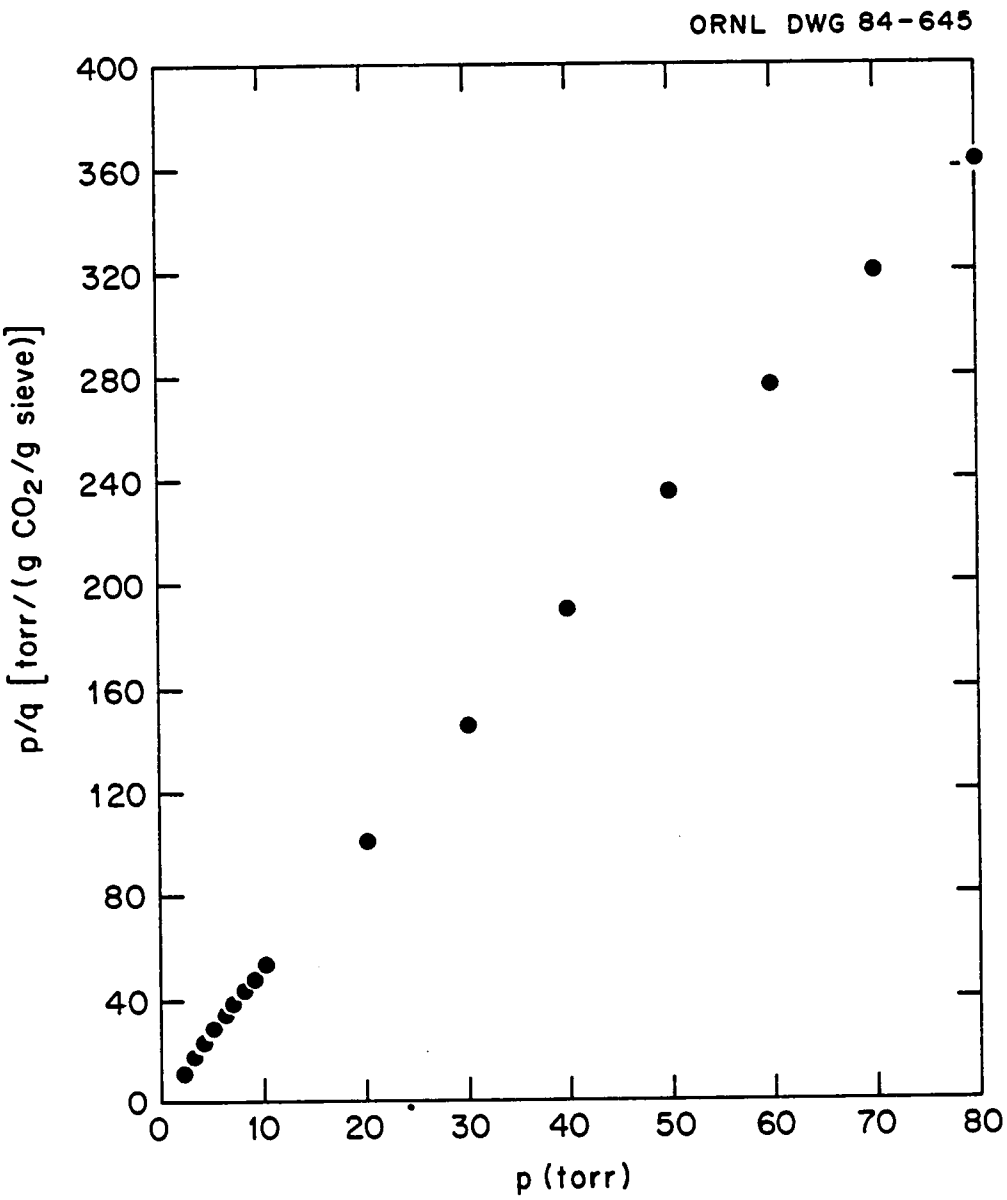

Figure C-2. Equilibrium adsorption data for CO_2 on Davison 4A molecular sieves at 198 K.

VITA

Katherine Samuels Crabb was born in Oak Ridge, Tennessee, on March 11, 1957. She attended elementary, junior high, and high school in Oak Ridge before entering the University of Tennessee, Knoxville, in September 1974. In March 1978, she graduated at the top of the College of Liberal Arts with a Bachelor of Arts degree in English. During these four years, she was elected to Phi Kappa Phi and Phi Beta Kappa honor societies.

From June 1978 to May 1980, Katherine worked as a technical reports editor in the Technical Publications Department at the Oak Ridge National Laboratory. She returned to The University of Tennessee, Knoxville, in June 1980 to pursue a Master's degree in Chemical Engineering. As a chemical engineering student, she received an AIChE Scholarship Award and was elected to Tau Beta Pi honor society.

Katherine is married to Charles Clarence Crabb, a PhD candidate in Polymer Chemistry at The University of Tennessee. Mr. and Ms. Crabb will both graduate from the university in August 1984. After graduation, they will be employed by Rohm & Haas Company in Philadelphia, Pennsylvania.